Steady States of Passive Particles Sliding on Fluctuating Surfaces

A Thesis
Submitted to the
Tata Institute of Fundamental Research, Mumbai
For the degree of Doctor of Philosophy
in Physics

by

Apoorva Nagar

Department of Theoretical Physics
School of Natural Sciences
Tata Institute of Fundamental Research
Mumbai

October, 2006

Acknowledgements

I would like to express my sincere gratitude to Mustansir for his guidance, constant encouragement and support. His open mindedness towards new ideas and interpretations coupled with his critical analysis of arguments made my interactions with him most enjoyable and enlightening. While he has always encouraged me to develop my positive qualities, he has also most patiently and kindly pointed out my inadequacies as a researcher and helped me overcome them. It has indeed been my pleasure and privilege to have worked with him. I would also like to thank him for the wonderful courses he has taught us.

I would also like to thank Deepak, talking to whom has been a learning experience. His keen insight and original approach to problems are a source of inspiration. The graduate courses at TIFR have been some of the best I have taken, in particular attending Sumit and Mustansir's courses was a treat.

My collaboration with Satya has been most fruitful and I would like to thank him for his help in the equilibrium calculations reported in this thesis.

Numerical simulations have been an important tool for my thesis work and the following people have been very kind in helping me with computers. Anindya is the friend, philosopher and guide in the world of machines, not just mine but of the entire theory department and many people in the institute. I thank him for the selfless help he provides anyone who asks for it. I would also like to acknowledge help from Sanjeeb, Arti and Swagato.

The office staff at the theory department are most co-operative, helpful and polite. I am grateful to Raju, Girish, Mohan, Rajendra and Ajay for making my life in the department easier.

I have had some most lively and intelligent people as my colleagues in the theory students' room. Punyabrata is not only my collaborator but also a good friend. I have learnt a lot from discussions with him, Kavita, Sakuntala and Shamik. I hope that I get a chance to interact and collaborate with them in the future. I have thoroughly enjoyed discussions, both physics and non-physics, with Suresh, Ashik, Basu, Aniket, Anandamohan, Shamik, Punyabrata, Arti, Ramanan, Dariush and Lars. Many thanks to all my friends in the theory room.

My stay at TIFR has been a learning experience, most eventful and memorable. I will always cherish my friendship with Vaibhav, Aditya, Deepankar and Anand. I would like to thank all my friends in TIFR, those who are in the following list and those who are not, for making my stay here a wonderful experience — Deepak, Ashok, Gautam, Arati, Amala, Shanta, Ashutosh, Ayesha, Garima and Ajay. A special thanks to my best friend, now my wife, Deepshikha. Thank you for being in my life, loving me, tolerating me, unconditionally.

Siddharth Verma has been an important influence in my life, my teacher and dearest friend, who introduced me to the beautiful world of Physics. Prashanth Jaikumar and Asim Mehmood who started out discussing Physics and became good friends. Thank you for making this journey possible, and interesting.

My family — Bhai, Mummy, Papa and Deepshikha who have believed in me, supported me in every venture. All this would not mean anything if it could not be shared with you.

Declaration

This thesis is a presentation of my original research work. Wherever contributions of others are involved, every effort is made to indicate this clearly, with due reference to the literature, and acknowledgment of collaborative research and discussions.

The work was done under the guidance of Professor Mustansir Barma, at the Tata Institute of Fundamental Research.

Apoorva Nagar

In my capacity as supervisor of the candidate's thesis, I certify that the above statements are true to the best of my knowledge.

Mustansir Barma

To my parents

Contents

Publications

0.1 Related to thesis

- *Passive Sliders on Fluctuating Surfaces: Strong-Clustering States*, A. Nagar, M. Barma and S. N. Majumdar, Phys. Rev. Lett. **94**, 240601 (2005)
- *Strong clustering of non-interacting, passive sliders driven by fluctuating surfaces*, A. Nagar, S. N. Majumdar and M. Barma, Submitted to Phys. Rev. E.
- *Clustering of advected passive sliders on a fluctuating surface*, A. Nagar, M. Barma and S. N. Majumdar, Proceedings of National conference on nonlinear systems and dynamics (NCNSD-2003), 85 (2003). cond-mat/0403711.

0.2 Other publications

- *Residence Time Distribution of Sand Grains in the 1-Dimensional Abelian Sandpile Model*, P. Pradhan, A. Nagar, Proceedings of National conference on nonlinear systems and dynamics (NCNSD-2003), 97, (2003). cond-mat/0403769.
- *First passage time distribution in random walks with absorbing boundaries*, A. Nagar and P. Pradhan, Physica A, Vol. 320, 141, (2003).

Introduction

In this thesis, we study the clustering of passive, non-interacting particles driven by fluctuating surfaces that evolve through stochastic dynamics. In particular, we consider fluctuating surfaces that evolve according to the Kardar-Parisi-Zhang (KPZ) equation where the dynamics do not respect reflection symmetry and Edwards-Wilkinson (EW) equation which respects reflection symmetry. The particles slide downward, following the local slope of the surface. This problem belongs to a general class of problems dealing with coupled driven diffusive systems and we will begin this chapter with a discussion of this topic. We will then discuss a specific example of such systems — the passive scalar problem in fluid dynamics. The passive scalar problem has a connection to our problem — the Kardar-Parisi-Zhang equation can be mapped to the Burgers equation for a compressible fluid. This mapping and a detailed description of our problem will be discussed next. The following section will describe previous work which is of direct relevance to our problem. The final portion of this chapter contains a brief discussion of our results and the plan of the thesis.

1.1 Coupled driven diffusive systems

The term driven diffusive systems refers to multiparticle systems in which individual particles have a diffusive motion apart from an overall systematic drive. This general area describes a vast variety of physical systems — from stirred fluids and growing thin films [1] to traffic [2]. The attempts at theoretical modeling of these systems include setting up and trying to solve continuum equations like the Navier-Stokes [3] or Burgers [4] equations for fluids or studying lattice models like the asymmetric exclusion process (ASEP) [2], a simple model for traffic. While this is an extremely interesting area attracting a lot of current attention, our interest in this thesis is to study what happens when two such systems are coupled together.

The coupling of two or more driven diffusive systems can give rise to complex and interesting behaviour. There are diverse physical systems where such coupling arises, for instance, growth of binary films [5], motion of stuck and flowing grains in a sandpile [6], movement of ants along a trail [7], coupled motion of magnetic fields and fluids in magnetohydrodynamic turbulence [8] and the flow of passive scalars like ink or dye particles in a fluid [9, 10].

Coupled systems can be further subclassified into two categories. The first category is systems with a bidirectional coupling i.e. the evolution of each field affects the other, an example being ant trails [7]. Here, the density of ants and density of pheromones are the two coupled fields. Pheromones are substances dropped by moving ants to guide subsequent ants. Ants prefer to move towards the direction of increasing pheromone density and while moving, keep dropping more pheromones for other ants to follow. This coupling leads to interesting patterns in ant traffic and studies are underway to look for these features in real ant trails.

The other category, one of interest to us, is semiautonomously coupled systems. Here, one of the fields evolves independently and drives the other field. The problem of passive scalars like ink or dye in stirred fluids [9, 10] is an example of such systems. In this case, fluid flow is the independent field to which the dye particles are coupled. The word passive in "passive scalars" implies that the ink or dye particles follow the local flow of the fluid, but the flow is not affected by their presence; the word scalar qualifies the passive field e.g. the density of the dye particles. The passive scalars, apart from being driven by the fluid, also diffuse, and this combination leads to intricate and interesting behaviour.

1.2 Passive Scalars

As we mentioned earlier, our problem of sliding particles on a fluctuating surface can be mapped to the passive scalar problem which describes the behaviour of particles or fields driven by a fluid. In this section, we will provide a brief description of the important work done in the general area of passive scalar advection. The examples of passive scalars which we encounter in daily life — ink, dye mixing in fluids, smoke particles mixing in air, etc. describe passive particles which are driven by incompressible fluids. Here we see that the passive particles spread out and mix evenly in the large time limit. However, if the fluid in question is compressible, the behaviour can change

drastically and it is possible that the passive scalar particles cluster together rather than mixing with the fluid and reaching a more homogeneous state. Thus we can see that the nature of the driving fluid is of great importance in this problem. The subsection below discusses in brief the properties of the driving fluids. We will address the problem of passive fields driven by these fluids in the subsection after that.

1.2.1 The Navier-Stokes and Burgers fluids

The dynamics of incompressible fluids like water are described by the Navier-Stokes equations

$$\frac{\partial \vec{v}}{\partial t} + (\vec{v}.\nabla)\vec{v} = -\frac{1}{\rho}\nabla p + \nu\nabla^2\vec{v} + f \tag{1.1}$$

and

$$\nabla.\vec{v} = 0. \tag{1.2}$$

Let us first consider Eq. (1.1) above. The L.H.S. of this equation describes the total derivative of velocity $\vec{v}$, which takes into account the motion of the fluid. The first term on the R.H.S. describes the force due to the pressure differences inside the fluid, p is the pressure and ρ is the fluid density. The second term arises from viscous interactions and ν is the coefficient of viscosity. The last term on the R.H.S. is the forcing term and corresponds to the external force applied to the liquid to drive it. The second equation, Eq. (1.2) is derived from the equation of continuity

$$\frac{\partial \rho}{\partial t} + \nabla.(\rho\vec{v}) = 0 \tag{1.3}$$

by demanding that ρ is a constant independent of space and time.

Although the Navier-Stokes equations are of immense practical importance since they model realistic fluids, they are difficult to approach analytically and have eluded a solution. Most of the methods adopted to solve these equations require considerable computational power. Apart from trying to solve these equations directly, alternative approaches have been tried, which include studying the simpler and more approachable Burgers equation[4, 11], or in the context of passive scalars, replacing the fluid by a random Gaussian field [12]. While these approaches may not offer us solutions which are directly useful in practical situations, they afford us an insight into the physics of

the problem. We discuss below the Burgers equation which is of direct relevance to our problem.

The Burgers equation is similar to the Equation (1.1) above with the difference that the pressure term $-\frac{1}{\rho}\nabla p$ is not present

$$\frac{\partial \vec{v}}{\partial t} + (\vec{v}.\nabla)\vec{v} = \nu\nabla^2\vec{v} + f. \tag{1.4}$$

The removal of this term changes the character of the fluid significantly; since there is no pressure inside the fluid, it becomes highly compressible. An example of a compressible fluid that we see around us is vehicular traffic where traffic jams are regions of high fluid density while empty stretches of road in front of such a jam are regions of low density. The Burgers equation provides a simplified model for vehicular traffic [13]. Interestingly, in the case of irrotational flow (curl of the velocity is zero), this equation can be mapped to the well known Kardar-Parisi-Zhang (KPZ) equation for evolving interfaces by the transformation $\vec{v} = -\nabla h$, where h is the height of the interface. This mapping is important to our problem and we shall discuss the KPZ equation and the mapping in detail later.

The Burgers equation has been the subject of much research since its introduction in 1930s by J. M. Burgers [4]. When the forcing $f = 0$, we have what is called the unforced Burgers equation which describes a decaying fluid flow field. Any initial velocity given to the fluid particles will decay due to the viscosity. Here, one is interested in studying the solutions when the viscosity is very small and the initial conditions are random. The mapping to the KPZ equation is useful here; the Hopf-Cole transformation $h = 2\nu \ln \theta$ changes the nonlinear KPZ equation into a linear diffusion equation in θ which can be solved exactly. There are various methods adopted to study the evolution of the particle trajectories as the system evolves from a random initial state. It has been shown in this case that there is an emergence of shocks as the system evolves in time [11, 14]. A shock is a region in space where velocity of a particle jumps discontinuously from a higher to a lower value as it crosses it. Thus similar to a traffic jam, there is an aggregation of particles at the position of a shock and the density of the fluid increases. The motion of the particles is deterministic in this case and the velocity curves show a sawtooth or a ramp like structure with the slope of the ramp being proportional to $1/t$, and the number or ramps falling in time [11].

The other case of interest is that of a stochastic driving force f. This is the case

of interest to us as we consider the KPZ equation with noise as our driving field. The noise in our case is delta correlated white noise and the structure of shocks is different in this case. We shall see later that instead of a large, smooth, sawtooth like structure, one sees a state with statistical fluctuations around a uniform slope and an absence of shocks. We will discuss the solution in detail later in the KPZ context.

1.2.2 Passive scalars driven by fluids

In this subsection, we will discuss some important results in the general area of passive scalar advection. Before going to the results, let us describe the two points of view that are relevant to the study of fluids and passive scalars — the Lagrangian and the Eulerian points of view. A fluid is a dynamical system with a macroscopic motion apart from the motion of individual particles and to characterise such a system one can take two points of view. We will take weather measurement as an illustrative example for describing these. One can measure the relevant quantity over a period of time at a given point in space, which is the Eulerian point of view. This is like monitoring the quantity of interest, temperature in this case, from a weather station. The other possibility is to tag a given element e.g. a small fluid or passive scalar parcel, and to move along with it as one takes measurements, which is the Lagrangian point of view. This is similar to taking measurements from a weather balloon which is free to move with the wind. The fluid dynamics Equations (1.1) and (1.4) above involve total derivatives and are written from an Eulerian point of view i.e. they describe the velocity of a fluid at time t at a point r in the fixed or the laboratory reference frame.

One can write the generic equation for the density ρ of passive scalars in an Eulerian frame

$$\frac{\partial \rho}{\partial t} + \nabla.(\rho \vec{v}) = \kappa \nabla^2 \rho \tag{1.5}$$

where $\vec{v}$ is the fluid velocity. The first term on the R.H.S. is a diffusive term and indicates that the passive scalars, apart from being advected by the fluid also have a random motion due to thermal noise. This diffusive motion allows the particles to switch fluid streamlines and makes the study of passive scalars nontrivial and interesting. The $\nabla.(\rho \vec{v})$ term makes the equation above difficult to solve.

One can also study the passive field using the trajectory of individual particles. The noninteracting passive particles follow the equation

$$\frac{d\vec{x}_m}{dt} = a\vec{v}|_{\vec{x}_m} + \zeta_m(t) \tag{1.6}$$

where m is a label for the particle. The equation shows that the trajectory of a passive particle is governed by the local fluid velocity and a random noise. Equation (1.6), as we will see in the later chapters, is of importance to us; we will be constructing models for Monte-Carlo simulations and the equation provides a natural way of looking at the trajectories of individual particles. Equation (1.6) also shows us why the passive scalar problem is nontrivial — it requires the knowledge of the field at the exactly the point where the particle is present.

Previous work

From our experience with fluids around us, we know that the addition of passive scalars like ink/dye to a stirred, incompressible fluid like water leads to spreading and mixing at various length scales till the density becomes homogeneous. This process is however not as simple as releasing the scalars in a stationary fluid and letting them diffuse through the entire fluid by diffusion. It has been observed that the addition of fluid drive to diffusion hastens the mixing process but also introduces intermittency [9]. The term intermittency implies an activity that occurs in bursts and in this case refers to the fluctuations in the density of the passive scalars. The mathematical measure for this intermittent behaviour is usually provided by correlation functions; exponents describing the higher order correlation functions of the quantity of interest (e.g. density) do not grow linearly with the order.

While various models have been proposed to understand this sort of intermittent behaviour [14, 15], a simpler and quite successful approach has been developed by Kraichnan [12]. In the Kraichnan model, instead of considering the turbulent velocity field from the complex fluid dynamics equations, the driving field is modelled in a much simpler way. The fluid velocity field is assumed to be a random, incompressible field which is Gaussian and delta correlated in time. So, in Eq. (1.5) above, the statistical properties of the velocity field $\vec{v}$ are fully specified by the two point correlator $\langle v^\alpha(t,\vec{r})v^\beta(t',0)\rangle = \delta(t-t')[d_0^{\alpha\beta} - d^{\alpha\beta}(\vec{r})]$. The form of $d^{\alpha\beta}$ is chosen such that the condition for incompressibility $\partial_\alpha d^{\alpha\beta}(\vec{r}) = 0$ (which follows from $\partial_\alpha v^\alpha = 0$) is satisfied.

While neglecting the time correlations and choosing a simple Gaussian ensemble for space distribution are big simplifications over the realistic Navier-Stokes velocity

fields, the model still gives non-trivial statistics for the passive scalar field and is believed to capture much of the essential physics of the process. It can be shown that the second order correlation of the passive scalar field follows a power law r^{γ} as a function of distance r [12, 9]. In this model, γ is a free parameter, in particular, the choice of $\gamma = 2/3$ is close to the experimental value [16] and consistent with previous results (Kolmogorov-Obukhov-Corrsin (KOC) theory [9]). The importance of the model lies in the fact that it predicts anomalous scaling of the higher order moments [12] and thus shows intermittency. So, the study of this simpler model leads to the understanding that the complex nature of the passive scalar statistics originates from the mixing process rather than the complexity of the turbulent velocity field of a realistic fluid. It also opens up a gateway for investigation of passive scalar properties by analytical methods. Recent work [17] has shown that though the Kraichnan model shows multiscaling in equal time correlation functions, it does not show dynamic or time dependent multiscaling. This is a result of neglecting the time correlations in the driving field.

Till now, we have considered non-inertial passive scalars in incompressible fluids. We have seen that there is a mixing on larger and larger scales with the presence of intermittency. While the picture of spreading and mixing is intuitive, being realised in everyday incompressible fluids like water, there can be interesting, counter-intuitive consequences if the fluid is highly compressible or if the passive scalars possess inertia. Let us consider the case of inertial passive scalars first.

Let us consider a driven fluid with a homogeneously distributed initial passive scalar density. We would expect that when the passive particles possess no inertia they would follow the lines of flow strictly, if there is no diffusion. The presence of diffusion would tend to homogenise the density field at smaller length scales. In either case, we expect that the passive scalar paricles would not show clustering at large times if the passive particles do not possess inertia. The situation is different when the passive particles possess inertia. They do not tend to follow the flow lines faithfully and might lag behind. This opens up the possibility of the particles clustering together and causes the passive scalar flow to be compressible (the divergence of the passive scalar velocity field is non zero), even though the fluid is incompressible (the divergence of the fluid velocity field is zero) [18]. Deutsch [19] and later Wilkinson and Mehlig [20] have studied the clustering transition under the change in inertia. They model the medium in which particles are moving through a random force with correlations that decay rapidly and show how the path coalescence mechanism causes a clustering of the scalars. Wilkinson

and Mehlig [21] have also shown the formation of structures called caustics in spatial dimensions larger than one. The nomenclature caustics originates from the similarity of the structures to optical caustics. They show that these structures further enhance the clustering. In the presence of turbulence and vortices, there is another mechanism by which clustering or large fluctuations can occur [22, 23]; due to their inertia, the passive particles inside the vortices and eddies are driven outwards due to the centrifugal force and thus tend to aggregate in the boundary regions between the eddies.

Apart from considerable work on the theoretical aspects of passive scalar clustering, there also has been experimental work in this direction. While the driven particles in these experiments might not necessarily be passive, the results still shed light on aspects of the dynamics which relate to clustering. Fessler et. al. [24] have studied the motion of inertial particles driven by a turbulent fluid. They measured the density distribution and found that it shows significant departure from the expected random distribution of particles. Their measurements show formation of clusters which are separated from each other at much larger scales than the scales on which clustering occurs. Apart from inertial effects, clustering can also be caused if the flow of the passive particles can be made compressible. Cressman et. al. [25] and Sommerer and Ott [26] have achieved this compressibility in the following way. They have made an arrangement where the fluid flow can be manipulated in three dimensions while the passive particles are extremely light and thus tend to float on the two dimensional top surface of the fluid. Turbulence is created in the fluid such that the top fluid layer is dynamic, with fluid entering the top layer from below at certain places and leaving at others. The passive particles follow the fluid flow while always floating on the surface and thus tend to cluster in the areas where the fluid is flowing downwards i.e. leaving the surface layers. Thus they are able to create a two dimensional compressible subsystem in a system with three dimensional incompressible flow. Cressman et. al. [25] have studied the amount of clustering using the mean squared separation of tagged particles, they show that this separation increases slower than if the motion were diffusive. Sommerer et. al. [26] have studied the fractal structure of the passive particle concentration and show that the fractal has a dimension approximately equal to 1.73.

We now turn to the case of direct interest to us — noninertial passive scalars in a compressible fluid. Compressible fluids, as we saw in the case of the Burgers equation, have a tendency towards shock formation. Shocks are regions where the velocity suddenly changes its value and the fluid density increases; this causes the

passive scalars, which are carried by the fluid, to accumulate in these shocks. Gawedzki and Vergassola [27, 10] have studied the effect of compressibility on passive scalars using the Kraichnan approach. They consider a Gaussian random velocity field and the velocity-velocity correlation is chosen so as to allow for the compressibility of the fluid. They study the separation of two marked particles as a function of time. When the fluid is incompressible, two particles separated by an infinitesimal distance reach an $O(1)$ separation in finite time; there is an explosion of trajectories. On the other hand, when the compressibility of the fluid is increased, one sees a transition. The trajectories of particles are now seen to implode and collapse leading to clustering of particles. They have also measured the density-density correlation function for the passive particles and find that it diverges at small values of separation. This indicates strong clustering and is a feature that we observe in our system as well; however, they did not find scaling with system size, which is an important feature of the steady state of our system. Though these and other studies have shown that clustering of particles is possible in compressible fluids, there has been limited work on the detailed description of the steady states in such systems. A major aim of our thesis is to describe such steady states. The equation we have considered for this purpose is the Burgers equation which describes a perfectly compressible fluid.

The general problem studied in this thesis is that of passive, noninteracting particles sliding on fluctuating surfaces. As we will see below, in the specific case of a Kardar-Parisi-Zhang (KPZ) surface, this problem can be mapped to the passive scalar problem in fluid dynamics by using the mapping of the KPZ equation to the Burgers equation. We have studied other types of fluctuating surfaces as well, which do not correspond to a fluid problem.

1.3 Passive Sliders on fluctuating surfaces

The general problem of growing or evolving interfaces has been the centre of much attention in the recent past. The surface of a growing thin film, burning paper fronts or the surface of an evolving sandpile are the kind of systems one is interested in modeling [1]. These interfaces can be thought of as evolving height fields and one can write continuum equations for the evolution of the height. In our work, we have considered two such well known equations — The Kardar-Parisi-Zhang (KPZ) and the Edwards-Wilkinson (EW) equations [1]. In our problem, these equations describe

the independently evolving field, similar to the fluid in the passive scalar problem. Coupled to this field are particles that slide over the surface, following the local slope. A general discussion of the KPZ and EW equations will be followed by the discussion of the coupled problem.

1.3.1 Fluctuating surfaces

The Edwards-Wilkinson equation

$$\frac{\partial h}{\partial t} = \nu \nabla^2 h + \zeta_h(\vec{x}, t) \tag{1.7}$$

describes an evolving height field $h(\vec{x}, t)$. ζ_h is a Gaussian white noise satisfying $\langle \zeta_h(\vec{x}, t)\zeta_h(\vec{x}', t')\rangle = 2D_h\delta^d(\vec{x} - \vec{x}')\delta(t - t')$. The term $\nu\nabla^2 h$ in the above equation can be thought of as a surface tension term because it tends to smoothen out the surface features. The noise term $\zeta_h(\vec{x}, t)$ describes a random drive causing fluctuations in the surface profile. Thus according to the above equation, the local change in height is governed by a random fluctuation term and the surface tension term which smoothens the surface profile.

Given the above equation, we would like to describe the physical attributes of the surface, e.g. how rough it is, how does it evolve in time, etc.? A measure of the surface roughness is provided by the width W of the surface in a finite system of size L

$$W(L, t) \equiv \sqrt{\overline{\frac{1}{L}\sum_{i=1}^{L}[h(x, t) - \overline{h(t)}]^2}} \tag{1.8}$$

where $\overline{h(t)}$ is the average height. The quantity defined above is the root mean square fluctuation in the height. It is well known [1] that for the surfaces under consideration, the width scales as

$$W(L, t) \sim L^{\alpha} f\left(\frac{t}{L^z}\right). \tag{1.9}$$

The exponent α in the above equation is called the roughness exponent since it provides a measure for the height fluctuations. A portion of the surface having a length l will

have typical height fluctuations (hills and valleys) of size $\sim l^{\alpha}$. The exponent z is the dynamic exponent and describes how fast surface fluctuations evolve. To understand the significance of z, again consider a section of length l. Hills/valleys present in this section will typically be replaced by valleys/hills in time of order l^z. For the EW equation, it can be shown that $\alpha = (2-d)/2$ and $z = 2$, where d is the spatial dimension under consideration [1].

The KPZ equation

$$\frac{\partial h}{\partial t} = \nu \nabla^2 h + \frac{\lambda}{2}(\nabla h)^2 + \zeta_h(\vec{x}, t) \tag{1.10}$$

contains the nonlinear term $\frac{\lambda}{2}(\nabla h)^2$ in addition to the linear terms of the EW equation. This term breaks the $h \rightarrow -h$ symmetry and changes the behaviour of the height fluctuations significantly. In one dimension, one can calculate the value of the exponents $\alpha = 1/2$ and $z = 3/2$ exactly [28], but in higher dimensions, one only has numerical estimates. As we have mentioned before in the subsection on Burgers fluid, the transformation $v = -\nabla h$ maps Eq. (1.10) (with $\lambda = 1$) above to the Burgers equation for a compressible fluid

$$\frac{\partial \vec{v}}{\partial t} + \lambda(\vec{v}.\nabla\vec{v}) = \nu\nabla^2\vec{v} + \nabla\zeta_h(\vec{x}, t). \tag{1.11}$$

The restriction on the velocity field in the above equation is that it has no vorticity; the velocity field can be written as a gradient of the height field, implying that the curl of the velocity is zero.

1.3.2 Sliding particles on fluctuating surfaces

With this background, let us consider the coupled problem. We consider non-interacting particles which slide over the fluctuating surfaces described by the above equations. These particles see the local slope and try to move downwards as if they are subject to gravity. This problem was first studied by Drossel and Kardar [5, 29]. A brief description of their work has been provided in a later subsection. The motion of the particles is described by the following equation

$$\frac{d\vec{x}_m}{dt} = -a\nabla h|_{\vec{x}_m} + \zeta_m(t) \tag{1.12}$$

where $\vec{x}_m$ is the position of the m^{th} particle. The term $-a(\nabla h)$ shows that the particle tends to follow the local slope and brings in the effect of gravity. The white noise $\zeta_m(t)$ represents the randomising effect of temperature, and satisfies $\langle \zeta_m(t)\zeta_m(t')\rangle = 2\kappa\delta(t-t')$. The non-interacting nature of the particles means that the equation for motion of each particle evolves independently and does not involve the effects of the presence of other particles. Thus, in terms of the continuum equations, we want to solve the coupled equations Eqs. (3.9) and (4.2), and, Eqs. (1.10) and (4.2). The transformation $\vec{v} = -\nabla h$ in Eq. (4.2) above leads to

$$\frac{d\vec{x}_m}{dt} = a\vec{v}|_{\vec{x}_m} + \zeta_m(t) \tag{1.13}$$

which is the equation of motion for a passive scalar particle driven by the Burgers fluid. Thus, the problem of passive sliding particles on a KPZ surface is equivalent to the problem of passive scalars in a Burgers fluid. As mentioned earlier, the nonlinear term in the KPZ equation breaks the $h \to -h$ symmetry. This allows for two kind of coupled dynamics depending on the sign of a/λ. The case $a/\lambda > 0$ corresponds to the sliding particles moving in the same direction as the surface. In the fluid picture, this corresponds to particles moving in the direction of flow (advection). The other case, $a/\lambda < 0$ corresponds to the particles and surface moving in the opposite direction to each other, which corresponds to particles moving opposite to the flow or anti-advection in the fluid picture. We will henceforth refer to these dynamics as the KPZ advection and the KPZ anti-advection dynamics. Since the EW equation does not contain the symmetry breaking nonlinear term, one does not have the two distinct cases as for the KPZ equation.

1.3.3 Relevant parameters: ω and K

The coupled problem described above involves two time time scales, that of particle motion τ_p and that of surface motion τ_s. We are interested in studying the change in the steady state properties of the system when the relative value of the time scales $\omega \equiv \tau_p/\tau_s$ is varied. In particular, the limit of $\omega = 0$ i.e. particles moving on a static surface under the effect of temperature can be solved exactly. We will present our results on this problem in a separate chapter. We have also studied the variation of the steady state under the change in the parameter K which is a measure of the bias for the particle motion. One can think of the tendency of the particles to slide preferentially

downward as being caused by a gravitational field. The parameter K depends on the gravitational field and temperature, and will be defined precisely in the next chapter.

1.4 Passive Sliders: Known results

While we are studying passive particles whose dynamics is governed by the surface fluctuations and diffusion, we should remember that it is possible that the particles themselves might interact with each other. This inter-particle interaction can affect the steady state properties strongly. Two of the simpler cases that one can consider are (i) hard core exclusion interaction and (ii) no interaction i.e. particles moving independently of each other. Our work deals with noninteracting particles, and as we might expect, and will show later, this property leads to a very strong clustering of particles. The resulting clustered state has very interesting scaling properties and its characterisation is one of the principal results of this thesis. However, before we go to a description of our results and the plan of the thesis, let us describe in brief what is known from work on related problems.

1.4.1 Passive particles with hard core exclusion

Das et. al. [30, 31] have studied passive particles, interacting via hard core exclusion, sliding on fluctuating surfaces in one dimension. The evolution of the KPZ and EW surfaces leads to the formation of hill and valley like structures which are dynamical in nature. It was observed by them that the particles tend to cluster in the valleys of the surface. They characterised the clustering by measuring the two point density-density correlation function $C(r)$ in the steady state. The correlation function was shown to be a scaling function of the distance r divided by the system size L and the scaling function was observed to exhibit a cusp in the limit $r \to \infty$, $L \to \infty$, $|r/L| \to 0$ [30, 31]

$$C(r) = m_c^2(1 - b\left|\frac{r}{L}\right|^{\alpha}) \tag{1.14}$$

with $\alpha < 1$. The constant m_c^2 in the above equation is the intercept of the curve on $y-$axis and describes the behaviour of the correlations at large distances. A non-zero value of m_c^2 implies that the correlations are present at large distances and thus the system possesses long range order. The above result is to be contrasted to the normal phase ordering results where we have $\alpha = 1$, corresponding to a linear drop. This linear

behaviour leads to a power law decay in the structure function for large wavevectors, and the result is known as Porod law [32]. An example of phase ordered systems which follow this law is the low temperature phase of an Ising system with conserved magnetisation. The Porod law indicates the presence of large regions of either phase separated by boundaries that are sharp on the scale of system size.

Another feature of the steady state of this problem is that the probability $p(l)$ of a cluster having having a size l decays as a power law, $p(l) \sim l^{-\theta}$. This indicates that clusters of all sizes are present in the system. The cuspy decay and the power law distribution of cluster sizes in the hard core case shows the presence of large clusters of particles and large stretches of empty sites separated by a boundary region where the particles are loosely scattered. The size of the boundary region itself scales as the system size and the region has a lot of structure. Thus we see that this system shows a very different kind of phase ordering than the one seen in ordinary phase separated systems. A study of the Fourier components of the density profile shows that the large clusters themselves are of a dynamic nature and the system shows fluctuations that do not damp down in the thermodynamic limit. These results characterise a new kind of steady state — the fluctuation dominated phase ordered (FDPO) state. This feature of fluctuations again distinguishes the steady state from the Porod law steady state where the fluctuations vanish in the thermodynamic limit. Later work by Gopalakrishnan and Barma [33] has shown that FDPO is the steady state for the system in two dimensions as well. Chatterjee and Barma [34] have studied the dynamical properties of FDPO. Their measurements on the autocorrelation function show that it is a function of t/L^z (z being the dynamic exponent of the surface) and decays with a cusp at small argument. The cuspy decay is again a special feature of FDPO and distinguishes it from normal phase separating systems where one sees a linear decay. These authors have also studied the approach to steady state and ageing effects. They show that if one starts from a random disordered state and starts measuring the autocorrelation function at time t_1, one again sees that the autocorrelation function shows a cuspy decay, with L being replaced by $t_1^{1/z}$ in the argument.

1.4.2 Non-interacting passive particles

We now discuss the non-interacting particles case, which is of direct interest to us. Drossel and Kardar [29] were the first to study this problem, with a KPZ surface as

the driving field, albeit with slightly different dynamics for the driven particles. They considered a solid on solid model for surface dynamics with particles being updated at the site of a recent surface update, and considered both the cases — advection and anti-advection. They observed strong clustering of particles, which they monitored by studying the number of particles in bins of variable sizes. We will comment on this result in the next chapter (KPZ advection). Part of the motivation for their study came from a solid on solid model for an evolving surface composed of two species of particles [5]. They claim that in a specific region of the parameter space, the domain walls separating the regions occupied by the two components can behave like passive particles sliding on the KPZ surface. They reported numerical results for the density-density correlation function for the KPZ anti-advection case. They reported that this function decays as a power law with the power being close to 0.3.

The above work, however does not report the crucial property of system size dependence of the scaling properties of the correlation function or the probability distribution of occupancy. In [29], Drossel and Kardar have also described results from a perturbative renormalization group calculation. These results, however, do not agree with numerical results. As we will show in Chapter 2, the particles show extremely strong clustering and fluctuations that grow with the system size. Thus the renormalization group approach, which works well for normal critical point behaviour, is not directly applicable to our system. These points will be discussed further in Chapter 2 (Section 2.2.6).

Apart from this work, Bohr and Pikovsky [35] and Chin [36] have studied dynamical quantities for a model similar to our KPZ advection (one dimension), with the difference that they do not consider noise acting on particles. In the absence of noise, all the particles coalesce and ultimately form a single cluster in steady state, very different from the strongly fluctuating, distributed particle state under study here. References [35] and [36] study the process of coalescence in time. Further, they find that the RMS displacement for a given particle increases in time t as $t^{1/z}$, where z is equal to the dynamic exponent of the surface, indicating that the particles have a tendency to follow the valleys of the surface. Drossel and Kardar [29] have studied the RMS displacement in the same problem in the presence of noise and observe the same behaviour. For the case of KPZ anti-advection, Drossel and Kardar [29] show evidence for the dynamic exponent for particle motion being continuously dependent on K; the parameter K characterises the random noise which acts on the particles in addition to

the surface drive. We have addressed this point in our work and our numerical results point to this dependence being just a crossover effect. Gopalakrishnan [37] has studied the variation of RMS displacement of passive sliders on a one dimensional EW surface, and the possibility was raised that there are two different exponents characterising this quantity for $\omega \leq 1$ and for $\omega > 1$. We will present numerical evidence that the apparent change in exponent with change in ω is due to a crossover effect and that there is a single exponent which describes the RMS displacement.

1.5 Our results, plan of the thesis

We begin with results on KPZ advection in one dimension. We have performed Monte-Carlo simulations on a lattice version of the problem and numerically evaluated the quantities of interest. We see that in the steady state, the two point density-density correlation function is a function of the distance r divided by the system size L and diverges at small r/L, indicating a strong clustering of the particles. We take this as the defining property of a new kind of steady state — the strong clustering state (SCS). Our results imply that the two point correlation function in the SCS is a function of the system size, and diverges in the thermodynamic limit for any finite value of the separation. Contrasting the divergence in our case to the cusp in the FDPO case, we see that there is much more clustering in our case. The removal of the hard core constraint allows for very high densities and thus leads to such strong aggregation of particles.

The other quantity we measure is the probability density of occupancy of a site. We again see that this quantity shows scaling with system size, showing that a large number of particles aggregate in a few sites. We see that the clusters are highly dynamic in nature, breaking and re-forming all the time. This leads to fluctuations which are significant even in the thermodynamic limit. This feature of SCS is similar to FDPO where again one sees giant fluctuations that do not damp down in the thermodynamic limit. We have measured dynamic quantities like the RMS displacement of a tagged particle and see that the particles have an overall tendency to follow the valleys in which they are clustered. The model for Monte-Carlo simulation and the above results are discussed in detail in the second chapter.

We describe our results on the KPZ anti-advection and the EW dynamics (one

dimension) in the third chapter. We see that the steady state in these cases is again an SCS but the amount of clustering is less than the KPZ advection case. Apart from these general results, we discuss specific issues, like the possibility of the dynamic exponent depending continuously on the parameter K in the case of KPZ anti-advection and the apparent change in the dynamic exponent with change in ω, proposed earlier, in the EW case.

The limit $\omega = 0$ for the above dynamics corresponds to particles moving under the effect of temperature on a static surface. This is the well known Sinai model of random walkers on a random landscape. This equilibrium problem can be solved exactly by using a mapping to a quantum mechanics problem [38]. We show that the equilibrium state is again an SCS and surprisingly, the results match very well with the nonequilibrium KPZ advection case. The calculation and the correspondence to the nonequilibrium problem will be discussed in detail in the fourth chapter.

We have also performed simulations in two dimensions for all the three dynamics discussed above. In the fifth chapter, we discuss the Monte-Carlo model and the results from the simulations. We show that the steady state is an SCS, even in two dimensions. The last chapter is devoted to conclusions and a discussion of our results.

KPZ advection, one dimension

In this chapter, we will describe our results on the Kardar-Parisi-Zhang (KPZ) advection case where the particles and the surface move in the same direction. In the fluid language, the problem is equivalent to studying passive scalars that move with the flow in the Burgers fluid. We will consider the surface/fluid evolving in one spatial dimension. In the first section, we will describe the lattice Monte-Carlo model used for the simulations and discuss its connection to the continuum description. We will then describe our results from the simulations. We will begin with results on statics and define the strong clustering state (SCS). The results on dynamics will be next, followed by a discussion on fluctuations in the steady state. We will end with our results on the change in steady state when ω is varied and when the surface is tilted.

2.1 Lattice model for Monte-Carlo simulations

2.1.1 Lattice model details

As described in the previous chapter, for the KPZ advection case, we want to solve the coupled equations below (in one dimension)

$$\frac{\partial h}{\partial t} = \nu \nabla^2 h + \frac{\lambda}{2}(\nabla h)^2 + \zeta_h(\vec{x}, t). \tag{2.1}$$

and

$$\frac{d\vec{x}_m}{dt} = -a \nabla h|_{\vec{x}_m} + \zeta_m(t) \tag{2.2}$$

with $a/\lambda > 0$. As shown in the previous chapter, the transformation $v = -\nabla h$ maps the KPZ equation to the Burgers equation, thus mapping the problem to the passive

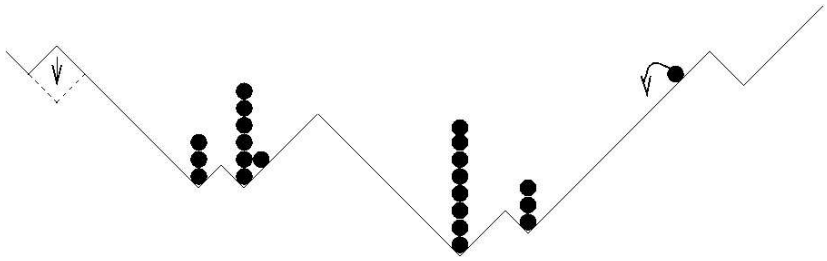

Fig 2.1: Schematic diagram of the surface and non-interacting particles sliding on top of it. Arrows show possible surface and particles moves.

scalar problem in fluid dynamics.

The method we have adopted to deal with the above coupled equations is to perform Monte-Carlo simulations on a discrete lattice model which mimics the behaviour of the equations at large length and time scales. The model we have considered, consists of a flexible, one-dimensional lattice in which particles reside on sites, while the links or bonds between successive lattice sites are also dynamical variables which denote local slopes of the surface. The total number of sites is L and the total number of particles N is taken to be equal to L in our simulations. Each link takes either of the values $+1$ (upward slope $\rightarrow$ /) or -1 (downward slope $\rightarrow$ \). The rules for evolution are:

We choose a site at random, and if it is on a local hill (/\), we change the local hill to a local valley (\/) (Fig. 2.1, extreme left), otherwise, we leave it unchanged. After every such N_s surface moves, we perform N_p particle updates according to the following rule: we choose a particle at random and move it one step downward with probability $(1 + K)/2$ or upward with probability $(1 - K)/2$. The parameter K ranges from 1 (particles totally following the surface slope) to 0 (particles moving independently of the surface). If a downward move is performed on a particle sitting on a local hill (/\), it is moved to either side with equal probability and an attempted upward move is neglected. Similarly, a particle inside a local valley can be moved upward in either direction with equal probability while a downward move is neglected. In our simulations, we update the surface and particles at independent sites, reflecting the independence of the noises $\zeta_h(x, t)$ and $\zeta_m(t)$; this is in contrast to Drossel and Kardar's update rule [29] where only particles at a site affected by the surface evolution are moved. The ratio $\omega \equiv N_s/N_p$ controls the relative time scales of the surface evolution and particle movement. In particular, the limit $\omega \rightarrow 0$, with L held fixed, corresponds to the adiabatic limit of the problem where particles move on a static surface and the steady state is a thermal equilibrium state.

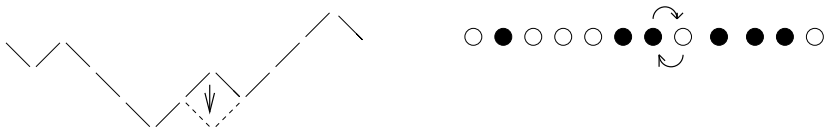

Fig 2.2: The figure on the left shows a KPZ lattice configuration with a possible move. The figure on the right shows the equivalent configuration and lattice move for the ASEP.

2.1.2 Connection with the continuum equations

To see how the lattice model described above describes a KPZ surface, we will consider the mapping of the above model to the well known asymmetric simple exclusion process (ASEP) [39, 40].

The ASEP consists of a lattice with empty sites (holes), and particles. The particles interact with each other via hard core repulsions which means that no more than one particle is allowed at a given site. The dynamics is as follows: particles are chosen at random and a move is attempted to the right hand neighbouring site with probability p and to the left neighbouring site with probability q, $p > q$. The move is successful if the neighbouring site is empty, otherwise the particle stays at the same site. This model can be solved exactly for various boundary conditions. For periodic boundary condition, which is of interest to us, it is known that all possible configurations in the steady state occur with equal probability [39]. The current in the ASEP can be calculated by the following argument. There is a movement to the right if the site under consideration is occupied and the site to the right is unoccupied; this process has a probability $p[\rho(1-\rho)]$ where ρ is the density of particles. Similarly one can reason for movement to the left and the average current is given by the expression $(p-q)[\rho(1-\rho)]$.

Now, let us consider the mapping of ASEP to our lattice model (Fig. 2.2): An up slope in our surface model is equivalent to a particle on a lattice in ASEP and a down slope to an empty space (hole). The flipping of a hill to a valley then corresponds to the motion of a particle (exchange of particle and hole). In our lattice model $p = 1$, $q = 0$.

A coarse grained description of the ASEP leads to the KPZ equation [41]. The continuum description of the ASEP, obtained by coarse graining over regions which are large enough to contain many sites, involves the density of particles $\rho(x)$ and the local current $J(x)$. These are connected through the continuity equation

$$\frac{\partial \rho}{\partial t} + \frac{\partial J}{\partial x} = 0 \tag{2.3}$$

$$J(x) = -\nu \frac{\partial \rho}{\partial x} + j(\rho) + \eta \tag{2.4}$$

where ν is the particle diffusion constant, η is a Gaussian noise variable and $j(\rho)$ is the systematic contribution to the current associated with the local density ρ. Using the expression for the bulk ASEP with density ρ for j, we have

$$j(\rho) = (p - q)\rho(1 - \rho) \tag{2.5}$$

where p and q are the particle hopping probabilities to the right and left respectively, with our one-step model corresponding to $p = 1$ and $q = 0$.

Since we identify the presence (absence) of a particle in the lattice model with an up (down) slope, we may write

$$\rho = \frac{1}{2}(1 + \frac{\partial h}{\partial x}) \tag{2.6}$$

Using Eqs. (2.4),(2.5) and (2.6) in Eq. (2.3) leads to

$$\frac{\partial h}{\partial t} = -\frac{1}{2}(p - q) + \nu \frac{\partial^2 h}{\partial x^2} + \frac{1}{2}(p - q)(\frac{\partial h}{\partial x})^2 - 2\eta \tag{2.7}$$

which is the KPZ equation (Eq. (3.1)) in one dimension with an additional constant term, and $\lambda = (p - q)$ and $\zeta_h = -2\eta$. Note that the signs of the constant term and λ are opposite. Thus a downward moving surface (corresponding to $p > q$) has positive λ. The constant term can be eliminated by the boost $h \to h - \frac{1}{2}(p - q)t$, but its sign is important in determining the overall direction of motion of the surface. The case $(a/\lambda) > 0$ which is of interest to us thus corresponds to the lattice model in which particles move in the same direction as the overall surface motion.

The parameters ω and K defined in the lattice model are connected to the continuum equations as follows. In the limit of a stationary surface, we achieve equilibrium

and the particles settle into a Boltzmann state with particle density $\sim e^{-\beta h(x)}$, here $h(x)$ is the surface height profile and β is the inverse temperature. β is related to K by $\beta = \ln\left(\frac{1+K}{1-K}\right)$ and to the parameters a and κ in Eq. (4.2) by $\beta = a/\kappa$. Thus

$$K = \frac{e^{a/\kappa} - 1}{e^{a/\kappa} + 1} \tag{2.8}$$

The parameter ω cannot be written simply in terms of the parameters in the continuum equations, because it modifies Eqs. (3.1) and (3.9) as we now show. ω is the ratio of the update speeds or equivalently the time between successive updates of the particles Δt_p and surface Δt_s. The noises $\zeta_h(\vec{x}, t)$ and $\zeta_m(t)$ in Eqs. (3.1) and (4.2) can be written as $\sqrt{\frac{D_h}{\Delta t_s}}\widetilde{\zeta_h}(\vec{x}, t)$ and $\sqrt{\frac{\kappa}{\Delta t_p}}\widetilde{\zeta_m}(t)$ respectively. Here $\widetilde{\zeta_h}(\vec{x}, t)$ is noise of $O(1)$, uncorrelated in time, white in space while $\widetilde{\zeta_m}(t)$ is uncorrelated noise of $O(1)$. The factors of $\sqrt{\frac{1}{\Delta t}}$ in the terms indicate that the strength of the noise depends on how frequently noise impulses are given to the particles; the square root arises from the random nature of these impulses. Thus the change in height Δh in time Δt_s and the distance travelled $\Delta \vec{x}_m$ in time Δt_p are respectively

$$\Delta h = \Delta t_s[\nu \nabla^2 h + \frac{\lambda}{2}(\nabla h)^2] + \sqrt{\Delta t_s D_h}\widetilde{\zeta_h}(\vec{x}, t) \tag{2.9}$$

$$\Delta \vec{x}_m = \Delta t_p[-a \nabla h|_{\vec{x}_m}] + \sqrt{\Delta t_p \kappa}\widetilde{\zeta}(t) \tag{2.10}$$

We now identify Δt_s and Δt_p with the Monte-Carlo time step δt as $\Delta t_s = N_s \delta t$ and $\Delta t_p = N_p \delta t$. We can thus replace Δt_s by $\omega \Delta t_p$ and take it to be the natural continuous time. We thus get

$$\frac{\partial h}{\partial t} = \omega[\nu \nabla^2 h + \frac{\lambda}{2}(\nabla h)^2] + \sqrt{\omega}\zeta_h(\vec{x}, t) \tag{2.11}$$

$$\frac{d\vec{x}_m}{dt} = -a \nabla h|_{\vec{x}_m} + \zeta_m(t) \tag{2.12}$$

We can see that the ω dependence in the above equation cannot be removed by rescaling space and time. Eq. (3.1) is recovered as a special case of Eq. (2.11) on setting $\omega = 1$. The same analysis can be carried through for the EW equation by dropping the nonlinear term in the equations above.

2.1.3 Details of the simulations

In our simulations, we started with a random surface and particle configuration. As we know, the largest valleys/hills in the system have breadth of the order of system size and they overturn to form hills/valleys in time $\sim L^z$, where $z = 3/2$. In our simulations, we evolved the system for approximately $10 \times L^2$ number of steps before we started our measurements. This ensures that we have reached steady state before taking the numerical data. We sampled the data every 1000 Monte Carlo time steps to reduce correlation between the samples. The average was taken over a total of $30,000$ samples.

We used the RAN3 random number generator for our Monte-Carlo simulations. RAN3 is a lagged Fibonacci generator [42, 43] and has a large period of $2^{55} - 1$. It is also known to be one of the faster generators [43]. We have checked our results from the simulations by using another random number generator, the Mersenne Twister [44]. We saw that changing the generator does not make a difference to our results.

The values of system size that we have worked with are $256, 512, 1024, 2048$. The values were chosen such that we have minimal finite size effects while keeping the time of the simulation for the complete run within reasonable limits (up to 2 days).

2.2 Numerical results

We begin this section with the simplest case $\omega = K = 1$; surface updates are attempted as frequently as particle updates, and both particles and surface always move only downwards.

2.2.1 Two Point Density Density Correlation Function

The two point density-density correlation function is defined as

$$G(r, L) \equiv \langle n_i n_{i+r} \rangle_L, \tag{2.13}$$

where n_i is the number of particles at site i. We obtained numerical data for various system sizes L and tried to scale the data such that it lies on a single curve. Figure 2.3

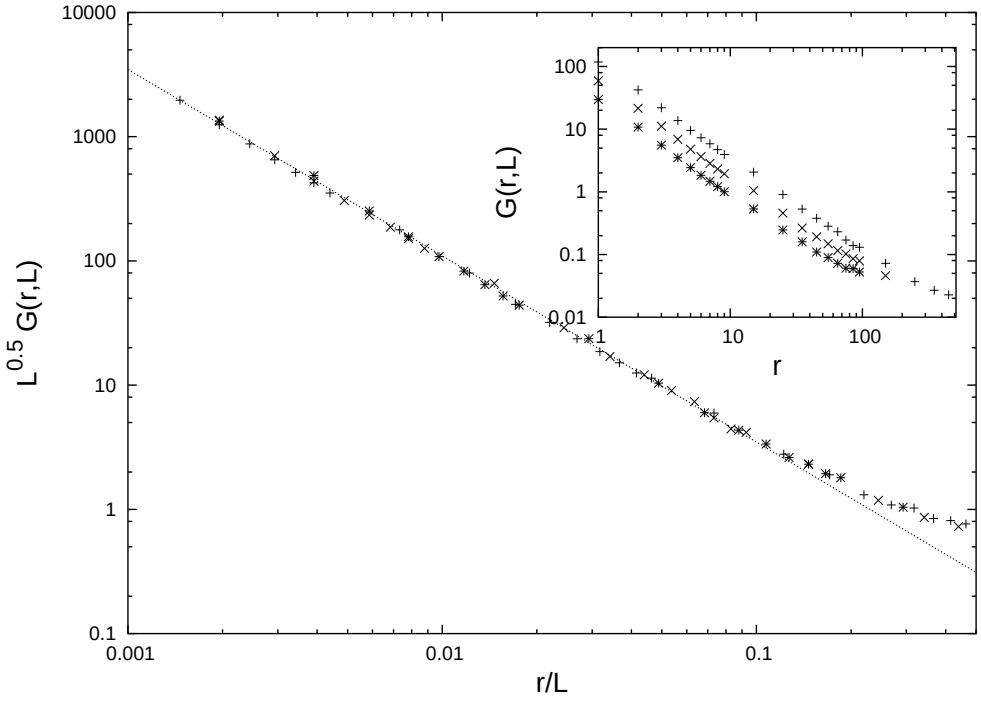

Fig 2.3: The inset shows $G(r, L)$ versus r for different values of L. The main plot shows the scaling collapse when r is scaled with L and $G(r, L)$ with $1/L^{0.5}$. The dashed, straight line shows a power law with exponent -1.5. The lattice sizes for both plots are L= 512 ($*$), 1024 ($\times$), 2048 ($+$).

shows the scaling collapse of numerical data for various system sizes L which strongly suggests that for $r > 0$, the scaling form

$$G(r, L) \sim \frac{1}{L^{\theta}} Y\left(\frac{r}{L}\right) \tag{2.14}$$

is valid with $\theta \simeq 1/2$. The scaling function $Y(y)$ has a power law divergence $Y(y) \sim y^{-\nu}$ as $y \to 0$, with ν close to 3/2 (1.48 $\pm$ 0.04). The data for $r = 0$, which is not a part of the scaling function (Eq. 2.14) above, points to $G(0, L) \sim L$ (Fig. 2.4).

The result in Eq. (2.14) is in agreement with an exact result of Derrida et. al. [45] for a slightly different model. As we have seen in the previous section, the single step model which we use for Monte-Carlo simulations, can be mapped on to an asymmetric simple exclusion process (ASEP). The particles/holes in the ASEP map to the up/down slopes in our model and the flipping of a hill to a valley is equivalent to swapping a particle with a hole. In [45], apart from particles and holes, a third species, namely second-class particles, is introduced which act as holes for the particles and particles for the holes. When translated to the surface language, these second class particles

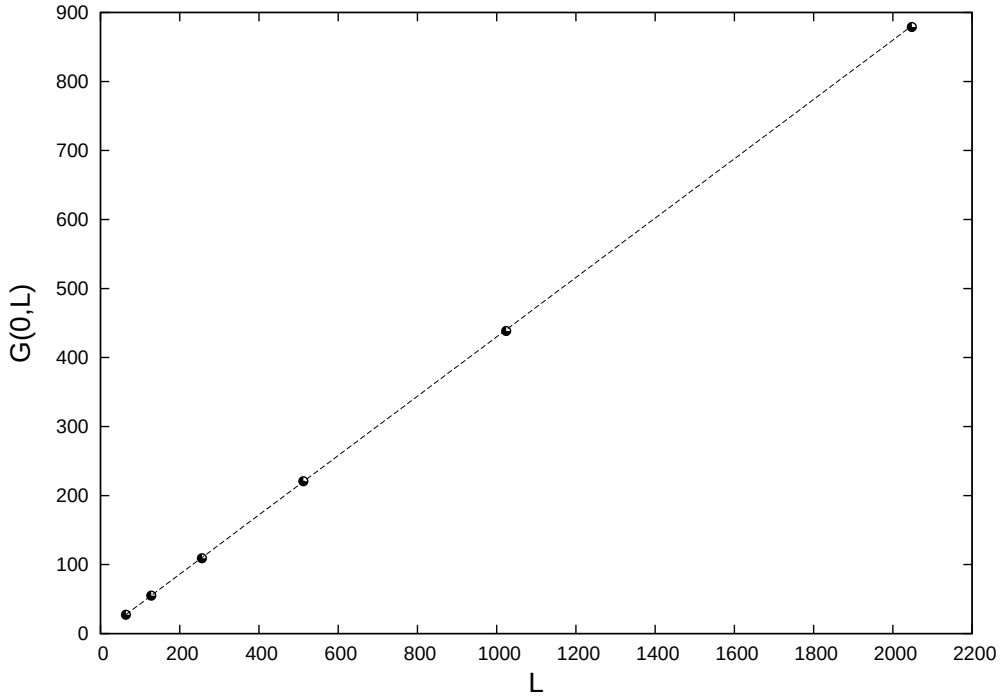

Fig 2.4: The graph shows $G(0, L)$ versus L. The dashed line shows that $G(0, L)$ depends linearly on L.

behave like the sliders in our model, with the difference that they are not passive: there is no surface evolution at a site where second-class particles reside. The effect of non-passivity is relatively unimportant for KPZ advection-like dynamics of the surface, as particles mostly reside on stable local valleys while surface evolution occurs at local hilltops. Moreover, if the number of second class particles is small, the probability of the rare event where they affect the dynamics of local hills goes down even further. With only two such particles in the full lattice, the probability $p(r)$ that they are at a distance r goes as [45] $p(r) \sim \frac{1}{r^{3/2}}$. This quantity can be connected to the two point correlation function $G(r, L)$ as follows. The probabilty p_r is proportional to the probability that there is, simultaneously, a particle at the site i and a particle at the site $i + r$. Thus

$$p_r \sim \sum_i \langle P_i P_{i+r} \rangle, \tag{2.15}$$

P_i being the probability of having a particle at site i. The correlation in the above sum is a probability density - probability density correlation and can be connected to the density-density correlation as below.

$$p_r \sim L\langle \frac{n_i}{N}\frac{n_{i+r}}{N}\rangle = \frac{L}{N^2}\langle n_i n_{i+r}\rangle \tag{2.16}$$

where we perform the sum in Eq. (2.15) using the fact of translational invariance. Using $L = N$, the scaling form $G(r, L) \equiv \langle n(0)n(r)\rangle \sim L^{-\theta}Y(r/L)$ and the functional form for small r/L — $Y(y) \sim y^{-\nu}$ ($\nu = 3/2$), we obtain

$$p_r \sim r^{-3/2}. \tag{2.17}$$

Thus our scaling form (Eqs. (2.14)) is consistent with Derrida et. al.'s exact result

Number of particles in a bin

The result for $G(r, L)$ also allows us to calculate a quantity $N(l, L)$, first defined in [29], which monitors the degree of clustering. To calculate $N(l, L)$, the lattice is divided into L/l bins of size l and we ask for the number $N(l, L)$ of particles in the same bin as a randomly chosen particle. $N(l, L)$ is a good measure of clustering — if $N(l, L)$ rises linearly with l, one concludes that the particles are fairly spread out, while if $N(l, L)$ saturates or shows a decreasing slope, one concludes that particles are clustered. $N(l, L)$ can be related to the two point correlation function $G(r, L)$ as follows

Suppose that the number of particles in the k^{th} bin is $N(k)$ ($N(k) = \sum_{i\epsilon k} n_i$). We denote by p_k, the probability of choosing the k^{th} bin ($p_k = \frac{N(k)}{N}$). Then

$$N(l, L) = \sum_k \langle p_k N_k\rangle = \sum_k \left\langle \frac{N_k^2}{N}\right\rangle \tag{2.18}$$

$$N(l, L) = \frac{1}{N}\sum_k \sum_{i=1}^{l}\sum_r \langle n_i n_{i+r}\rangle \tag{2.19}$$

$$\Rightarrow N(l, L) = \frac{L}{l}\frac{l}{N}\sum_r \langle n_i n_{i+r}\rangle \tag{2.20}$$

Since $L = N$,

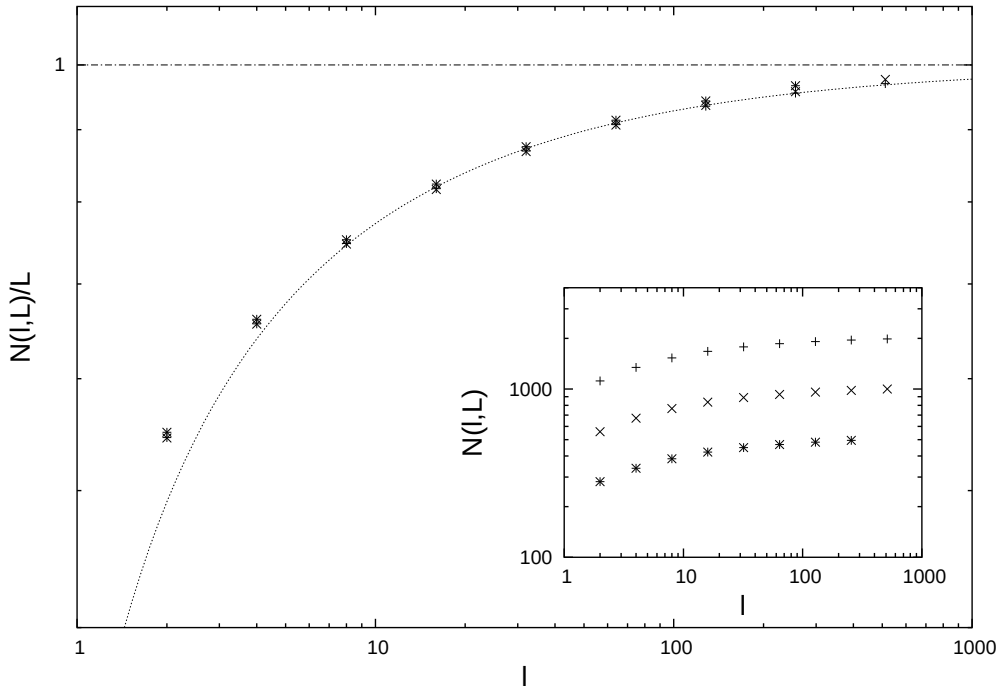

Fig 2.5: The inset shows $N(l, L)$ versus bin size l for different system sizes (L). The main plot shows $N(l, L)$ scaled with L versus bin size l. The curve shows $c_1 L(1 - c_2 l^{-\nu+1})$ with $c_1 = 1$ and $c_2 = 0.72$. The straight line shows $N(l, L) = L$, the form predicted in [29]. The lattice sizes for both plots are L= 512 ($*$), 1024 ($\times$), 2048 ($+$).

$$N(l, L) = \int_{-l/2}^{l/2} \langle \rho(0)\rho(r) \rangle dr \tag{2.21}$$

So, the two point correlation function

$$G(l, L) = \frac{\partial}{\partial l} N(l, L) \Rightarrow N(l, L) = \int_0^l G(r, L) dr \tag{2.22}$$

We know that $G(r, L)$, in the advection case, has the form

$$G(r, L) = L\delta(r) + \frac{1}{L^{\nu-1}} \left(\frac{r}{L}\right)^{-\nu} \tag{2.23}$$

$$\Rightarrow N(l, L) = c_1 L(1 - c_2 l^{-\nu+1}) \tag{2.24}$$

The value of ν according to us is 3/2, using which we obtain a very good fit to the binning data.

The form for $N(l, L)$ proposed in [29] is

$$\Rightarrow N(l, L) \sim l^{2\chi_\rho - 1} L^{2-2\chi_\rho} \tag{2.25}$$

The L dependence is obtained by demanding that $N(L, L) = L$. Their proposed value $\chi_\rho = 1/2$ removes the l dependence; the claim is that this is correct for large l where $N(l, L)$ becomes independent of l. As we can see in Fig. 2.5, our form in Eq.(2.24) captures the curvature of the curve correctly and thus describes the binning data much better than the l-independent form of [29].

2.2.2 Probability Density of Occupancy

Another quantity of primary interest is the fraction of sites $P(n, L)$ that are occupied by n particles, which is the same as the probability that any given site has an occupancy n. If $\mathcal{N}_n$ is the number of sites which have an occupancy of n, we define $P(n, L)$ as

$$P(n, L) \equiv \langle \mathcal{N}_n / L \rangle \tag{2.26}$$

where the brackets indicate a time average over configurations in the steady state. For $n > 0$, this quantity shows a scaling with the total number of particles, which in turn is equal to the system size L. We have (see Fig. 2.6)

$$P(n, L) \sim \frac{1}{L^{2\delta}} f\left(\frac{n}{L^\delta}\right), \tag{2.27}$$

with $\delta \simeq 1$ (1 ± 0.07). The scaling function $f(y)$ seems to fit well to a power law $y^{-\gamma}$ with $\gamma \simeq 1.15$ (1.15 ± 0.02) (Fig. 2.6), though as we shall see in the chapter on the Sinai equilibrium limit, the small y behaviour may follow $y^{-1} \ln y$. We can use the scaling form in the above equation to calculate $G(0, L)$, $\langle n^2 \rangle \equiv G(0, L) = \int_0^L n^2 P(n, L) dn \sim L^\delta = L$, which, as we have seen above, is borne out independently by the numerics. Numerical data for $P(0, L)$ (which is not a part of the scaling function in Eq. (2.27)) shows that the number of occupied sites $N_{occ} \equiv (1 - P(0, L))L$ varies as L^ϕ with $\phi \simeq 0.23$, though the effective exponent seems to decrease systematically with increasing system size L (Fig. 2.7).

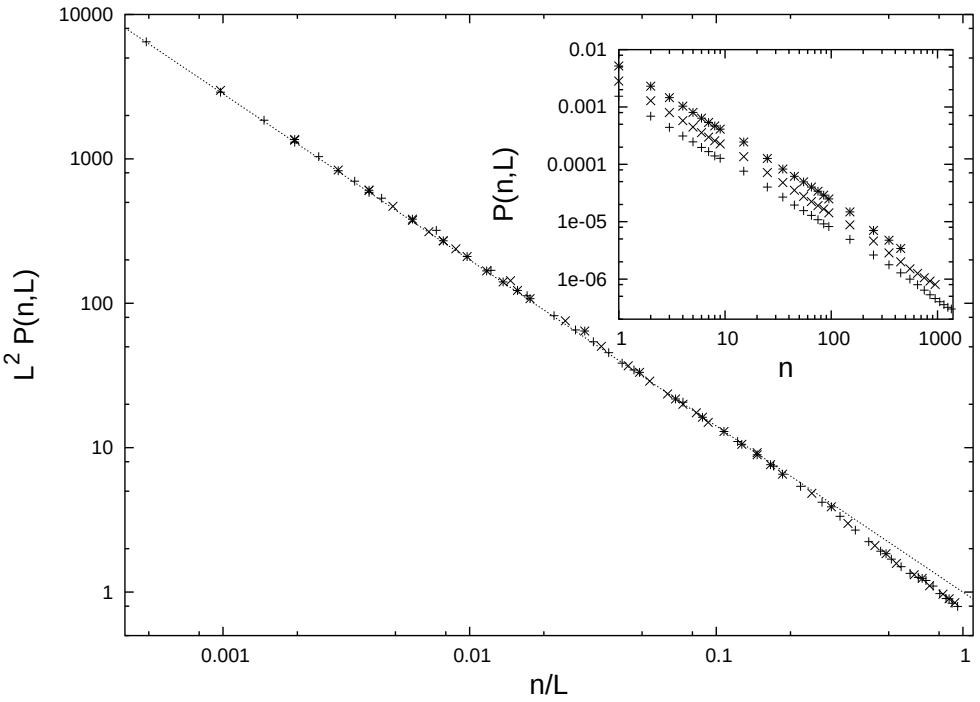

Fig 2.6: The inset shows $P(n, L)$ versus n for different values of L. The main plot shows $L^2 P(n, L)$ versus n/L. The straight line shows a power law with exponent -1.15. The lattice sizes are L= 512 ($*$), 1024 ($\times$), 2048 ($+$).

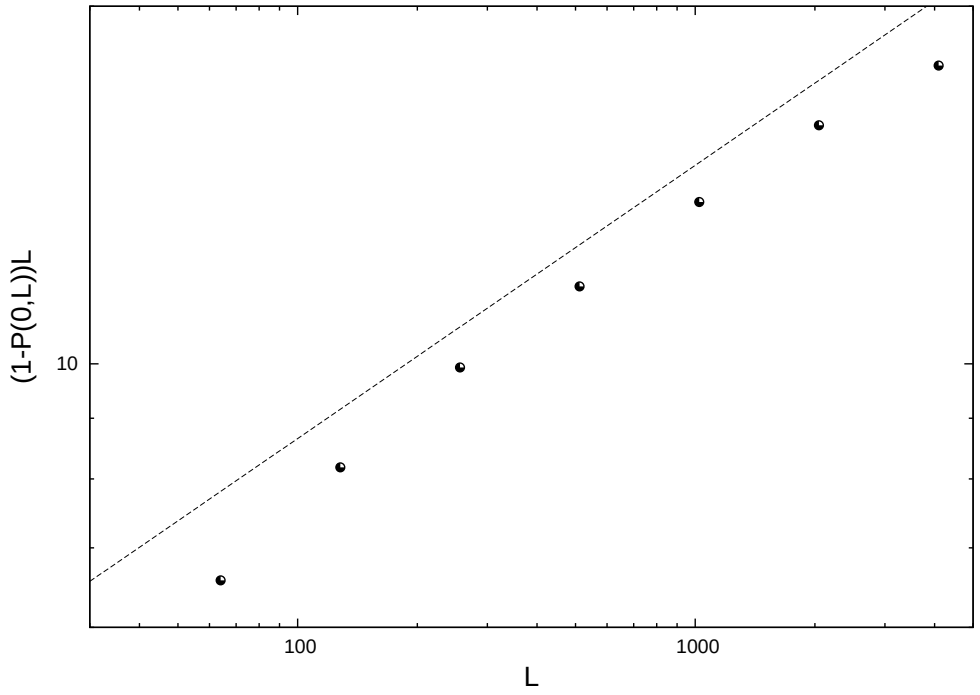

Fig 2.7: The figure shows data for $(1 - P(0, L)L)$ versus L. The straight line shows power law with exponent 0.23. The data for large L shows a deviation from the power law showing that the true power might be smaller than the plotted power law value.

2.2.3 Results on Dynamics

One of the simplest ways of studying the dynamics of the passive sliders is to tag a particle and track its movement. In particular, we can ask for the root mean square (RMS) displacement $R(t)$

$$R(t) \equiv \langle (x(t) - x(0))^2 \rangle^{1/2} \tag{2.28}$$

where $x(t)$ is the position of the particle at time t. This quantity has been studied earlier [29, 36] and $R(t)$ is found to obey the scaling form

$$R(t) = L^{\chi} h\left(\frac{t}{L^z}\right) \tag{2.29}$$

where $h(y) \sim y^{1/z}$, with $z = 3/2$ for small y. The requirement that $R(t)$ has to be independent of L in the limit $L \to \infty$ leads to $\chi = 1$. The value of z above is the same as the dynamic exponent z_s of the KPZ surface. As discussed in the introduction chapter, the dynamic exponent z_s of a surface carries information about the time scale of evolution of valleys and hills; the landscape evolves under surface evolution and valleys/hills of breadth L' are typically replaced by hills/valleys in time of order L'^{z_s}. Thus the observation $z = z_s$ suggests that the particles follow the valley movement. We have verified the above results in our simulations (Fig. 2.8). At large times ($t \sim L^z$), due to the hills/valleys getting decorrelated, the value of z changes from 3/2 to the diffusion value 2 as can be seen in Fig. 2.8 (large t/L^z).

We have also evaluated the density-density autocorrelation function $\widetilde{G}(t, L)$

$$\widetilde{G}(t, L) \equiv \langle n_i(0) n_i(t) \rangle_L \tag{2.30}$$

and find that it scales with the system size as (Fig. 2.9)

$$\widetilde{G}(t, L) \sim \widetilde{Y}\left(\frac{t}{L^z}\right). \tag{2.31}$$

Again, $z = z_s = 3/2$, reaffirming our conclusion that particles tend to follow valleys. The scaling function shows a power law behaviour $\widetilde{Y}(\tilde{y}) \sim \tilde{y}^{-\psi}$ with $\psi \simeq 2/3$ as $\tilde{y} \to 0$.

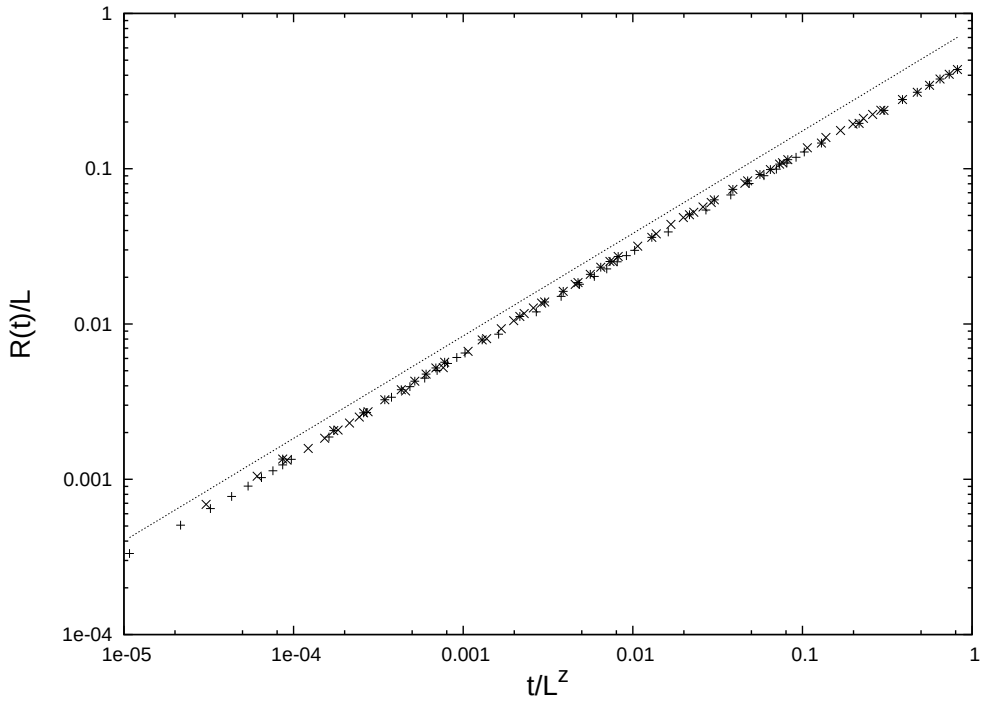

Fig 2.8: Scaled RMS displacement $R(t)$ for various lattice sizes. The line shows a power law with exponent 2/3. The lattice sizes are L= 512 ($*$), 1024 ($\times$), 2048 ($+$).

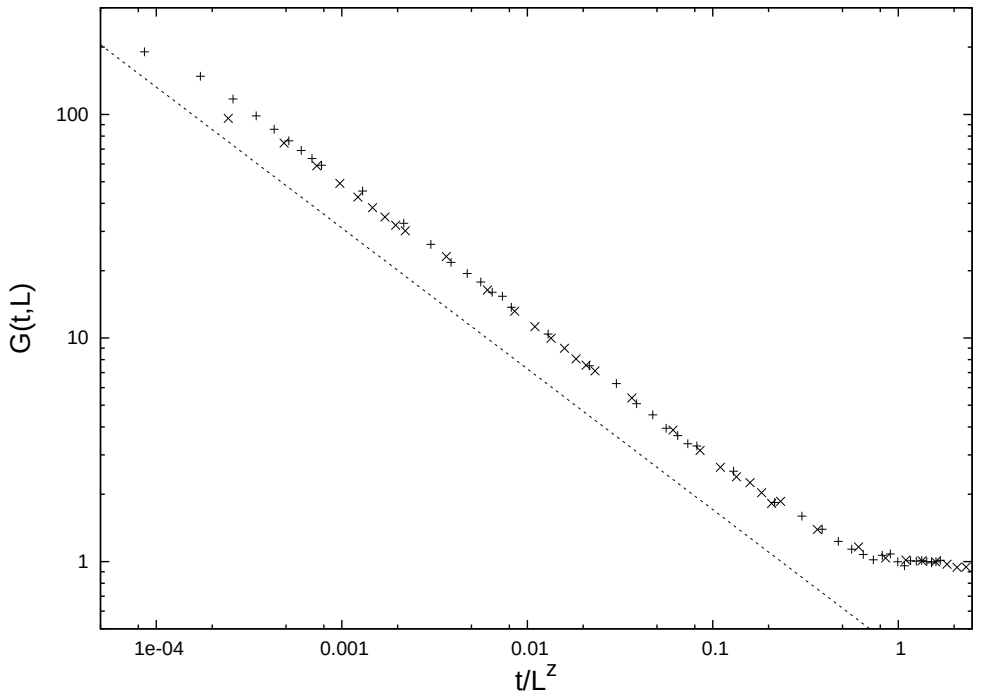

Fig 2.9: Scaled density-density autocorrelation function $\widetilde{G}(t, L)$. The dashed line shows a power law with exponent $-2/3$. The lattice sizes are L=256 ($\times$), 512 ($+$).

2.2.4 Relations Between the Exponents

The exponents defined in the above sections can be connected to each other by simple relations using scaling analysis. For instance, δ, ν and θ are related by

$$\delta = \nu - \theta \tag{2.32}$$

This can be proved as follows. Using $N = L$, it can be easily shown that

$$\int_0^L \langle n(0)n(r)\rangle dr = L \tag{2.33}$$

$$\Rightarrow \langle n(0)^2\rangle + \int_1^L \langle n(0)n(r)\rangle dr = L \tag{2.34}$$

We will first show that the first term on L.H.S. of the above equation goes as L^δ. We know that

$$\langle n(0)^2\rangle = \langle n^2\rangle = \int_0^L n^2 P(n,L)dn \tag{2.35}$$

Using Eq.(2.27), we have

$$\langle n^2\rangle \sim \frac{1}{L^{2\delta}} \int_0^L n^2 f\left(\frac{n}{L^\delta}\right) dn \tag{2.36}$$

Defining $X = n/L^\delta$, we have

$$\langle n^2\rangle \sim L^\delta \int_0^{L^{1-\delta}} X^2 f\left(X\right) dX \tag{2.37}$$

Our numerical results suggest that the integral in the above equation is convergent for large L. We thus have $\langle n^2\rangle \sim L^\delta$. We use this in Eq.(2.34) to obtain

$$\int_1^L \langle n(0)n(r)\rangle dr = L - aL^\delta \tag{2.38}$$

Using the scaling form in Eq.(2.14), we have

$$a'\frac{1}{L^\theta}\int_1^L Y(\frac{r}{L})dr = L - aL^\delta \tag{2.39}$$

a' and a are positive constants. Guided by numerical evidence, we substitute $Y(y)$ to be a power law for y in the range $0 < y < bL$ (where b is a constant between 0 and 1) and a constant in the range $bL < y < L$. This is consistent with the fact that we are working on a periodic lattice and the scaling function has to be symmetric and thus have a zero slope at $y = 1/2$. We thus have

$$\frac{a'}{L^{\theta-\nu}}\int_1^{bL} r^{-\nu}dr + cL^{1-\theta} \sim L - aL^\delta \tag{2.40}$$

$$\Rightarrow a'\int_1^{bL} r^{-\nu}dr + cL^{1-\nu} \sim L^{1+\theta-\nu} - aL^{\delta+\theta-\nu} \tag{2.41}$$

$$\Rightarrow eL^0 - dL^{1-\nu} + cL^{1-\nu} = L^{1+\theta-\nu} - aL^{\delta+\theta-\nu} \tag{2.42}$$

$$\Rightarrow eL^0 - fL^{1-\nu} = L^{1+\theta-\nu} - aL^{\delta+\theta-\nu} \tag{2.43}$$

We will now consider the two cases $\nu \geq 1$ and $\nu < 1$. When $\nu \geq 1$, the second term on the L.H.S. either goes to zero in the large L limit ($\nu > 1$) or has the same form as the first term ($\nu = 1$). Thus, balancing powers on both sides, we have $\delta + \theta - \nu = 1 + \theta - \nu = 0$. We thus get $\delta = 1$ and $\delta = \nu - \theta$. (We have assumed, guided by numerical evidence, that $\delta + \theta - \nu$ is not negative). If $\nu < 1$, then the second term on the L.H.S. of Eq.(2.43) does not go to zero in the large L limit. Balancing the powers on both sides we have, $\delta + \theta - \nu = 0$ (b and f in Eq.(2.43) are negative constants when $\nu < 1$) and $1 + \theta - \nu = 1 - \nu$. Thus $\theta = 0$ and $\beta = \nu$. We regain the form $\delta = \nu - \theta$.

We can also relate ϕ, δ and γ by

$$\phi = \delta(\gamma - 2) + 1 \tag{2.44}$$

which can be seen below. Using the normalisation condition on $P(n, L)$, we have

$$\int_1^L P(n, L)dn = 1 - P(0, L) \sim L^{\phi-1} \tag{2.45}$$

Using Eq. (2.27) we have

$$\frac{1}{L^{2\delta}} \int_1^L f\left(\frac{n}{L^\delta}\right) dn \sim L^{\phi-1} \tag{2.46}$$

Defining $X = n/L^\delta$ we have

$$\frac{L^\delta}{L^{2\delta}} \int_{1/L^\delta}^{L^{1-\delta}} f(X)dX \sim L^{\phi-1} \tag{2.47}$$

Using the form $f(y) \sim y^{-\gamma}$ we have

$$\int_{1/L^\delta}^{L^{1-\delta}} X^{-\gamma} dX \sim L^{\phi-1+\delta} \tag{2.48}$$

$$\Rightarrow \frac{X^{-\gamma+1}}{-\gamma+1}\Bigg|_{L^{-\delta}}^{L^{1-\delta}} \sim L^{\phi-1+\delta} \tag{2.49}$$

$$\Rightarrow \frac{L^{(1-\delta)(-\gamma+1)}}{-\gamma+1} - \frac{L^{(-\delta)(-\gamma+1)}}{-\gamma+1} \sim L^{\phi-1+\delta} \tag{2.50}$$

If $1 \geq \delta > 0$, $\gamma > 1$, the second term on the L.H.S. is dominant

$$\Rightarrow L^{\delta\gamma-1} \sim L^{\phi-1+\delta} \tag{2.51}$$

$$\Rightarrow \delta\gamma - \delta = \phi - 1 + \delta \tag{2.52}$$

$$\Rightarrow \phi = \delta(\gamma - 2) + 1 \tag{2.53}$$

From our simulations we have $\beta = 1$, $\phi = 1/4$, so Eq. (2.53) predicts $\gamma = 5/4$, which is close to the simulation result $\gamma \approx 1.15$.

2.2.5 Fluctuations and Non Self-averaging

It is known for the problem of hard core particles sliding on fluctuating surfaces [30, 31, 33] that there is a clustering of particles and the clusters are highly dynamic in nature — they are continuously breaking into smaller clusters and then recombining to form larger clusters. In fact these fluctuations are so strong that they do not damp down in the thermodynamic limit, leading to the nomenclature fluctuation dominated phase ordering (FDPO). The strong clustering state (SCS) in our system also shows strong fluctuations, which we characterise using the fraction of sites $\mathcal{N}_n/L$ with occupancy n. This fraction fluctuates from sample to sample and has a very broad distribution. Its mean is given by $P(n,L) = \langle \mathcal{N}_n \rangle / L$ and its variance by

$$\sigma^2 \equiv \left\langle \left(\frac{\mathcal{N}_n}{L} \right)^2 \right\rangle - \left\langle \frac{\mathcal{N}_n}{L} \right\rangle^2 . \tag{2.54}$$

We found that if n is held fixed and we take the limit $L \to \infty$, the ratio $\sigma / \langle \mathcal{N}_n/L \rangle$ approaches a constant (Fig. 2.10). This is to be contrasted with a normal, self-averaging system where this ratio vanishes in the limit $L \to \infty$. Thus we see that our steady state has strong fluctuations and the clusters are not stable objects but break and reform all the time as the surface evolves.

2.2.6 The strong clustering state (SCS)

The following picture of the steady state emerges from our results. The scaling of the probability distribution $P(n,L)$ as n/L and the vanishing of the probability of finding an occupied site ($\equiv N_{occ}/L$) suggest that a large number of particles (often of the order of system size) aggregate on a few sites. The scaling of the two-point density-density correlation function with L implies that the particles are distributed over distances of the order of L, while the divergence of the scaling function indicates clustering of large-mass aggregates. Thus the evidence points to a state where the particles form a few, dense clusters composed of a small number of large mass aggregates and these clusters are separated on the scale of system size. We choose to call this state as the Strong Clustering State (SCS). The divergence at the origin of the two-point density-density correlation function as a function of the separation scaled by the system size, is its hallmark. The information we get from results on dynamics is that the particles

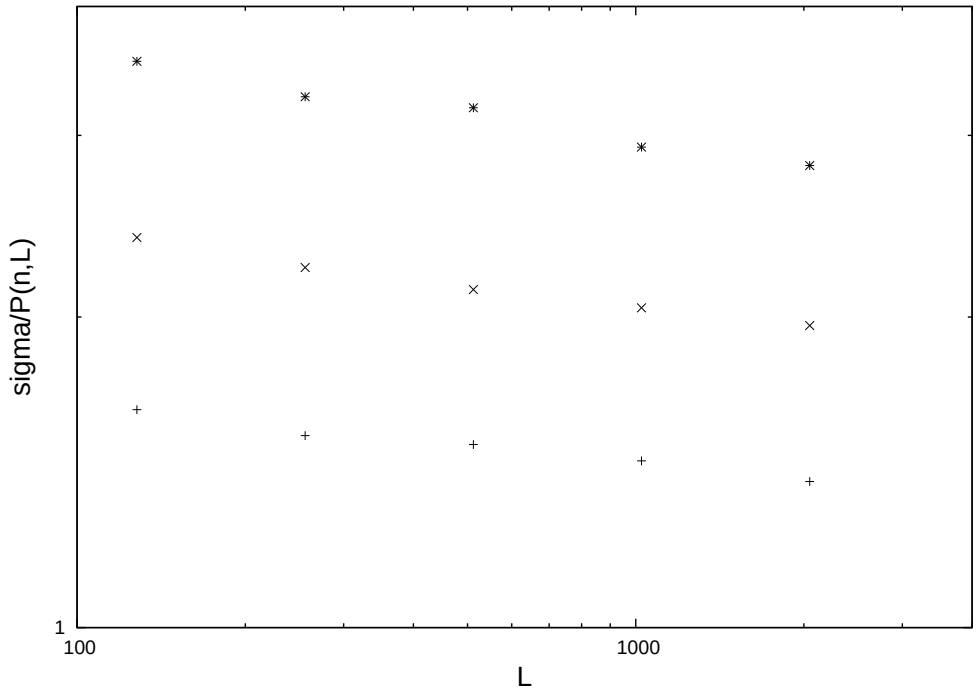

Fig 2.10: The figure shows data for the quantity $\sigma/\langle \mathcal{N}_n/L \rangle$ for 3 values of n, $n = 4$ (+), 8 ($\times$), 16 ($*$). We see that for large L, this quantity approaches a constant, showing the presence of large fluctuations that do not damp down in the thermodynamic limit.

have a tendency to follow the surface. This is brought out by the fact that the scaling exponent describing the RMS displacement comes out to be equal to the dynamic exponent of the KPZ surface.

At this point, we would like to comment on the renormalization group (RG) calculation of Drossel and Kardar [29]. They have tried a perturbative RG approach to determine the density-density correlation. The answers from their calculation do not match well with the numerical results, as we have shown in section 2.2.1. The reason, we believe, lies in the strong clustering feature of the steady state. The crucial point is that the two point correlation function in the SCS is a function of the system size and diverges in the thermodynamic limit for any finite value of the separation. This can be seen by substituting the power law form for $Y(y)$ in Eq. (2.14). The calculation in [29] assumes a well defined value for the correlation function, for any finite separation, in the thermodynamic limit. Neglecting this infra-red divergence which is inherent to the system would lead to incorrect results. The fluctuations in our system diverge with increasing system size and thus are much stronger than those near a critical point. Thus the usual renormalization group approach, which is well suited to critical point

behaviour, is not directly applicable to our system. We have seen that in the steady state, the particles cluster in a few sites which contain a diverging number of particles and most of the sites are empty. This state is very far removed from a diffusive state where the particles are distributed uniformly. Treating the coupling term in the equation for evolution of the density as a perturbation around the diffusive solution would then not be expected to yield the correct form of the correlation function.

2.2.7 Variation of ω and K

In this section, we describe our results on how the steady state of the system changes with a change in the parameters ω and K. To see how the system behaves when we change the relative speeds of the surface and particle evolution, we vary the parameter $\omega \equiv N_s/N_p$ (N_s and N_p being respectively the number of successive surface and particle update attempts) in the range $1/4 \leq \omega \leq 4$. When $0 < \omega < 1$ (particles faster than the surface), we regain the scaling form of Eq. (2.14) for the two point correlation function. The scaling function also diverges with the same exponent. While the probability distribution for occupancy $P(n, L)$ shows similar scaling with system size as Eq. (2.27), the scaling function $f(y)$ shows a new feature — it develops a peak at large n (Fig. 2.11). This peak at large n indicates that the probability of finding nearly all the particles at a single site is substantial.

A heuristic argument for the appearance of this peak is now given. Consider a configuration in which a large number of particles (nearly equal to the total number of particles) reside in a local valley. When this valley is replaced by another one nearby under surface dynamics , all the particles tend to move to the new one. If the number of particle updates is greater than surface updates, there is a substantial probability that all the particles are able to move to the new valley before it is itself replaced by another one. Thus there is a significant probability of the initial cluster surviving intact for a fair amount of time. Numerically, we also find that

$$\frac{P(n = N, L)}{P(n = N - 1, L)} = \frac{1}{\omega} \tag{2.55}$$

As mentioned in the introduction, the case of $\omega = 0$ (with the limit $L \to \infty$ taken later) is special. In this case, the problem reduces to an equilibrium problem and can be approached analytically. We will describe the calculations in a separate section

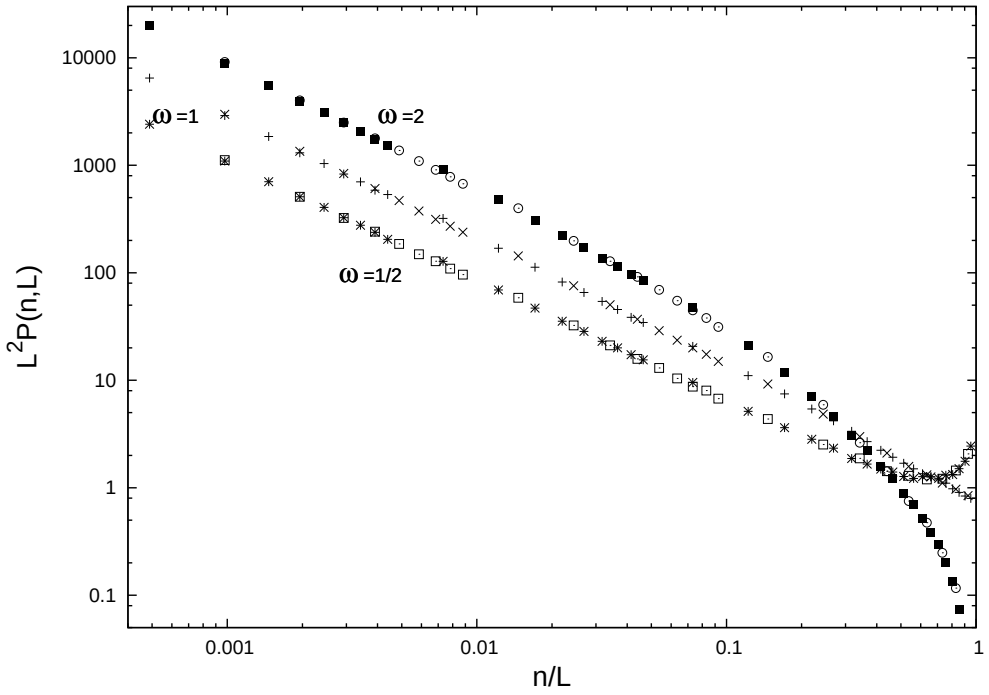

Fig 2.11: Scaled probability distribution $P(n, L)$ for $\omega = 1/2, 1, 2$ ($K = 1$). The line is a fit to Eq. (4.50) with $\beta = 2.3$. The lattice sizes are L= 1024 ($\circ$, $\times$, $\Box$), 2048 ($\blacksquare$, $+$, $*$).

below but point out the main result here — the strong clustering state survives for $\omega = 0$ and the results (scaling exponents, functional forms of the scaling functions) match very well with our non-equilibrium numerical results for $\omega = 1$. This close correspondence between a nonequilibrium system and a disordered equilibrium system is quite unexpected.

For $\omega > 1$, the particles settle down slowly in valleys and $\tau_{surf} \gg \tau_{part}$ where τ_{surf} and τ_{part} are respectively the times between successive surface and particle updates. Though $\tau_{surf} \gg \tau_{part}$; for large enough L, the survival time of the largest valley $\sim \tau_{surf} L^z$ is always greater than the particle sliding time $\sim \tau_{part} L$. Thus we expect that particles will lag behind the freshly formed valleys of small sizes but would manage to cluster in the larger and deeper valleys, which survive long enough. We thus expect a clustering of particles and scaling to hold beyond a crossover length scale $r_c(\omega)$. We can estimate the crossover length by equating the time scales of surface and particle rearrangements — $\tau_{surf} r_c^z(\omega) \sim \tau_{part} r_c(\omega)$, which yields $r_c(\omega) \sim \omega^{\frac{1}{z-1}}$. Using $z = 3/2$, we have $r_c \sim \omega^2$. Numerical simulation results are shown in Fig. 2.13 which shows that the data deviates from scaling and power law behaviour at small r, due to a crossover

effect. The data suggests that

$$G(r,L) \sim\sim \frac{1}{L^{\theta}} Y\left(\frac{r}{L}\right) g(\frac{r}{r_c(\omega)}) \tag{2.56}$$

As we can see from Fig. 2.13 (main graph), the curve flattens out at small values of r, so for $y < 1$ ($r < r_c(\omega)$), the function $g(y)$ in the equation above should follow $g(y) \sim y^{1.5}$ while it should go to a constant for $y > 1$. We can determine $r_c(\omega)$ from $G(r,L)$ by separating out the r dependent part; if we scale $G(r,L)$ by L, we obtain the quantity $\frac{1}{r^{1.5}} g(\frac{r}{r_c(\omega)})$). We can now determine $r_c(\omega)$ as the value or r where the scaled data starts deviating from the power law behaviour $r^{-1.5}$. From Fig. 2.13, (inset) $r_c(\omega = 2) \simeq 10$. A similar exercise for $\omega = 3$ leads to $r_c(\omega = 3) \simeq 20$. A clean determination of $r_c(\omega)$ for $\omega > 3$ requires data for very large values of system size, beyond the scope of our computational capabilities.

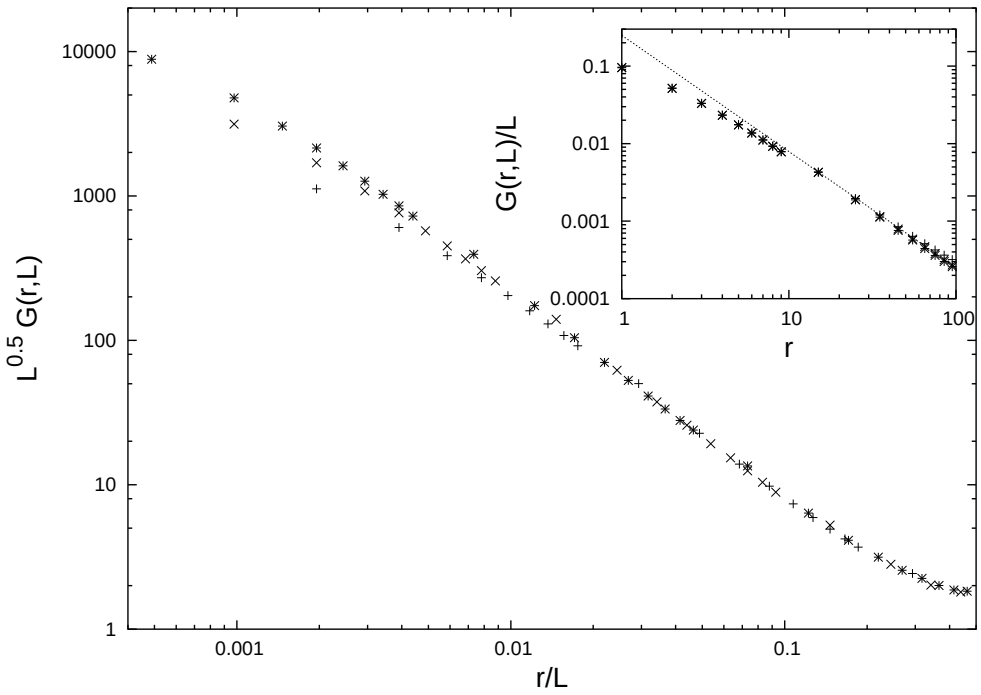

Fig 2.12: The main plot shows the scaled two point correlation function for $\omega = 2$, ($K = 1$), we see deviation from scaling at small r/L. The inset shows a plot of $G(r,L)/L$ versus r. The straight line shows depicts the power law with exponent -1.5. The lattice sizes are L= 512 (+),1024 ($\times$), 2048 ($*$).

The probability distribution $P(n,L)$ continues to show the same scaling form (Eq. (2.27)) for $\omega > 1$, but the scaling function $f(y)$ in this case dips at large values of y (Fig. 2.11)

in contrast to the peak seen for $\omega < 1$. The exponent z describing the RMS displacement of particles remains unchanged under a change in ω, again indicating that particles follow the movement of valleys on the large scale.

In the limit $\omega \to \infty$, the surface movement is much faster than the particle response time. The valleys evolve quickly and disappear before the particles can cluster in them, thus, the particles essentially move like random walkers or free particles on a flat landscape.

The other parameter of interest is K, defined in the section on Monte-Carlo simulations above. When we make a particle update, we move the particle downhill with probability $(1+K)/2$ and uphill with probability $(1-K)/2$. So far we have discussed the results for the case $K = 1$, where particles always move downhill. Decrease in K reduces the average downhill speed of particles, while the valley evolution rates are unaffected. Thus decreasing K causes an effect similar to increasing ω and a crossover length scale is introduced. The particles lag behind the freshly formed local valleys but settle down in the deeper, longer surviving global valleys. The numerical results again guide us to the form

$$G(r, L) \sim \frac{1}{L^{\theta}} Y\left(\frac{r}{L}\right) g(\frac{r}{r_c(K)}) \tag{2.57}$$

for the correlation function. Analogous to $\omega > 1$ case, we have extracted r_c from the numerical data. We find $r_c(K = 0.75) \simeq 10$. Values of K lower than 0.75 require data for system sizes that are beyond our computational limitations.

2.2.8 Tilting the surface

Up till now, we have considered a surface with no average slope and we see that the steady state is a strong clustering state (SCS) and that this state is robust under change in various parameters. The question that we will address in this section is — what happens to the steady state if the surface has an average slope? Addition of an average slope or tilting the KPZ surface is the same as adding an average velocity to the Burgers fluid. Thus the transformation $v' = v + v_0$ leads to the transformed coupled equations (see Equations (1.11) and (1.13))

$$\frac{\partial(v+v_0)}{\partial t} + \lambda(v+v_0).\frac{\partial(v+v_0)}{\partial x} = \nu\left(\frac{\partial(v+v_0)}{\partial x}\right)^2 + \frac{\partial\zeta_h(x,t)}{\partial x} \tag{2.58}$$

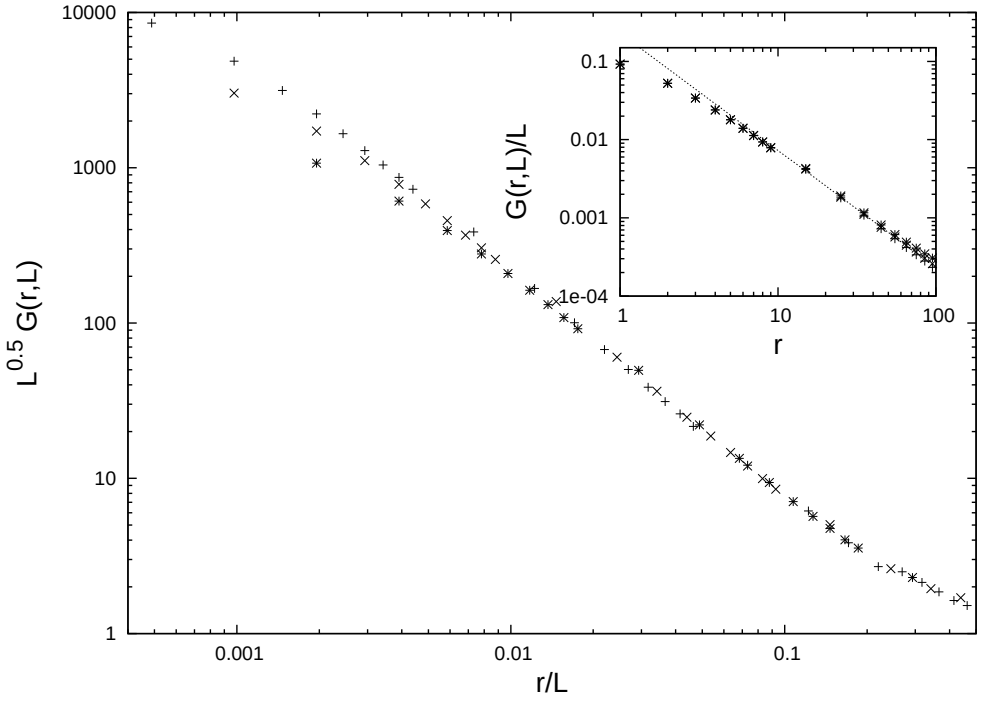

Fig 2.13: The main plot shows the scaled two point correlation function for $K = 0.75$ ($\omega = 1$), we see deviation from scaling at small r/L. The inset shows a plot of $G(r, L)/L$ versus r. The straight line shows depicts the power law with exponent -1.5. The lattice sizes are L= 512 ($*$),1024 ($\times$), 2048 ($+$).

The particles respond only to the local velocity, so

$$\frac{dx_m}{dt} = av|_{\vec{x}_m} + v_0 + \zeta_m(t) \tag{2.59}$$

It can be shown that the Galilean shift $x' = x - \lambda vt$ and $t' = t$ will simultaneously shift the extra term in both the equations above, given $\lambda = 1$. In our simulations, we have $\lambda = 1$ ($p = 1, q = 0$ in Eq. 2.7), thus, the steady state in this case is again an SCS (Fig. 2.14). Let us contrast this result to the the fluctuation dominated phase ordering (FDPO) in the hard core particles case. It was seen that FDPO does not survive when the surface is tilted and the clustering is lost [31]. As the hills and valleys sweep across at a finite speed, the particles are not able to keep up. Thus, the particles are not able to cluster in the newly formed valleys and the phase ordering is lost. In our case, the particles are non interacting and it suffices to consider a single particle, which, as we have seen above, keeps moving along with the valley.

Thus, to summarise — In this chapter we described our method and results for the Monte-Carlo simulations of the KPZ advection case. We saw that there is a new kind

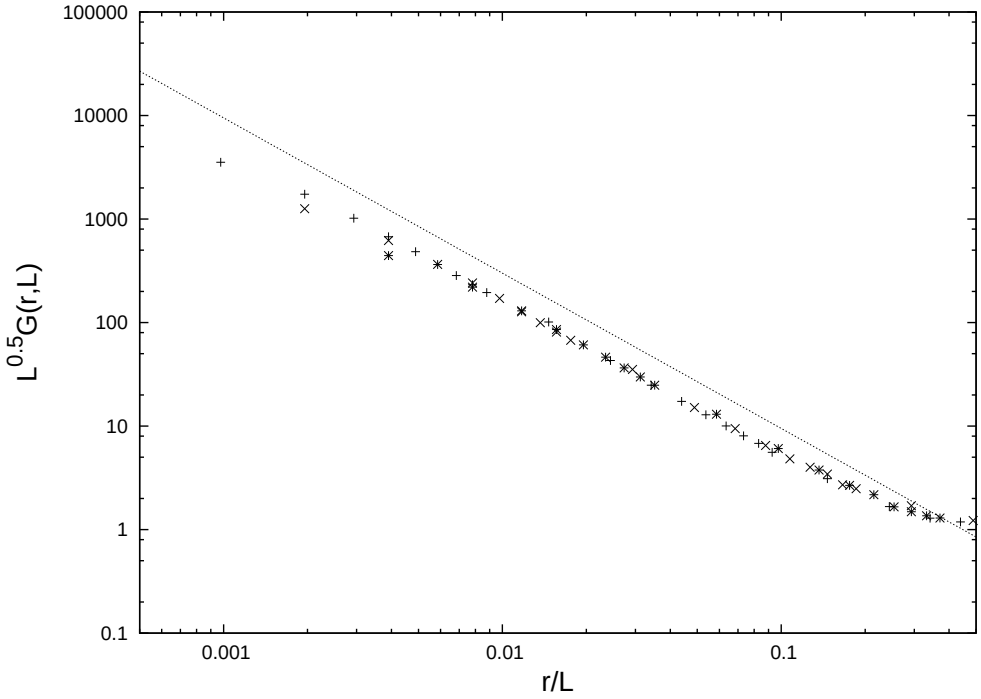

Fig 2.14: The plot shows the scaled two point correlation function for a tilted surface (3 negative slopes per positive slope). We see that the correlation function scales as for the untilted case.The straight line shows depicts the power law with exponent -1.5. The lattice sizes are L= 256 ($*$), 512 ($\times$), 1024 ($+$).

Exponent	Related Quantity	Definition	Scaling relation
θ	$G(r,L)$ Two point density-density correlation	$G(r,L) \equiv \langle n_i n_{i+r} \rangle$ $n_i \rightarrow$ No. of particles at site i	$G(r,L) \sim \frac{1}{L^\theta} Y(\frac{r}{L})$
ν	$G(r,L)$		$Y(y) \sim y^{-\nu}$
δ	$P(n,L)$ Probability of having occupancy n	$P(n,L) \equiv \langle \mathcal{N}_n/L \rangle$ $\mathcal{N}_n \rightarrow$ No. of sites with occupancy n	$P(n,L) \sim \frac{1}{L^{2\delta}} f\left(\frac{n}{L^\delta}\right)$
ϕ	N_{occ} No. of occupied sites	$N_{occ} = (1 - P(0,L))L$	$N_{occ} \sim L^\phi$
z	$R(t)$ RMS displacement of tagged particle	$R(t) \equiv \langle (x(t) - x(0))^2 \rangle^{1/2}$ $x(t) \rightarrow$ Position of tagged particle at time t	$R(t) \sim L^\chi h\left(\frac{t}{L^z}\right)$

Table 2.1: Table for the various exponents defined in the chapter.

of steady state in this case, called the strong clustering state (SCS). We saw that the steady state is robust under the change of parameters and the tilting of the surface. In the next chapter, we will describe our results on the remaining two cases under consideration — the KPZ anti-advection case and the EW case. We will see that while the steady state is again an SCS, the details vary from case to case.

KPZ anti-advection, EW

We will begin this chapter with a discussion of the KPZ anti-advection dynamics where the particles and the surface move in opposite directions. Thus, while the particles try to settle in local valleys, the valleys themselves are unstable, evolving all the time. This leads to declustering, and the question arises — Do we still have an SCS? The answer to this question, as we will see, is yes, though the degree of clustering is less than the KPZ advection case.

The KPZ anti-advection dynamics was first studied by Drossel and Kardar [5, 29]. In [5], they studied a model for the growth of binary films i.e. thin films which are grown by the deposition of two kinds of materials. The film is composed of regions or phases consisting of either of the two materials and these regions are separated from each other by phase boundaries. The phase boundaries are dynamic in nature and can be thought of as a driven field, the drive being the growth of the film itself. In a certain region of parameter space, these domain walls behave similarly as the passive particles in the KPZ anti-advection case. It is to be remembered though, that unlike our non-interacting passive scalars, these domain boundaries can annihilate each other on contact or create new boundaries. Thus, the number of boundaries, unlike our passive scalars, is not conserved. Nevertheless, as a starting point, Drossel and Kardar [5] considered the noninteracting particle case as a reference. As we proceed, we will compare our results with results from these papers.

The other dynamics that we will consider in this chapter is one where the particles are driven by a surface governed by the EW equation. The EW equation is different from the KPZ equation in that it does not have the symmetry breaking nonlinear term. We see that the steady state here is again an SCS, the amount of clustering is less than the KPZ advection case but more than the KPZ anti-advection case. We will end this chapter with a comparison of results from all the three dynamics considered by us.

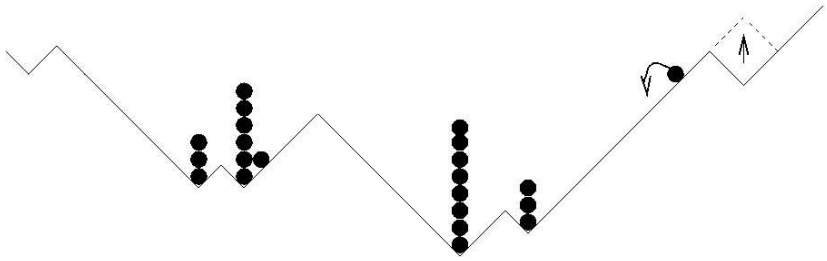

Fig 3.1: Schematic diagram of the surface and non-interacting particles sliding on top of it. Arrows show possible surface and particles moves. Only the hill to valley move is allowed for the KPZ anti-advection dynamics.

3.1 KPZ anti-advection

Let us once more consider the coupled pair of equations

$$\frac{\partial h}{\partial t} = \nu \nabla^2 h + \frac{\lambda}{2}(\nabla h)^2 + \zeta_h(\vec{x}, t). \tag{3.1}$$

and

$$\frac{d\vec{x}_m}{dt} = -a \nabla h|_{\vec{x}_m} + \zeta_m(t), \tag{3.2}$$

this time with $a/\lambda < 0$. As we have seen in the last chapter, λ determines the direction of average surface motion and $a/\lambda < 0$ corresponds to particles moving in the opposite direction of average surface motion. Again, to solve the above system of equations, we performed Monte-Carlo simulations with the following rules:

We again have the same kind of lattice as in KPZ advection, with particles residing on sites and the link between sites have slopes of either 1 (upward slope $\rightarrow$ /) or -1 (downward slope $\rightarrow$ \). We choose a site at random, but instead of considering hills, we concentrate on local valleys — if the chosen site is on a local valley (\/), we change the local valley to a local hill (/\) (Fig. 3.1, extreme right), otherwise, we leave it unchanged. The particles are updated in exactly the same fashion as in the KPZ advection case — a randomly chosen particle is always attempted to move downwards.

As one can see from the above Monte-Carlo rules, while the particles are trying to move into local valleys, the valleys are themselves unstable and overturn to form hills. Thus one expects that there would be less clustering in this case. This is borne out by our numerical results.

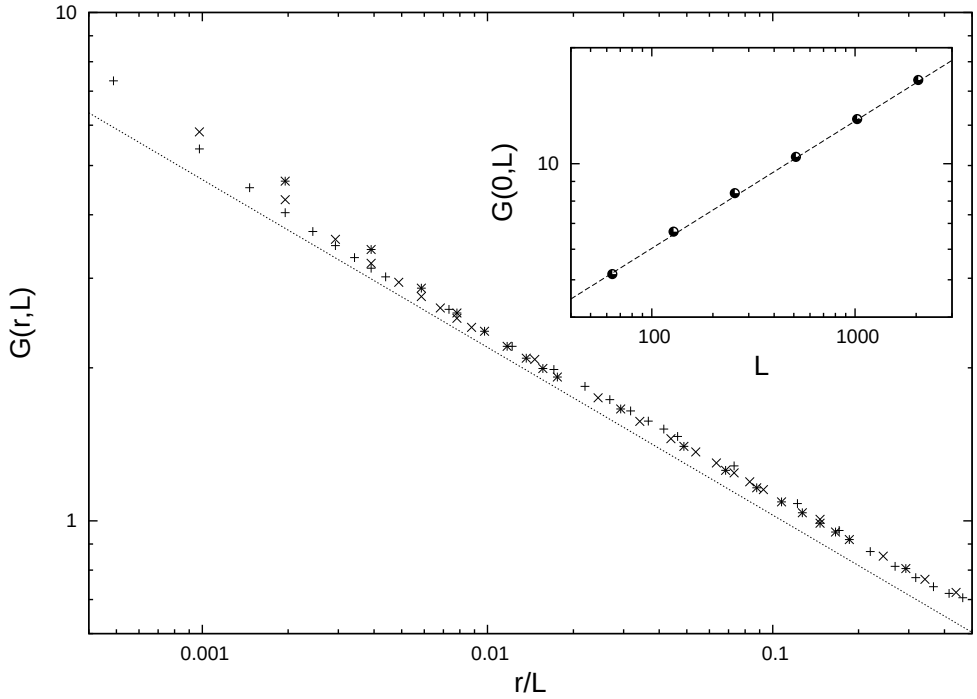

Fig 3.2: The main figure shows $G(r, L)$ versus r/L for the anti-advection case. The straight line shows a power law with exponent $-1/3$. The lattice sizes are L= 512 ($*$), 1024 ($\times$), 2048 ($+$). The inset shows $G(0, L)$ versus L and the straight line shows a power law with exponent $1/3$.

3.2 Numerical Results, KPZ anti-advection

We begin with the simplest case $\omega = K = 1$.

3.2.1 Statics

We measured the two point correlation function $G(r, L)$ and obtained a scaling collapse for data for various values of system size L. Our data suggests that for $r > 0$, the same scaling form as for the advection case is valid (Fig. 3.2)

$$G(r, L) \equiv \langle n_i n_{i+r} \rangle_L \sim \frac{1}{L^\theta} Y\left(\frac{r}{L}\right). \tag{3.3}$$

The value of θ is zero in this case. The scaling function $Y(y)$ again has a power law divergence $Y(y) \sim y^{-\nu}$ as $y \to 0$, with ν close to $1/3$ (see Table 3.1, Fig. 3.2). This power law behaviour and the value of the exponent ν is in agreement with results in [5]. However, as we have mentioned before, the scaling with system size has not

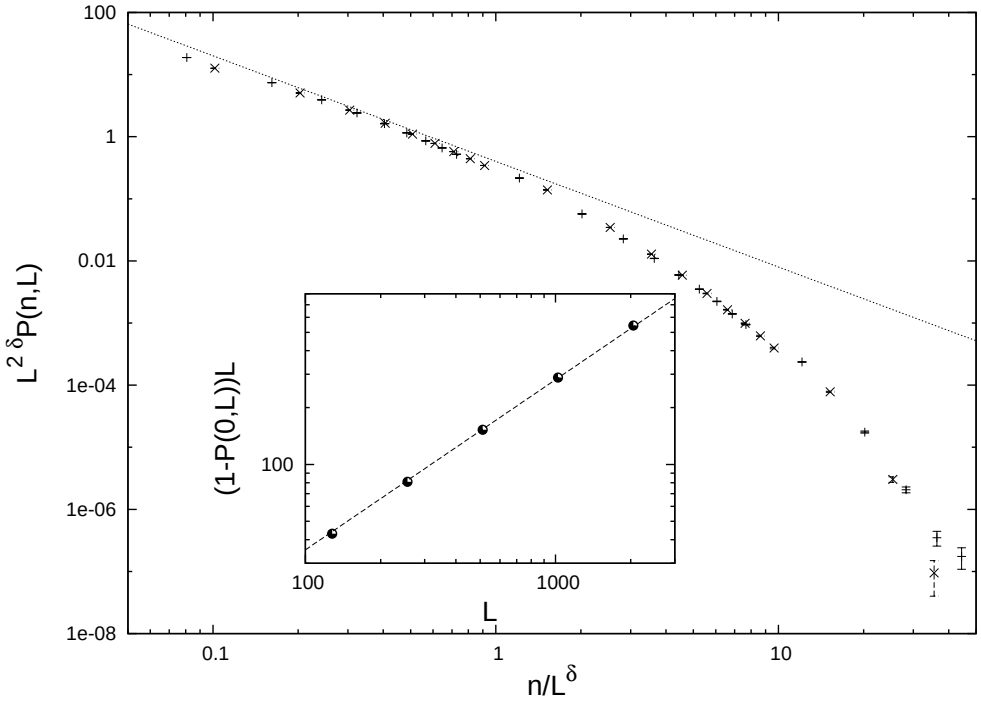

Fig 3.3: The main figure shows $P(n, L)$ versus n/L^{δ} for the anti-advection case. The straight line shows a power law with exponent -1.7. The lattice sizes are L= 512 ($*$), 1024 ($\times$), 2048 ($+$). The inset shows $(1 - P(0, L))L$ versus L and the straight line shows a power law with exponent 0.9.

been mentioned in [5].

Thus, the above results show that there is clustering and the steady state is an SCS. The value of the exponent ν, which is an indicator of the amount of clustering, is less in this case ($\nu \simeq 0.33$) than the value for the advection case ($\nu \simeq 1.5$) indicating that there is less clustering. These results again do not match with the results from the renormalization group calculation in [29] because the steady state, as we have shown above, is an SCS and the perturbative approach is not expected to work, as discussed in Section 2.2.6.

The probability $P(n, L)$ of a site having an occupancy n again has a similar scaling form as in the advection case

$$P(n, L) \equiv \langle \mathcal{N}_n/L \rangle \sim \frac{1}{L^{2\delta}} f\left(\frac{n}{L^{\delta}}\right) \tag{3.4}$$

with $\delta \simeq 1/3$ (see Table 3.1, Fig. 3.3). We thus see that the relation

$$\delta = \nu - \theta \tag{3.5}$$

is true for anti-advection also. The function $f(y)$ seems to fit a power law $y^{-\gamma}$ with $\gamma \simeq 1.7$ (see Table 3.1, Fig. 3.3) for small values of y. The behaviour of the function at small y describes the distribution of large but finite clusters in the limit of system size going to infinity ($n \to \infty$, $L \to \infty$, $n/L^{\delta} \to 0$). As in the KPZ advection case, we can use the scaling form of $P(n, L)$ to show that $G(0, L) \sim L^{\delta}$, which, is borne out independently from the numerics (Fig. 3.2). The singular part $P(0, L)$ satisfies $N_{occ} \equiv (1 - P(0, L))L \sim L^{\phi}$ with $\phi \simeq 0.9$ (Fig. 3.3). Substituting this value of ϕ in the scaling relation

$$\phi = \delta(\gamma - 2) + 1 \tag{3.6}$$

leads to $\gamma \simeq 1.7$, which is the same as the numerical value from direct measurement.

We have explored the ω and K dependence of the above results. For the range of values studied ($1 \leq K \leq 0.75$, $1/5 \leq \omega \leq 5$), we found the scaling relation and the values of scaling exponents to be the same as the values for the $\omega = 1$, $K = 1$ case. There are no significant crossover effects. There is an interesting feature present in the density-density correlation data for small values of ω; the numerical value of $G(r = 1, L)$ is less than the value expected from the scaling function $Y(y)$. This is a feature induced by the lattice model that we are using for the simulations; when a local hill turns into a local valley, all the particles present inside the local valley slide quickly to either side, thus decreasing the probability of finding two particles at distance one from each other.

3.2.2 Dynamics

We measured the RMS displacement $R(t)$ and found that it follows

$$R(t) \equiv \langle (x(t) - x(0))^2 \rangle^{1/2} = L^{\chi} h\left(\frac{t}{L^z}\right) \tag{3.7}$$

where $h(y) \sim y^{1/z}$, with $z = 1.75$ for small y, and $\chi = 1$. Similarly, the measurements on autocorrelation function (Fig. 3.4) show that $\widetilde{G}(t, L)$ has the same form as in the advection case

$$\widetilde{G}(t, L) \equiv \langle n_i(0) n_i(t) \rangle_L \sim \widetilde{Y}\left(\frac{t}{L^z}\right) \tag{3.8}$$

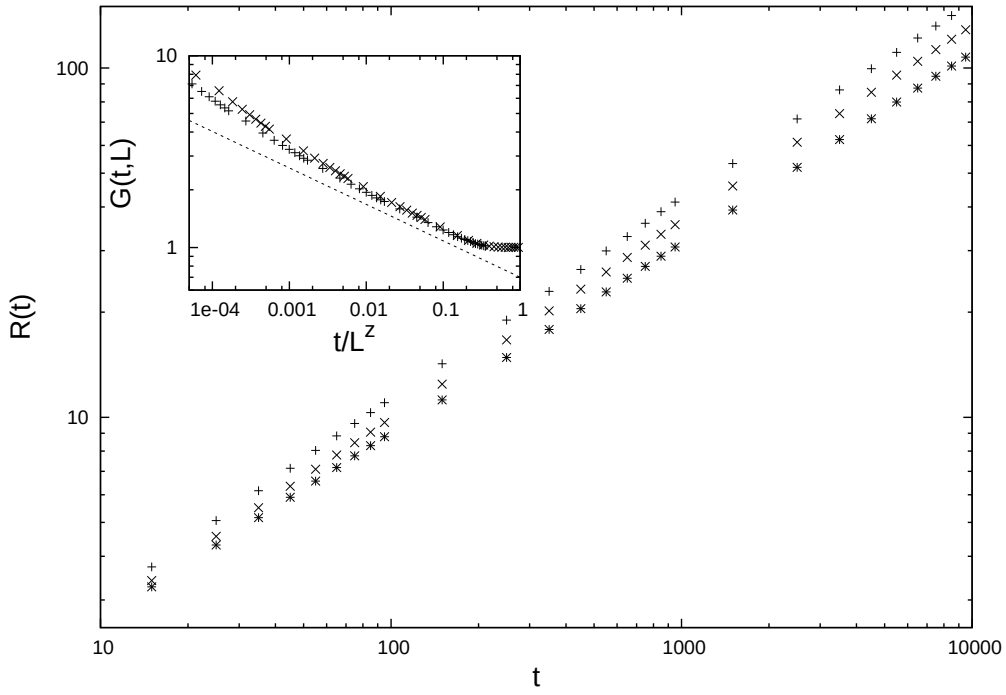

Fig 3.4: The main figure shows the RMS displacement $R(t)$ versus t for various values of K. We see that $R(t) \sim t^{1/z}$ with $z = 1.75, 1.82, 1.85$ for $K = 1, 0.5, 0.25$ respectively. $L = 1024$ for all the data. The inset shows the autocorrelation function $\tilde{G}(t, L)$ versus t/L^z for $L = 256,\ 512$. The straight line shows a power law with exponent -0.19.

with $z = 1.75$ and $\widetilde{Y}(\tilde{y}) \sim \tilde{y}^{-\psi}$, $\psi = 0.19$ (Fig. 3.4). A point to note is the following: if we substitute $r \sim t^{1/z}$ in the Equation (3.3) for the static correlation, we get the autocorrelation scaling form above with the correct scaling exponent $\psi = 0.19$. We thus see that a simple scaling picture is valid where one can think of taking a time correlation measurement as equivalent to a space correlation measurement, provided distance r scales as $t^{1/z}$. The value of z obtained from these two measurements is different from the advection case where it is equal to the dynamic exponent for the surface, $z_s = 1.5$. Since the surface is the same in both the cases, one would have a priori expected z to be the same, thus an increase in z is surprising. The reason, we believe, lies in the dynamics. In the advection case, the dynamics cause the particles to faithfully follow a deep valley and thus the movements of the valley reflect in the movement of the particles. In the anti-advection case where the valleys themselves are unstable, the particles can get distributed into different valleys when the particular valley they were aggregated in gets destabilised. The particles thus move slower than the KPZ advection case and the dynamic exponent value is somewhere between the KPZ surface dynamic exponent value (1.5) and the random walk value (2).

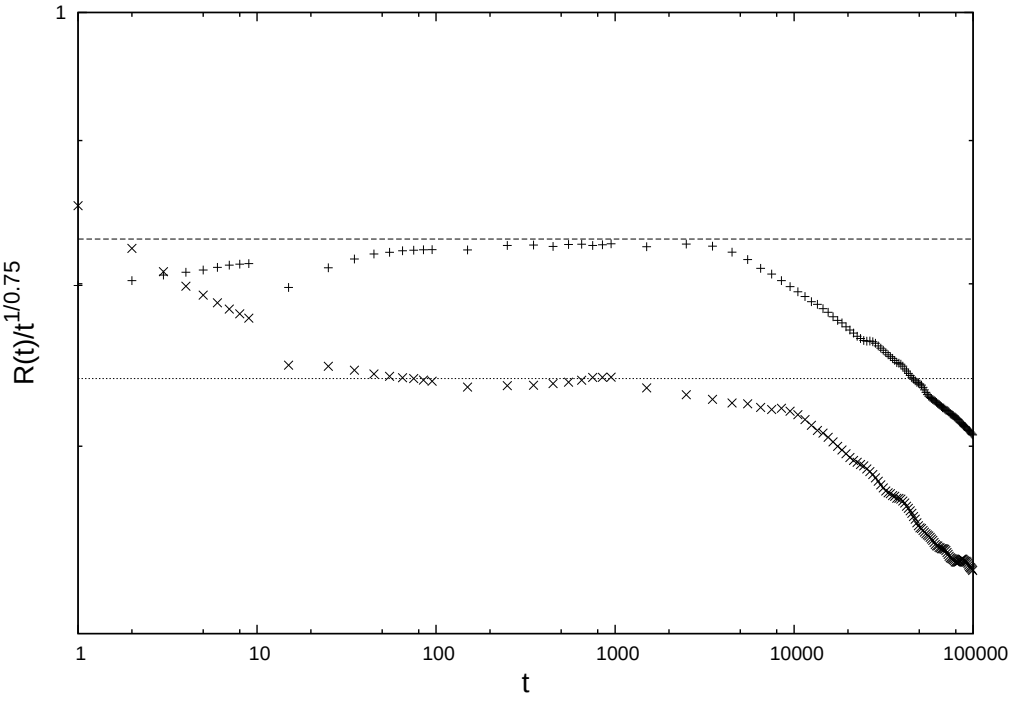

Fig 3.5: The figure shows $R(t)/t^{1/z}$ ($z = 1.75$) versus t for $K = 1$ (+), $K = 0.5$ (×). We see that $z = 1.75$ is indeed the correct exponent for both K values. $L = 1024$ for both the data.

We studied the effect of varying the parameter K on the RMS displacement, first studied in [29]; at first look one sees that z appears to increase continuously as we decrease K (Fig. 3.4), apparently in accordance with [29]. However, a more careful look at the data reveals a different picture. If we divide the RMS displacement data for various values of K by $t^{1/z}$, where z is taken to be 1.75 (the value for $K = 1$), one sees that the curve is indeed flat in the middle region(Fig. 3.5). This shows that $z \simeq 1.75$ is the correct dynamical exponent for the particle motion irrespective of the value of K. At large times, one sees as expected that due to decorrelation in the surface and the destruction of the valley in which the particle was originally situated, the particles show diffusive behaviour. At small times one sees a transient behaviour due to the increased tendency of the particles to move independently of the surface slope.

3.3 Edwards-Wilkinson

In this section we will consider a surface evolving according to the Edwards-Wilkinson (EW) equation as our driving field. The EW equation

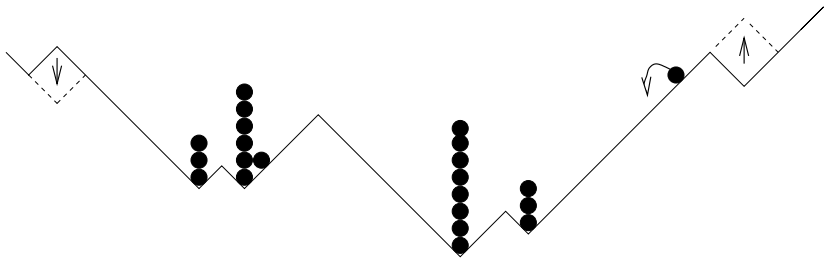

Fig 3.6: Schematic diagram of the surface and non-interacting particles sliding on top of it. Arrows show possible surface and particles moves. Both the valley to hill and hill to valley moves are allowed for the EW dynamics.

$$\frac{\partial h}{\partial t} = \nu \nabla^2 h + \zeta_h(\vec{x}, t) \tag{3.9}$$

does not contain the nonlinear term $\frac{\lambda}{2}(\nabla h)^2$ present in the KPZ equation above (Eq. (3.1)). The first thing to note is that the nonlinear term breaks the $h \rightarrow -h$ or up-down symmetry, thus the removal of the term restores this symmetry. Therefore, the surface in this case does not have an average motion; we also do not have the advection and anti-advection cases as in the KPZ advection case since the direction of the gravity with respect to the surface motion does not matter. These facts will be reflected in our Monte-Carlo simulation rules. The EW equation, owing to its linear character, can be solved exactly and the values of the exponents in one dimension are — roughness exponent $\alpha = 1/2$ and dynamic exponent $z = 2$. The roughness exponent in one dimension has the same value as for the KPZ surface, thus the static surface configurations are statistically the same. The difference in the passive slider steady state is caused by the dynamics of the surface. Our results show that the steady state for the EW surface is again an SCS, the amount of clustering is less than the KPZ advection and more than the KPZ anti-advection dynamics.

The basic Monte-Carlo model and the particle dynamics in this case are the same as for the KPZ advection and anti-advection cases above; the essential difference lies in the surface dynamics. Here, we choose a site at random, if the chosen site is on a local valley (\/), we change the local valley to a local hill (/\) (Fig. 3.6, extreme right) and if the chosen site is on a local hill (/\), we change it to a local valley (\/) (Fig. 3.6, extreme left). If the chosen site lies on a slope, we leave it unchanged. Since the valleys and the hills are treated on the same footing, the surface dynamics respects the $h \rightarrow -h$ symmetry of the EW equation.

3.3.1 Statics

The two point correlation function $G(r, L)$, for $r > 0$ has the same scaling form as Eq. (3.3) with $\theta = 0$ and $Y(y) \sim y^{-\nu}$ as $y \to 0$, $\nu \simeq 2/3$ (see Table 3.1, Fig. 3.7). The probability $P(n, L)$ of a site having an occupancy n again has a similar scaling form as in Eq. (3.4) with $\delta \simeq 2/3$ (see Table 3.1, Fig. 3.8). For small y, $f(y) \sim y^{-\gamma}$, $\gamma \simeq 1.49$. We have for $P(0, L)$ — $N_{occ} \equiv (1 - P(0, L))L \sim L^{\phi}$ with $\phi \simeq 0.75$ (Fig. 3.8) and Eq. (3.6) leads to $\gamma \simeq 1.62$, close to our numerical value from the data for $P(n, L)$. These results are universal in nature and show no significant deviation when the value of ω and k are varied in the range $1/5 \leq \omega \leq 5$ and $0.75 \leq K \leq 1$.

3.3.2 Dynamics

As we mentioned above, the value of the dynamic exponent of the EW equation in one dimension is $z_S = 2$. Our results for the RMS displacement of the tagged particle and the autocorrelation function show that the $z \simeq 2$, thus the particles do follow the valley movement in this case. The system is similar to KPZ advection in this regard. Specifically, we observe that the RMS displacement $R(t)$ has the same form as in Eq. (3.7) with $z \simeq 2$. This confirms Gopalakrishnan's result [37] for the same quantity. The autocorrelation function again shows the same behaviour as in Eq. (3.8) with $z \simeq 2$ and $\psi \simeq 1/3$. Regarding the dynamical exponent, Gopalakrishnan [37] suggested that there might well be two different values of z in the two regimes $\omega \leq 1$ ($z = 2$) and $\omega > 1$ ($z < 2$), but the possibility remained that this is a crossover effect. In order to answer this, we performed Monte-Carlo simulations (Fig. 3.9). We conclude that the apparent change in the dynamic exponent is indeed a transient phenomenon. The inset in Fig. 3.9 shows that the power law $R(t) \sim t^{0.6}$ seems to fit the data well at relatively low times while the main figure shows that if the data is divided by $t^{1/2}$, the resulting curve approaches a flat line at large times indicating that $R(t) \sim t^{1/2}$ at large times.

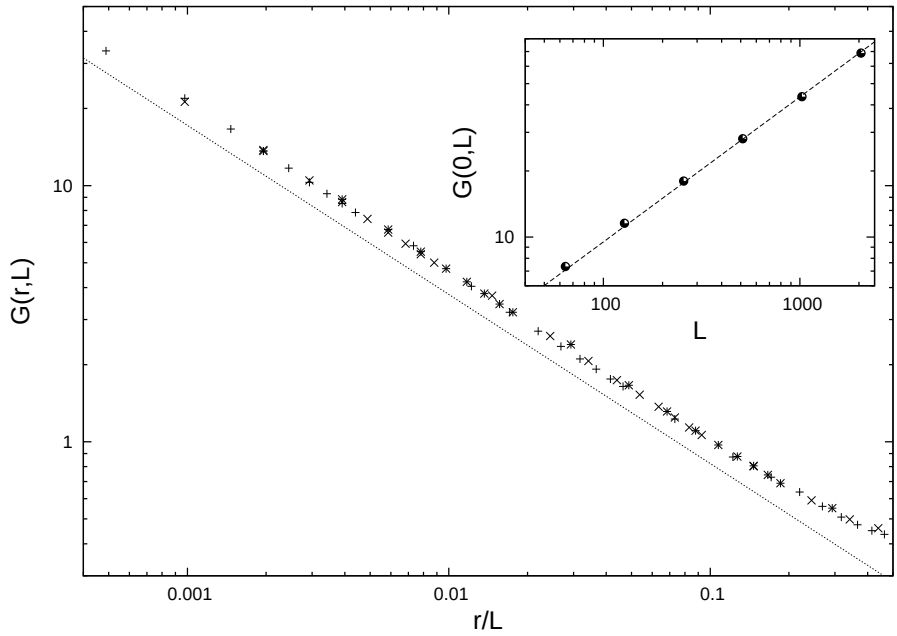

Fig 3.7: The main figure shows $G(r, L)$ versus r/L for the EW case. The straight line shows a power law with exponent $-2/3$. The lattice sizes are L= 512 ($*$), 1024 ($\times$), 2048 ($+$). The inset shows $G(0, L)$ versus L and the straight line shows a power law with exponent $2/3$.

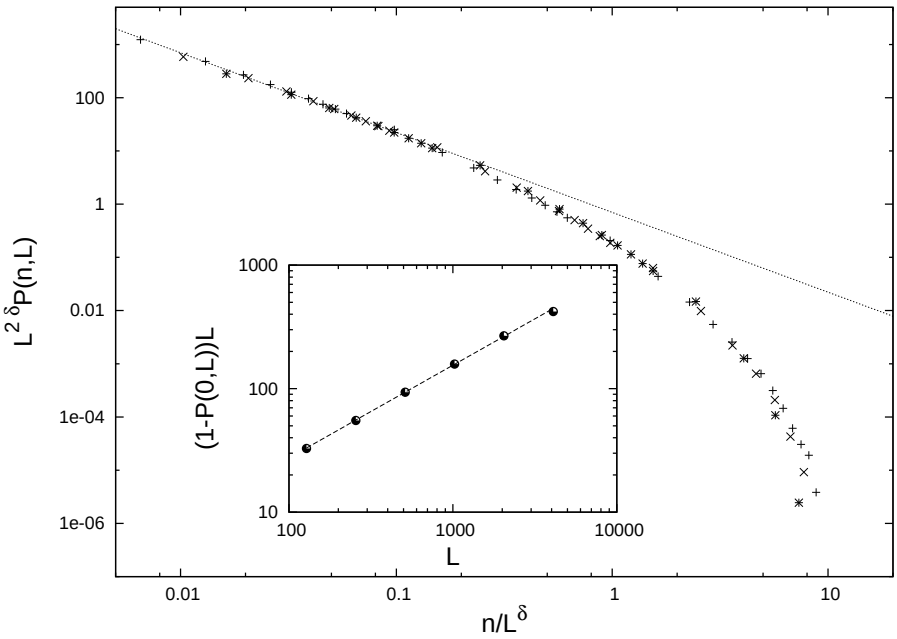

Fig 3.8: The main figure shows $P(n, L)$ versus n/L^{δ} for the EW case. The straight line shows a power law with exponent -1.49. The lattice sizes are L= 512 ($*$), 1024 ($\times$), 2048 ($+$). The inset shows $(1 - P(0, L))L$ versus L and the straight line shows a power law with exponent 0.75.

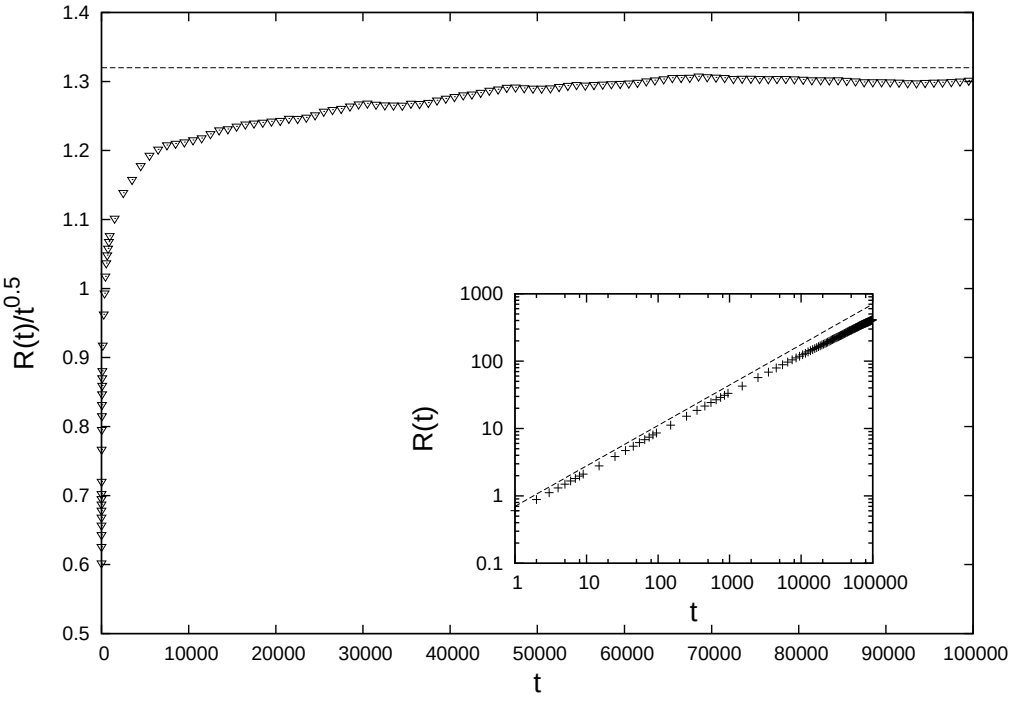

Fig 3.9: The inset shows $R(t)$ versus t for EW dynamics with $\omega = 2$. The straight line shows a power law with an exponent 0.6. The main figure shows $R(t)/t^{1/2}$ versus t which approaches a constant at larger values of t indicating that 0.6 is only an effective value st small times.

3.4 Comparison

To conclude our results from the simulations in one dimension, we show below a comparison of the various dynamics. As we have seen, SCS is the steady state for all three dynamics — KPZ advection, KPZ anti-advection and EW, showing that the state is not limited to a particular dynamics and arises under more general conditions. We have seen that the KPZ advection case, where the valleys are stable, shows the most clustering while the KPZ anti-advection case, where the valleys are unstable, shows the least clustering. For the EW surface, the valleys and hills have the same dynamics, and the clustering lies in between the KPZ advection and anti-advection cases. Figure 3.10 shows a visual confirmation of this picture of clustering. Figure 3.11 compares the density-density correlation function for the three dynamics, the larger the divergence, more the clustering. Finally, Table 3.1 below shows the values of the various exponents, with errors.

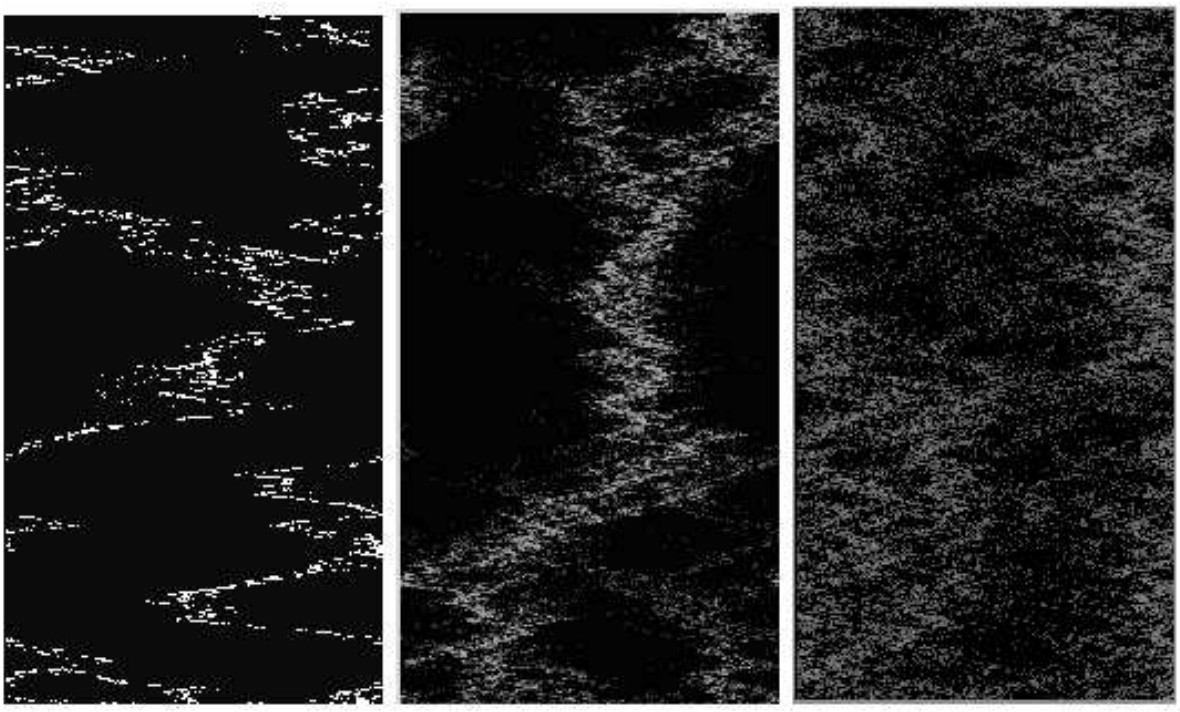

Fig 3.10: Time evolution for the KPZ advection, EW and KPZ anti-advection dynamics (from left to right). The vertical axis shows time and the horizontal axis shows the one dimensional lattice, the white spots show presence of particles. The lattice size and the number of particles are both 256 for all the three cases and so fewer white spots indicate a higher degree of clustering (fewer but more dense clusters).

	δ	ν	γ
Equilibrium Sinai Limit	1	3/2	1 with log corrections
KPZ Advection	1 ± 0.07	1.48 ± 0.04 1.5 (exact)	1.15 ± 0.02 or 1 with log corrections
KPZ Anti-Adv	0.33 ± 0.09	0.31 ± 0.02	1.70 ± 0.02
EW	0.68 ± 0.08	0.67 ± 0.02	1.49 ± 0.04

Table 3.1: The values of the exponents in one dimension for the three kinds of dynamics under consideration - KPZ advection, KPZ anti-advection and EW. The first row shows the values of exponents for the equilibrium Sinai limit of a stationary surface, to be discussed in the next chapter. For KPZ advection, the exact value for the exponent $\nu = 1.5$ is the result from Derrida's model of second class particles in the asymmetric exclusion process (ASEP).

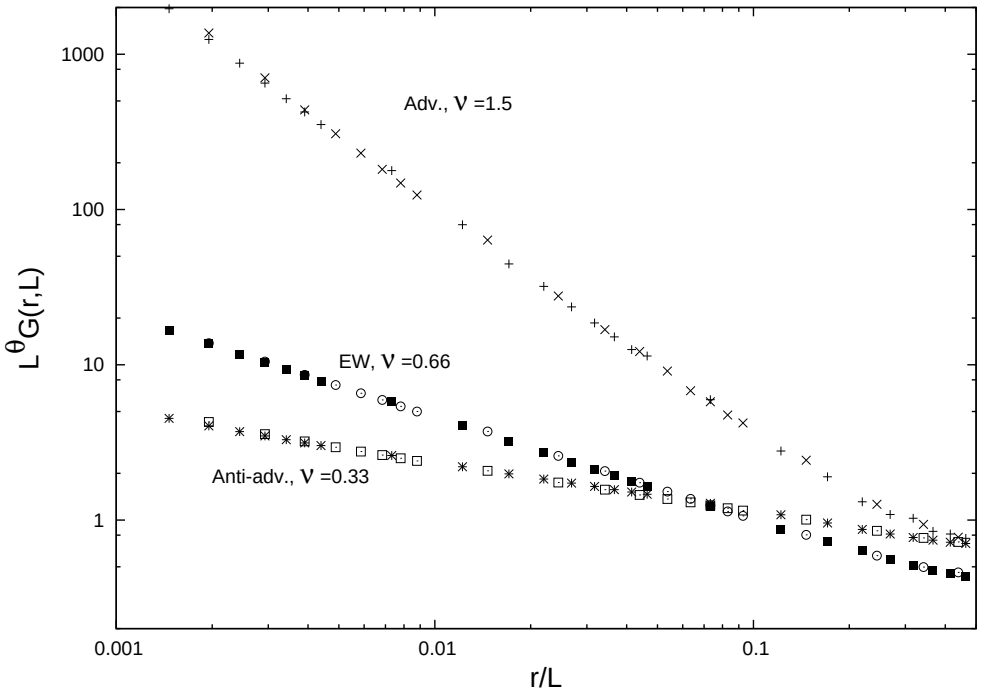

Fig 3.11: The figure shows $L^{\theta}G(r,L)$ versus r/L for the KPZ advection, KPZ anti-advection and the EW cases. Larger value of ν (steeper slope) implies more clustering.

IV. Equilibrium, Sinai Limit

In the previous chapters, we described our results on the nonequilibrium problem of passive particles sliding on fluctuating surfaces. Since the problem is difficult to approach analytically, we performed Monte-Carlo simulations on a lattice model. Our numerical results revealed a new kind of steady state — the strong clustering state (SCS) which we defined using the two point density-density correlation function. We studied the variation of the steady state with change in ω, which is the ratio of surface to particle update speeds. When the particles move faster than the surface ($\omega < 1$), we saw that the SCS persists and the clustering increases. For particles moving slower than the surface ($\omega > 1$), SCS is again the steady state but there are crossover effects due to the particles not being able to cluster in the valleys at small time scales.

To shed more light on the problem, let us consider the extreme limits — particles moving much faster than the surface ($\omega \to 0$) and the surface evolution being much faster than the particle motion ($\omega \to \infty$). The $\omega \to \infty$ limit is the free particle limit; the surface fluctuation is so fast that the particles are not able to react. Valleys appear and disappear before the particles can cluster in them. Thus the particles do not "feel" the valleys and move like free random walkers. The $\omega \to 0$ limit, as we will see below, is subtle and leads to surprising results.

This chapter is devoted to the extreme limit of passive sliders moving on a static surface or the $\omega \to 0$ limit, for all the three kinds of dynamics under consideration. As we discussed briefly in the Chapter on KPZ advection, this limit does not commute with the limit $L \to \infty$. In the numerical results described in the previous chapters, we have seen that as we go to smaller values of ω, the steady state remains the nonequilibrium SCS with the same exponents as for $\omega = 1$. Thus the $L \to \infty$ limit followed by the $\omega \to 0$ leads to the nonequilibrium steady state SCS.

We are now interested in the reverse limit, $\omega \to 0$ followed by $L \to \infty$. In this

limit, the surface is stationary. The particles move on this static surface under the effect of noise. A typical time scale of particle motion $\tau \sim e^{A\sqrt{L}}$ is the time in which the particles cross the largest hills in the landscape. The problem is now an equilibrium problem of particles moving in a random potential under the effect of temperature, and the statistics of the random potential governs the steady state properties. It is well known that for both the KPZ and the EW surfaces in one-dimension, the distribution of heights $h(r)$ in the stationary state is described by [1]

$$\text{Prob}[\{h(r)\}] \propto \exp\left[-\frac{\nu}{2D_h}\int\left(\frac{dh(r')}{dr'}\right)^2 dr'\right] \tag{4.1}$$

Thus, any stationary configuration can be thought of as the trace of a random walker in space evolving via the equation $dh(r)/dr = \xi(r)$ where the white noise $\xi(r)$ has zero mean and is delta correlated, $\langle\xi(r)\xi(r')\rangle = \delta(r-r')$. We thus have a problem of random walkers moving under the effect of gravity and temperature, on a landscape which can itself be seen as the trace of a random walk. This is a well studied equilibrium problem known as the Sinai model [46] for random walkers on a random landscape. We will work with periodic boundary conditions as for the lattice model and without loss of generality — $h(0) = h(L) = 0$.

The passive particles moving on this surface, as we remember, move according to the equation

$$\frac{d\vec{x}_m}{dt} = -a\nabla h|_{\vec{x}_m} + \zeta_m(t), \tag{4.2}$$

Since this is an equilibrium situation, $\langle\zeta_m(t)\zeta_m(t')\rangle = 2\kappa\delta(t-t') = 2K_BT\delta(t-t')$ where T is the temperature and K_B is the Boltzmann constant. We are interested in evaluating the same quantities as we did for the nonequilibrium cases — two point density-density correlation function and the probability of occupancy. Since the particles in our case are noninteracting, we can as well work with a single particle and deal with the probability $\rho(r)dr$ that the particle will be located between r and $r+dr$ instead of the number of particles n_r at a site r.

Before going to the calculations, let us roughly sketch the method we have adopted. We will average the quantities of interest over all possible configurations of the surface. As we have said before, the surface configurations are like the trace of a randomly moving particle; this fact will be used to map our problem to a quantum mechanics

problem. In the path integral formulation, the various surface configurations will look like the various possible paths of a fictitious quantum particle. The Hamiltonian of the quantum particle will carry information about our passive sliding particles. The calculation of the quantities of our interest now boils down to evaluating integrals which contain functions of the Hamiltonian in the integrand. These integrals can be evaluated by solving the eigenvalue problem for the Hamiltonian. This method of mapping the Sinai model to a quantum problem was introduced by Comtet and Texier [38]. We are interested in calculating the two point correlation function and the probability distribution of the particle density. While the correlation function was evaluated in [38], Satya Majumdar was the first to evaluate the probability density.

We now return to our calculations. In the long time limit, the passive particle moving on the surface will reach its thermal equilibrium in the potential $h(r)$ and will be distributed according to the Gibbs-Boltzmann distribution,

$$\rho(r) = \frac{e^{-\beta h(r)}}{Z}, \tag{4.3}$$

where $Z = \int_0^L dr e^{-\beta h(r)}$ is the partition function. The probability density $\rho(r)$ in Eq. (4.3) depends on the realisation of the potential $\{h(r)\}$ and varies from one realisation to another. Our goal would be to compute the distribution of $\rho(r)$ over different realisations of the random potential $h(r)$ drawn from the distribution in Eq. (4.1). Note that the distribution of $h(r)$ in Eq. (4.1) is invariant under the transformation $h(r) \to -h(r)$. In other words, the equilibrium density $\rho(r)$ defined in Eq. (4.3) will have the same distribution if one changes the sign of $h(r)$ in Eq. (4.3). For later simplicity, we will make this transformation now and replace $\rho(r)$ by the following definition

$$\rho(r) = \frac{e^{\beta h(r)}}{Z}, \tag{4.4}$$

where the transformed partition function is now given by $Z = \int_0^L dr e^{\beta h(r)}$.

4.0.1 The Exact Distribution of the Probability Density

We begin our calculations with the evaluation of the probability density $\rho(r)$. To calculate the probability of occupancy, our strategy would be to first compute the n-th moment $\overline{\rho^n(r)}$ of $\rho(r)$. We will then use the definition $\overline{\rho^n(r)} = \int_0^\infty \rho^n P(\rho, L) d\rho$ to

calculate the probability $P(\rho, L)$. From Eq. (4.4) we have

$$\rho^n(r) = \frac{e^{n\beta h(r)}}{Z^n} = \frac{1}{\Gamma(n)} \int_0^\infty dy\, y^{n-1} e^{-yZ + n\beta h(r)} \tag{4.5}$$

where we have used the identity $\int_0^\infty dy\, y^{n-1} e^{-yZ} = \Gamma(n)/Z^n$ to rewrite the factor $1/Z^n$. Here $\Gamma(n)$ is the standard Gamma function $\Gamma(n) = \int_0^\infty x^{n-1} \exp^{-x} dx$, $n > 0$. We now make a change of variable in Eq. (4.5) by substituting $\beta^2 e^{\beta u}/2 = y$. The limits of the new dummy variable u are $-\infty$ to ∞ corresponding to the limits 0 and ∞ for the variable y. Making this substitution in Eq. (4.5) we get,

$$\rho^n(r) \;=\; b_n \int_{-\infty}^{\infty} du\, \exp[-\frac{\beta^2}{2}\left\{\int_0^L dx\, e^{\beta(h(x)+u)}\right\} + n\beta(h(r)+u)] \tag{4.6}$$

where we have used the explicit expression of the partition function, $Z = \int_0^L dr e^{\beta h(r)}$. The constant $b_n = \beta^{2n+1}/[2^n \Gamma(n)]$.

We will now average the expression in Eq. (4.6) over all possible realisations of the random potential $h(x)$ drawn from the distribution in Eq. (4.1). We denote the average by an overbar. Using Eq. (4.1) we have,

$$\overline{\rho^n(r)} \;=\; A b_n \int_{-\infty}^{\infty} du \int_{h(0)=0}^{h(L)=0} \mathcal{D}h(x) \exp[-\left\{\int_0^L dx\, \left[\frac{1}{2}\left(\frac{dh(x)}{dx}\right)^2 + \frac{\beta^2}{2} e^{\beta(h(x)+u)}\right]\right\} + n\beta(h(r)+u)] \tag{4.7}$$

The constant A in the above equation will be chosen so as to satisfy the normalisation, $\int_0^L \overline{\rho(r)} dr = 1$. To get the integral in the above equation in a better form, we shift the potential by a constant amount u, i.e., we define a new function $V(x) = h(x) + u$ for all x. Doing this we get

$$\overline{\rho^n(r)} \;=\; A\, b_n \int_{-\infty}^{\infty} du \int_{V(0)=u}^{V(L)=u} \mathcal{D}V(x)\, \exp[-\left\{\int_0^L dx\, \left[\frac{1}{2}\left(\frac{dV(x)}{dx}\right)^2 + \frac{\beta^2}{2} e^{\beta V(x)}\right]\right\} + n\beta V(r)] \tag{4.8}$$

The above expression can be seen as a path integral for a quantum mechanics problem. One can view V as a space co-ordinate and x as a time co-ordinate. All paths (with the measure shown above) start from $V(0) = u$ and end at $V(L) = u$. At the fixed point r (where we are trying to calculate the density distribution), these paths take

a value $V(r) = V$ which can vary from $-\infty$ to ∞. Using the quantum mechanical bra-ket notation we have,

$$\overline{\rho^n(r)} \;=\; A\, b_n \int_{-\infty}^{\infty} du \int_{-\infty}^{\infty} dV \langle u|e^{-\hat{H}r}|V\rangle e^{n\beta V} \langle V|e^{-\hat{H}(L-r)}|u\rangle \tag{4.9}$$

The Hamiltonian $\hat{H}$ in the above equation corresponds to the operator $\hat{H} \equiv \frac{1}{2}\left(\frac{dV}{dx}\right)^2 + \frac{\beta^2}{2} e^{\beta V(x)}$. If we interpret $V(x)$ to be the "position" of a fictitious particle at the fictitious "time" x, this operator has a standard kinetic energy term and a potential energy which is exponential in the "position" V. The first bra-ket inside the integral in Eq. (4.9) denotes the propagation of paths from the initial value u to V at the intermediate point r and the second bra-ket denotes the subsequent propagation of the paths from V at r to the final value u at L. Rearranging the terms in the integral in the above equation

$$\overline{\rho^n(r)} \;=\; A\, b_n \int_{-\infty}^{\infty} dV\, e^{n\beta V} \int_{-\infty}^{\infty} du \langle V|e^{-\hat{H}(L-r)}|u\rangle\langle u|e^{-\hat{H}r}|V\rangle \tag{4.10}$$

Thus,

$$\overline{\rho^n(r)} \;=\; A\, b_n \int_{-\infty}^{\infty} dV\, e^{n\beta V} \langle V|e^{-\hat{H}L}|V\rangle \tag{4.11}$$

where we have used the completeness condition, $\int_{-\infty}^{\infty} du\, |u\rangle\langle u| = \hat{I}$ with $\hat{I}$ being the identity operator. At this point, it may be helpful and less confusing notationally if we denote the "position" V of the fictitious quantum particle by a more friendly notation $V \equiv X$, which will help us thinking more clearly. We thus have

$$\overline{\rho^n(r)} = A\, b_n \int_{-\infty}^{\infty} dX\, e^{n\beta X} \langle X|e^{-\hat{H}L}|X\rangle. \tag{4.12}$$

To evaluate the matrix element in Eq. (4.12), we need to know the eigenstates and the eigenvalues of the Hamiltonian operator $\hat{H}$. We will work in the "position" basis X where the eigenfunctions $\psi_E(X)$ of $\hat{H}$ satisfy the standard Schrödinger equation,

$$-\frac{1}{2}\frac{d^2\psi_E(X)}{dX^2} + \frac{\beta^2}{2} e^{\beta X}\psi_E(X) = E\psi_E(X), \tag{4.13}$$

valid in the range $-\infty < X < \infty$. To solve the equation above, we make the transformation $X' = 2e^{\beta X/2}$ and get the more familiar form

$$X'^2\frac{d^2\psi_E(X')}{dX'^2} + X'\frac{d\psi_E(X')}{dX'} - (X'^2 - \frac{8E}{\beta^2}\psi_E(X')) = 0 \tag{4.14}$$

The solutions of this differential equation are the modified Bessel functions $K_\nu(X')$ and $I_\nu(X')$, where $\nu = \frac{8E}{\beta^2}$. There are two possibilities for the energy E, we can have bound states $E < 0$ or scattering states $E \geq 0$. For bound states, ν is a real number and it can be shown using the properties of the modified Bessel functions that while K_ν diverges near the origin in this case, I_ν diverges at ∞. Thus the system can not have bound states. For the other possibility of scattering states ($E \geq 0$), ν is an imaginary number, $\nu = ik$. It can again be shown for this case that I_{ik} diverges at $X' \to \infty$ but K_{ik} is well behaved. Thus we take K_{ik} to be our solution and the eigenfunction $\psi_k(X)$ is given by

$$\psi_k(X) = a_k K_{ik}\left(2e^{\beta X/2}\right), \tag{4.15}$$

where a_k is a constant and we have substituted back $X' = 2e^{\beta X/2}$. To determine the constant a_k, we examine the asymptotic behaviour of the wavefunction in the regime $X \to -\infty$. Using the asymptotic properties of the Bessel function (when its argument $2e^{\beta X/2} \to 0$), we find that

$$\psi_k(X) \to a_k\left[\frac{\Gamma(ik)}{2}e^{-ik\beta X/2} - \frac{\pi}{2\sin(ik\pi)\Gamma(1+ik)}e^{ik\beta X/2}\right]. \tag{4.16}$$

In the same limit $X \to -\infty$, the Schrödinger equation (4.13) reduces to a free particle problem,

$$-\frac{1}{2}\frac{d^2\psi_k(X)}{dX^2} = \frac{\beta^2k^2}{8}\psi_k(X), \tag{4.17}$$

which allows plane wave solutions of the form,

$$\psi_k(X) \approx \sqrt{\frac{\beta}{4\pi}}\left[e^{ik\beta X/2} + r(k)e^{-ik\beta X/2}\right]. \tag{4.18}$$

The first term in the bracket $e^{ik\beta X/2}$ represents the incoming wave from $X = -\infty$ while the second term $e^{-ik\beta X/2}$ represents the reflected wave going back towards $X = -\infty$, with $r(k)$ being the reflection coefficient. The amplitude $\sqrt{\frac{\beta}{4\pi}}$ is chosen such that the plane waves $\psi_k(X) = \sqrt{\frac{\beta}{4\pi}}e^{ik\beta X/2}$ are properly orthonormalized so that $\langle\psi_k|\psi'_k\rangle = \delta(k-k')$, where $\delta(z)$ is the Dirac delta function. Comparing Eqs. (4.16) and (4.18) in the regime $X \to -\infty$, we determine the constant a_k (up to a phase factor)

$$a_k = \sqrt{\frac{\beta}{\pi^3}}\sin(ik\pi)\Gamma(1+ik). \tag{4.19}$$

The square of the amplitude $|a_k|^2$ (which is independent of the unknown phase factor) is then given by

$$|a_k|^2 = \frac{\beta k \sinh(\pi k)}{\pi^2}, \tag{4.20}$$

where we have used the identity, $\Gamma(1+ik)\Gamma(1-ik) = \pi k/\sinh(\pi k)$. We know the eigenstates of $\hat{H}$, $\hat{H}|k\rangle = \frac{\beta^2 k^2}{8}|k\rangle$. The wavefunction in the X basis $\psi_k(X) = \langle k|X\rangle$ is given by

$$\psi_k(X) = \frac{\sqrt{\beta k \sinh(\pi k)}}{\pi} K_{ik}(2e^{\beta X/2}). \tag{4.21}$$

Using the above result, we can now evaluate the integral in Eq. (4.12). The matrix $\langle X|e^{-\hat{H}L}|X\rangle$ in Eq. (4.12) can be expanded in terms of the eigenbasis $|k\rangle$ of $\hat{H}$ and we get

$$\begin{aligned}\overline{\rho^n(r)} &= A\, b_n \int_{-\infty}^{\infty} dX \int_0^{\infty} dk\, \langle X|k\rangle\langle k|X\rangle e^{n\beta X}\, e^{-\beta^2 k^2 L/8} \\ &= A\, b_n \int_0^{\infty} dk\, e^{-\beta^2 k^2 L/8} \int_{-\infty}^{\infty} dX |\psi_k(X)|^2 e^{n\beta X}.\end{aligned} \tag{4.22}$$

We can evaluate the X integral in the equation above

$$\langle k|e^{n\beta\hat{X}}|k\rangle = \int_{-\infty}^{\infty} dX |\psi_k(X)|^2 e^{n\beta X} = \frac{k\sinh(\pi k)}{\pi^2 2^{2n-1}} \int_0^{\infty} dy y^{2n-1} K_{ik}(y) K_{-ik}(y) \tag{4.23}$$

where we have substituted the form of $\psi_k(X)$ from Eq. (4.21). We can use the properties of the modified Bessel function [47] and perform the integral on the right hand side of Eq. (4.23) in closed form

$$\langle k|e^{n\beta\hat{X}}|k\rangle = \frac{k\sinh(\pi k)}{\pi^2 2^{2n-1}} \frac{\Gamma^2(n)}{\Gamma(2n)} \Gamma(n-ik)\Gamma(n+ik). \tag{4.24}$$

Substituting this expression in Eq. (4.22), we get

$$\overline{\rho^n(r)} = A \frac{\beta^{2n+1}}{4\pi^2 2^n} \frac{\Gamma(n)}{\Gamma(2n)} \int_0^{\infty} dk\, k \sinh(\pi k) |\Gamma(n-ik)|^2 e^{-\beta^2 k^2 L/8}. \tag{4.25}$$

To determine the value of the constant A in the expression above, we use the condition $\overline{\rho(r)} = 1/L$. This can be seen as follows: $\rho(r)$ being a probability density satisfies $\int_0^L \rho(r)dr = 1$. Now, taking the average over disorder and using translational invariance, we have $\overline{\rho(r)} = 1/L$. We can solve the integral in Eq. (4.25) for $n = 1$ using the identity $\Gamma(1+ik)\Gamma((1-ik) = \pi k/\sinh(\pi k)$ and then using the condition on $\overline{\rho(r)}$, determine the value of A

$$A = \sqrt{2\pi L}. \tag{4.26}$$

One can also check easily that as $n \to 0$, the right hand side of Eq. (4.25) approaches 1. This can be verified by using $\Gamma(x) \approx 1/x$ as $x \to 0$ and also the identity, $\Gamma(ik)\Gamma(-ik) = \pi/k\sinh(\pi k)$. For $n > 0$, one can make a further simplification of the right hand side of Eq. (4.25) by using the property of the Gamma function, $\Gamma(x+1) = x\Gamma(x)$, recursively. Thus $\Gamma(n-ik) = (n-1-ik)\Gamma(n-1-ik) = (n-1-ik)(n-2-ik)\dots(1-ik)\Gamma(1-ik)$. This gives us

$$\Gamma(n-ik)\Gamma(n+ik) \;=\; [(n-1)^2+k^2][(n-2)^2+k^2]...[1+k^2]\frac{\pi k}{\sinh(\pi k)} \tag{4.27}$$

where we have used the identity, $\Gamma(1+ik)\Gamma((1-ik) = \pi k/\sinh(\pi k)$. Substituting this expression in Eq. (4.25) we get

$$\begin{aligned}\overline{\rho^n(r)} \;=\; \sqrt{2\pi L}\frac{\beta^{2n+1}}{4\pi 2^n}\frac{\Gamma(n)}{\Gamma(2n)}\int_0^\infty dk\, k^2[(n-1)^2+k^2][(n-2)^2+k^2]\dots \\ [1+k^2]e^{-\beta^2k^2L/8}.\end{aligned} \tag{4.28}$$

Making the change of variable $\beta^2k^2L/8 = z$ in the integral, we finally obtain the following expression

$$\begin{aligned}\overline{\rho^n(r)} \;=\; \frac{1}{L\sqrt{\pi}}\frac{\beta^{2n-2}}{2^{n-2}}\frac{\Gamma(n)}{\Gamma(2n)}\int_0^\infty dz\, e^{-z}z^{1/2}\left[1^2+\frac{8z}{\beta^2L}\right] \\ \left[2^2+\frac{8z}{\beta^2L}\right]\dots\left[(n-1)^2+\frac{8z}{\beta^2L}\right].\end{aligned} \tag{4.29}$$

Let us consider the specific case $n = 2$. In this case, the formula in Eq. (4.29) gives

$$\overline{\rho^2(r)} = \frac{\beta^2}{12L}\left[1+\frac{12}{\beta^2L}\right], \tag{4.30}$$

which is valid for all L and not just for large L. Note that the second term on the right hand side gives a contribution which is exactly $1/L^2$. This means that the variance, $\overline{\rho^2(r)} - \overline{\rho(r)}^2 = \beta^2/[12L]$ for all L. For arbitrary integer $n \geq 1$, taking the large system size limit $L \to \infty$ in Eq. (4.29) we get

$$\overline{\rho^n(r)} \to \frac{1}{L}\left[\frac{\beta^{2n-2}}{2^{n-2}}\frac{\Gamma^3(n)}{\Gamma(2n)}\right]. \tag{4.31}$$

Now that we have an expression $\overline{\rho^n(r)}$, we use the definition $\overline{\rho^n(r)} = \int_0^\infty \rho^n P(\rho, L)d\rho$ to calculate the probability density $P(\rho, L)$. Note again that the range of ρ is from 0 to ∞ since it is a probability density and not a probability. The factor $1/L$ on the right hand side of Eq. (4.31) suggests that $P(\rho, L)$ has the following behaviour for large L,

$$P(\rho, L) = \frac{1}{L}f(\rho), \tag{4.32}$$

where the function $f(y)$ satisfies the equation,

$$\int_0^\infty y^n f(y)dy = \left[\frac{\beta^{2n-2}}{2^{n-2}}\frac{\Gamma^3(n)}{\Gamma(2n)}\right]. \tag{4.33}$$

To determine $f(y)$ from this equation, we first use the identity, $\Gamma(2n) = 2^{2n-1}\Gamma(n)\Gamma(n+1/2)/\sqrt{\pi}$, known as the doubling formula for the Gamma function. Next we use [48],

$$\int_0^\infty x^{n-1}e^{-ax}K_0(ax)dx = \frac{\sqrt{\pi}}{(2a)^n}\frac{\Gamma^2(n)}{\Gamma(n+1/2)}. \tag{4.34}$$

We can identify the right hand side of Eq. (4.34), with $a = 2/\beta^2$, with the right hand side of Eq. (4.33). This gives us the exact expression of $f(y)$,

$$f(y) = \frac{2}{\beta^2 y}e^{-2y/\beta^2}K_0\left(\frac{2y}{\beta^2}\right). \tag{4.35}$$

More cleanly, we can then write that for large L,

$$P(\rho, L) = \frac{4}{\beta^4 L}f_1\left[\frac{2\rho}{\beta^2}\right], \tag{4.36}$$

where the scaling function $f_1(y)$ is universal (independent of the system parameter β) and is given by,

$$f_1(y) = \frac{e^{-y}}{y}K_0(y). \tag{4.37}$$

This function has the following asymptotic behaviours,

$$f_1(y) \approx \begin{cases} \frac{1}{y}\left[-\ln(y/2) + 0.5772\ldots\right], & y \to 0, \\ \sqrt{\frac{\pi}{2y^3}}e^{-2y}, & y \to \infty. \end{cases} \tag{4.38}$$

The scaling form in Eq. (4.36) is valid only when ρ is of order $O(1)$. If the density is very low and ρ is a number of order $O(1/L)$, the scaling breaks down. This fact suggests that the correct behaviour of the distribution $P(\rho, L)$ for large L actually has two parts,

$$P(\rho, L) \approx \left[1 - \frac{\ln^2(L)}{\beta^2 L}\right] \delta(\rho) + \frac{4}{\beta^4 L} f'\left[\frac{2\rho}{\beta^2}\right] \theta\left(\rho - \frac{c}{L}\right), \tag{4.39}$$

where $f_1(y)$ is given by Eq. (4.37). This form in Eq. (4.39) is consistent with all the observed facts. For example, integrating the right hand side, the first term gives $1 - \frac{\ln^2(L)}{\beta^2 L}$ (with the convention $\int_0^\infty \delta(y)dy = 1$). The second term, when integrated, gives $\frac{\ln^2(L)}{\beta^2 L}$ (where we have used the small y behaviour of $f_1(y)$ from Eq. (4.38) and kept only the leading order term for large L) which exactly cancels the identical factor in the first term to give a total sum 1, as it should. On the other hand, for any finite moment of order n, the first term does not contribute and only the second term contributes to give the result in Eq. (4.31).

4.0.2 The Density-Density Correlation Function

We now consider the density-density correlation function between two points r_1 and r_2 at equilibrium. The calculation proceeds more or less along the same lines as in the previous section. The density-density correlation function is defined as

$$C(r_1, r_2) = \overline{\rho(r_1)\rho(r_2)}, \tag{4.40}$$

and evidently depends only on $r = |r_1 - r_2|$ due to the translational invariance. Using Eq. (4.4), we can write

$$\rho(r_1)\rho(r_2) = \frac{e^{\beta[h(r_1)+h(r_2)]}}{Z^2} = \int_0^\infty dy\, y e^{-yZ+\beta[h(r_1)+h(r_2)]}, \tag{4.41}$$

where the partition function, $Z = \int_0^L dr e^{\beta U(r)}$ and we have used the identity, $1/Z^2 = \int_0^\infty dy\, y e^{-Zy}$. As in the previous section, we now make a change of variable in Eq. (4.41) by writing $y = \beta^2 e^{\beta u}/2$. Then Eq. (4.41) becomes,

$$\begin{aligned} \rho(r_1)\rho(r_2) \;=\; & \frac{\beta^5}{4} \int_{-\infty}^{\infty} du\, \exp[-\frac{\beta^2}{2}\left\{\int_0^L dx e^{\beta[h(x)+u]}\right\} + \\ & \beta(h(r_1) + u + h(r_2) + u)], \end{aligned} \tag{4.42}$$

where we have used the explicit expression of the partition function, $Z = \int_0^L dr e^{\beta h(r)}$. Averaging over the disorder, we get

$$\begin{aligned}\overline{\rho(r_1)\rho(r_2)} &= B\frac{\beta^5}{4}\int_{-\infty}^{\infty} du \int_{h(0)=0}^{h(L)=0} \mathcal{D}h(x)\, \exp[-\left\{\int_0^L dx \right. \\ &\left.\left[\frac{1}{2}\left(\frac{dh(x)}{dx}\right)^2 [\frac{1}{2}\left(\frac{dh(x)}{dx}\right)^2 + \frac{\beta^2}{2}e^{\beta(h(x)+u)}\right]\right\} \\ &+\beta(h(r_1)+h(r_2)+2u)] \end{aligned} \tag{4.43}$$

where the normalisation constant B will be determined from the condition, $\int_0^L \int_0^L C(r_1, r_2) dr_1 dr_2 = 1$ (which follows from the fact that $\int_0^L \rho(r) dr = 1$). Alternatively, one can substitute $r = r_2 - r_1 = 0$ in the expression for the correlation function and then it should be same as $\overline{\rho^2(r)}$ already computed in the previous subsection.

As before, we next shift the potential, i.e., we define $V(x) = U(x) + u$ for all x. The Equation (4.43) then simplifies,

$$\begin{aligned}\overline{\rho(r_1)\rho(r_2)} &= B\frac{\beta^5}{4}\int_{-\infty}^{\infty} du \int_{V(0)=u}^{V(L)=u} \mathcal{D}V(x)\, \exp\left[-\left\{\int_0^L dx\, \left[\frac{1}{2}\left(\frac{dV(x)}{dx}\right)^2 + \right.\right.\right. \\ &\left.\left.\left. \frac{\beta^2}{2}e^{\beta V(x)}\right]\right\} + \beta(V(r_1)+V(r_2))\right]. \end{aligned} \tag{4.44}$$

Thus we have again reduced the problem to a path integral problem. However, unlike the previous calculation, we now have to divide the paths into three parts: (i) paths starting at $V(0) = u$ and propagating up to the point r_1 where $V(r_1) = V_1$ (V_1 can vary from $-\infty$ to ∞), (ii) paths starting at r_1 with $V(r_1) = V_1$ and propagating up to r_2 with $V(r_2) = V_2$ and (iii) paths starting at r_2 with $V(r_2) = V_2$ and propagating up to L where $V(L) = u$. We have assumed $r_2 \geq r_1$ for convenience. Using the bra-ket notation, we can then re-write Eq. (4.44) as

$$\begin{aligned}\overline{\rho(r_1)\rho(r_2)} &= B\frac{\beta^5}{4}\int_{-\infty}^{\infty} du \int_{-\infty}^{\infty} dV_1 \int_{-\infty}^{\infty} dV_2 \\ &\langle u|e^{-\hat{H}r_1}|V_1\rangle e^{\beta V_1}\langle V_1|e^{-\hat{H}(r_2-r_1)}|V_2\rangle \\ &e^{\beta V_2}\langle V_2|e^{-\hat{H}(L-r_2)}|u\rangle. \end{aligned} \tag{4.45}$$

The Hamiltonian $\hat{H} \equiv \frac{1}{2}\left(\frac{dV}{dx}\right)^2 + \frac{\beta^2}{2}e^{\beta V(x)}$ is the same as in the previous section. Using $\int_{-\infty}^{\infty} du\, |u\rangle\langle u| = \hat{I}$, Eq. (4.45) can be simplified,

$$\begin{aligned}\overline{\rho(r_1)\rho(r_2)} &= B\frac{\beta^5}{4}\int_{-\infty}^{\infty} dV_1 \int_{-\infty}^{\infty} dV_2\, \langle V_2|e^{-\hat{H}(L-r)}|V_1\rangle \\ &\langle V_1|e^{-\hat{H}r}|V_2\rangle e^{\beta(V_1+V_2)}, \end{aligned} \tag{4.46}$$

where $r = r_2 - r_1$. Note that Eq. (4.46) clearly shows that $C(r_1, r_2, L) = C(r = r_2 - r_1, L)$, which is expected from translational invariance. Furthermore, Eq. (4.46) also shows that function $C(r, L)$ is symmetric around $r = L/2$, i.e., $C(r, L) = C(L - r, L)$, which is expected due to the periodic boundary condition. As before, we change to a more friendly notation: $V_1 \equiv X_1$ and $V_2 \equiv X_2$, where X_1 and X_2 denote the "positions" of the fictitious quantum particle at 'times' r_1 and r_2. With this notation, Eq. (4.46) reads,

$$\begin{aligned} \overline{\rho(r_1)\rho(r_2)} &= B\frac{\beta^5}{4}\int_{-\infty}^{\infty} dX_1 \int_{-\infty}^{\infty} dX_2 \, \langle X_2|e^{-\hat{H}(L-r)}|X_1\rangle \\ &\quad \langle X_1|e^{-\hat{H}r}|X_2\rangle e^{\beta(X_1+X_2)}. \end{aligned} \tag{4.47}$$

This can be solved to obtain the correlation function

$$\begin{aligned} C(r, L) &= B\frac{\beta^5}{256}\int_0^{\infty}\int_0^{\infty} dk_1 dk_2 k_1 k_2 (k_1^2 - k_2^2)^2 \frac{\sinh(\pi k_1)\sinh(\pi k_2)}{[\cosh(\pi k_1) - \cosh(\pi k_2)]^2} \\ &\quad \exp\left[-\frac{\beta^2}{8}\left(k_1^2(L-r) + k_2^2 r\right)\right]. \end{aligned} \tag{4.48}$$

For $r = 0$, it is possible to perform the double integral in Eq. (4.48) and comparing the results with the expression of $\overline{\rho^2(r)}$ in Eq. (4.30) of the previous subsection, we can evaluate the normalisation constant $B = \sqrt{2\pi L}$. This exact expression of the correlation function was first derived by Comtet and Texier [38] in the context of a localisation problem in disordered supersymmetric quantum mechanics.

To extract the asymptotic behaviour for large L, we rescale $k_1\sqrt{L-r} = x_1$ and $k_2\sqrt{L} = x_2$ in Eq. (4.48), then expand the sinh's and the cosh's for small arguments, perform the resulting double integral (which becomes simple after the expansion) and finally get for $L \to \infty$ and $r > 0$,

$$C(r, L) = \frac{1}{\sqrt{2\pi\beta^2}L^{5/2}[x(1-x)]^{3/2}}, \tag{4.49}$$

where $x = r/L$ is the scaling variable.

To compare the above results for $P(\rho, L)$ and $C(r, L)$ with our nonequilibrium results, we will shift to the multiparticle language. The probability density ρ can be identified with n/L. Using this, we can identify the expressions for $P(\rho)$ and $C(r, L)$ with the corresponding equilibrium quantities — $P(n, L) = \frac{1}{L}P(\rho)$ and $G(r, L) = L^2 C(r, L)$. So, for $n \geq 1$ and $r \geq 1$

$$P(n,L) = \frac{4}{\beta^4 L^2} f_1\left[\frac{2n}{\beta^2 L}\right], \tag{4.50}$$

where $f_1(y)$ is given in Eq. (4.37), and

$$G(r,L) = \frac{1}{\sqrt{2\pi\beta^2}L^{1/2}[x(1-x)]^{3/2}}. \tag{4.51}$$

4.0.3 SCS, Agreement with KPZ advection

The primary result to emerge from the analytic results above is that the equilibrium state again is an SCS. The second and surprising result is that the above results describe very well, the numerical data for the KPZ advection case. A fit to the functional forms shows that these equilibrium results reproduce quite well the scaling exponents and scaling functions for $G(r,L)$ and $P(n,L)$ for $n \geq 1$ obtained numerically for the nonequilibrium KPZ advection case with $\omega = K = 1$. This can be seen in Figs. 4.1 and 4.2. However, the values of β required to fit the two quantities $G(r,L)$ and $P(n,L)$ are different. The correlation function matches with $\beta \simeq 4$ while $\beta \simeq 2.3$ describes the probability density of occupancy data. However, $P(0,L)$ (and thus N_{occ}) does not agree closely in the two cases. Also, as we can see in Fig. 4.2, the equilibrium and nonequilibrium results for $P(n,L)$ do not match very well for large values of n/L and the correspondence does not work well in this limit.

The equilibrium case can also be used to shed light on the dynamical properties of the nonequilibrium steady state for KPZ advection. We compared our results for $\widetilde{G}(t,L)$ with the density-density autocorrelation function in the adiabatic Sinai limit $\omega \to 0$. Though the equilibrium problem itself does not have any dynamics apart from fluctuations, we deduced the autocorrelation function using equilibrium calculations in the following way. We simulated a surface with height field $h(r,t)$ evolving according to KPZ dynamics, and evaluated the density using the equilibrium weight $\rho(r,t) = e^{-\beta h(r,t)}/Z$ for every configuration. As shown in Fig. 4.3, the results with $\beta = 4$ agree with the autocorrelation function in the nonequilibrium system, apart from an overall prefactor.

It is surprising that results in this equilibrium limit describe the non-equilibrium state so well. A partial explanation is as follows. In the nonequilibrium case, the driv-

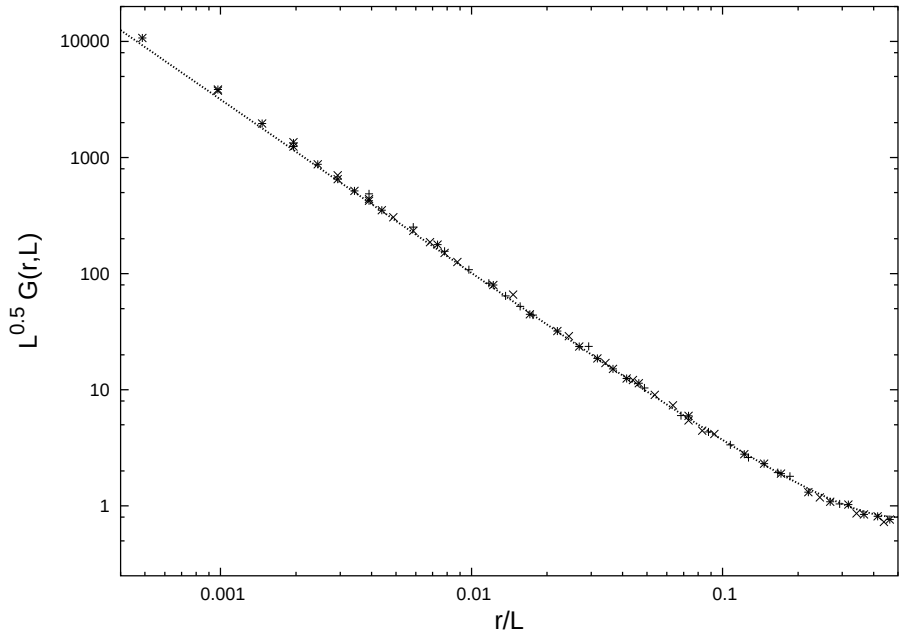

Fig 4.1: The two point scaled density correlation function $G(r, L)$ (advection) for $K = 1$, $\omega = 1$. The line is a plot of Eq. (4.51) with $\beta = 4$. We can see that there is a very good agreement of the nonequilibrium Monte-Carlo data with the analytic equilibrium result. The lattice sizes are $L = 512$ (+), 1024 ($\times$) and 2048 ($*$).

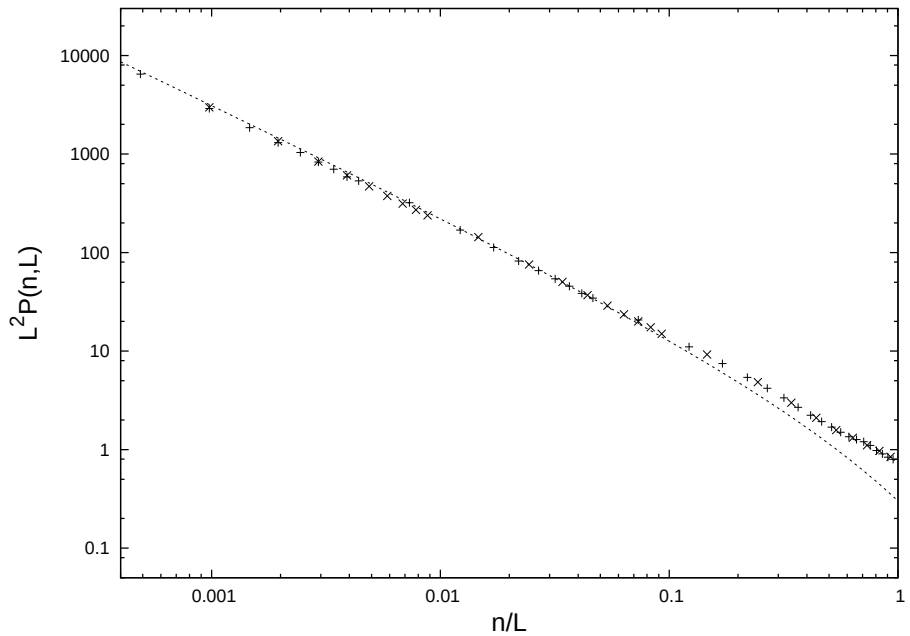

Fig 4.2: The scaled probability distribution $P(n, L)$ data for the KPZ advection case, for $K = 1$, $\omega = 1$, shown by (+) for system size $L = 2048$ and ($\times$) for system size $L = 1024$. The equilibrium prediction in Eq. 4.50 with $\beta = 2.3$ is shown by the dotted line.

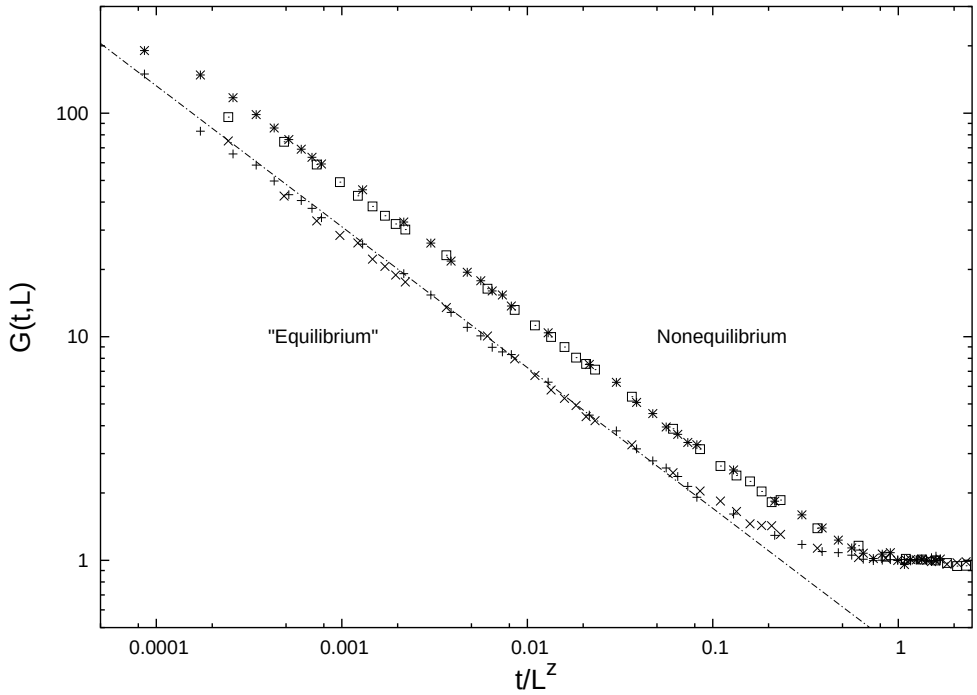

Fig 4.3: Scaled density-density autocorrelation function $\widetilde{G}(t, L)$ for the nonequilibrium KPZ advection and the equilibrium (adiabatic Sinai limit) cases. The dashed line shows $y \sim x^{-2/3}$. The lattice sizes are L=256 ($\Box$, $\times$), 512 ($*$, $+$).

ing force behind particle motion and clustering is the surface fluctuation; the values of the dynamic exponents of the surfaces under consideration are greater than one and thus the large valleys survive for a long enough time for the particles to cluster. In the equilibrium case the drive for particle motion is provided by the temperature. The common feature in both the cases is the exploration of the surface terrain. Thus, in some region of parameter space the surface motion mimics temperature and causes the particles to redistribute in a certain way. Why the equivalent temperature for various quantities is different is not clear and deserves further study. As we have mentioned before, the steady state height distribution for both the KPZ and EW surfaces are the same and so the the Sinai limit is the adiabatic limit for all the three kinds of dynamics under consideration, KPZ advection, KPZ anti-advection and EW dynamics. However only the KPZ advection results are well described by the equilibrium limit.

Two dimensions

Our studies till now have focussed on the problem of passive sliding particles on a one dimensional surface. We have seen that the steady state SCS describes all the three kinds of dynamics under consideration — KPZ advection and anti-advection, and EW dynamics. The question we would like to address in this chapter is — what happens to the steady state in higher dimensions, specifically, in two dimensions? It is known that the exponents characterising the surface vary with the dimension of the surface and we expect that this will have an effect on the clustering of the particles. Also, in two dimensions, we can have structures like saddle points which look like valleys in one direction and hills in the other. These kind of structures may also affect the dynamics of the particles. Thus one does not know a priori what to expect for the passive particles in two dimensions. We will describe below the model that we have used to approach the problem and our results, but before that we will describe the general properties of the KPZ and the EW surfaces in two dimensions.

As we mentioned earlier, the EW equation being linear, can be solved exactly and the results are known for all dimensions. The roughness exponent is known to be $(2-d)/2$ [1] where d is the spatial dimension. In two dimensions, the surface is only logarithmically rough [1, 49]. For the KPZ surface, the exponents are not known exactly. Renormalisation group calculations show that $d = 2$ is special dimension for the KPZ surface. For $d < 2$ the surface has a stable fixed point at finite value of the coupling constant and an unstable fixed point at zero, thus any finite value of nonlinearity λ leads to a rough surface and the exponents can be determined exactly [50, 51]. For $d > 2$, there exist stable fixed points at zero and a finite value of the coupling constant, separated by an unstable fixed point. The stable fixed point at zero is the EW fixed point, this means that at small values of λ, the nonlinear term is irrelevant and there is no roughening (EW surface is not rough for $d > 2$). The stable fixed point at finite λ is the strong coupling fixed point and the surface shows roughening [50, 51].

Thus when one passes a specific value of λ, one sees a transition from a non-roughening to a roughening behaviour. For $d > 2$, the values of the strong coupling exponents cannot be determined by perturbative calculations and one has to rely on numerical methods. The case of $d = 2$, which is of interest to us, shows a behaviour similar to $d < 2$, there is a stable strong coupling fixed point and a small enough nonlinearity leads to a rough surface, but like the $d > 2$ case, the values of the roughness and dynamic exponent cannot be determined from the perturbative calculations. The numerical values from various simulation approaches [1] point to the approximate value of the roughness exponent being nearly equal to 0.4 while the dynamic exponent $z \simeq 1.6$.

Keeping these in mind, we return to the discussion of our coupled problem. Our Monte-Carlo simulation data shows that even in two dimensions, the steady state is an SCS and the quantities characterising the clustering behave similarly to the one dimensional case. As in one dimension, the amount of clustering is different for the three kinds of dynamics and we see that KPZ advection dynamics shows the most clustering, followed by KPZ anti-advection and then the EW dynamics. This is in contrast to our results in one dimension where EW dynamics shows better clustering than the KPZ anti-advection dynamics. This can be ascribed to the fact that the surface roughness is much less for a two dimensional EW surface ($\chi = 0$) than for a strong-coupling KPZ surface ($\chi \simeq 0.4$).

5.1 Lattice Model in Two Dimensions

We consider a square lattice where the particles reside on sites and the links or bonds between successive lattice sites in the x and y directions are dynamical variables which denote local slopes of the surface as in one dimension. The total number of particles N which is taken to be equal to the total number of sites, is L^2. Each link takes either of the values $+1$ (upward slope $\rightarrow$ /) or -1 (downward slope $\rightarrow$ \). A local hill in this case is a site which is at a height one unit higher than all four of its nearest neighbours. In terms of slopes, one would see the configuration (/\) in both the x and y directions. Similarly a local valley is a site which is at a height one unit lower than all four of its nearest neighbours. The rules for the surface evolution are similar to the one dimensional ones and are based on the solid-on-solid (SOS) algorithm [52]. A site is chosen at random and if it is on a local hill, we change it to a local valley for KPZ

advection dynamics. KPZ anti-advection dynamics only allows the valley to hill move and the EW dynamics allows both the moves with equal probabilities.

The particle moves are as follows. We choose a particle at random and then find out the directions which are favourable for movement i.e. have a downward slope; we then move the particle in one of these directions chosen randomly. As before, N_p particle updates are made after every N_s surface moves and $\omega \equiv N_s/N_p$.

5.2 Results

We will start with results on KPZ advection dynamics and then describe the results for the KPZ anti-advection and EW cases.

5.2.1 KPZ advection

We define the two point density-density correlation function as

$$G(\vec{r}, L) \equiv \langle n(\vec{x})n(\vec{x}+\vec{r})\rangle_L \tag{5.1}$$

where $\vec{r}$ can have any direction. In our measurements, we computed the correlation along the directions of $\theta = 0, \pi/6, \pi/4$ and found that the results were independent of direction (Fig. 5.1) for small values of r. For $r > 0$, the correlation function scales as

$$G(\vec{r}, L) \sim Y_2\left(\frac{r}{L}\right), \tag{5.2}$$

the subscript 2 in Y_2 indicating two dimensions. We see that $G(\vec{r}, L)$ decays as a power law $Y_2(y) \sim y^{-\nu_2}$ with $\nu_2 \simeq 1.4$ (Fig. 5.1, Table. 5.1). Thus we find that SCS is the steady state in two dimensions as well.

We have also measured the probability distribution of occupancy $P(n, L)$. Before describing our results, we would like to mention again that we have worked with particle density equal to one, thus total number of particles is $N = L^2$ for two dimensions ($L \times L$ lattice). We find that for $n > 0$, $P(n, L)$ scales as

$$P(n, L) \sim \frac{1}{L^{2\delta_2}} f_2\left(\frac{n}{L^{\delta_2}}\right), \tag{5.3}$$

with $\delta_2 \simeq 1.4$ (Fig. 5.2, Table 5.1). The scaling function behaves as $f_2(y) \sim y^{-\gamma_2}$ with $\gamma_2 \simeq 1.38$ (Fig. 5.2, Table 5.1). We can define the number of occupied sites as $N_{occ} = (1 - P(0, L))L^2 \sim L^{\phi_2}$ and our data for $P(0, L)$ suggests $\phi_2 \simeq 1.37$ (Fig. 5.3, Table 5.1).

As in the case of one dimension, the exponents ν_2, δ_2, γ_2 and ϕ_2 can be connected to each other by scaling relations. We can show that $\delta_2 = \nu_2$ arguing similarly as in one dimension; in two dimensions $N = L^2$ and

$$\int_0^{2\pi} \int_0^L \langle n(0)n(r)\rangle r dr d\theta = L^2 \tag{5.4}$$

where we have made use of the rotational invariance and written the surface integral in polar co-ordinates. We thus have

$$\langle n(0)^2\rangle + \int_0^{2\pi} \int_1^L \langle n(0)n(r)\rangle r dr d\theta = L^2. \tag{5.5}$$

Exactly as in one dimension, it can be shown that $\langle n(0)^2\rangle \sim L^{\delta_2}$, thus

$$\int_0^{2\pi} \int_1^L \langle n(0)n(r)\rangle r dr d\theta = L^2 - aL^{\delta_2} \tag{5.6}$$

where a is a positive constant. Substituting the form in Eq. (5.2)

$$\int_0^{2\pi} \int_1^L Y_2\left(\frac{r}{L}\right) r dr d\theta = L^2 - aL^{\delta_2}. \tag{5.7}$$

Substituting the power law form $Y_2(y) \sim y^{-\nu_2}$ and performing the integration, we have

$$\frac{bL^{-\nu_2+2}}{(-\nu_2+2)L^{-\nu_2}} - \frac{c}{(-\nu_2+2)L^{-\nu_2}} = L^2 - aL^{\delta_2} \tag{5.8}$$

where b and c are positive constants. One can see from the above expression that $\nu_2 = \delta_2$, which agrees with our numerical result (see Table 5.1).

We can also show that ϕ_2, δ_2 and γ_2 are related by $\phi_2 = \delta_2(\gamma_2 - 2) + 2$, as below. The normalisation condition

$$P(0, L) + \int_1^{L^2} P(n, L)dn = 1 \tag{5.9}$$

implies

$$\int_1^{L^2} P(n, L)dn = 1 - P(0, L) \sim L^{\phi_2 - 2}. \tag{5.10}$$

If we substitute the scaling form of Eq. (5.3) and the power law form for the scaling function $f_2(y)$, we get after integrating

$$\frac{L^{(2-\delta_2)(-\gamma_2+1)}}{-\gamma_2 + 1} - \frac{L^{(-\delta_2)(-\gamma_2+1)}}{-\gamma + 1} = 1 - P(0, L) \sim L^{\phi_2 - 2 + \delta_2}. \tag{5.11}$$

Using our knowledge of the numerical values for δ_2 ($\simeq 1.4$) and γ_2 ($\simeq 1.38$), we can see that the first term on the LHS will decay to zero in the limit of $L \to \infty$. We thus get the relation

$$\phi_2 = \delta_2(\gamma_2 - 2) + 2 \tag{5.12}$$

by equating the powers on both sides. Substituting the numerical values of ϕ_2 and δ_2 in the above equation, we obtain $\gamma_2 \simeq 1.51$ which is slightly larger than the value of γ_2 obtained from the numerical data.

5.2.2 KPZ anti-advection and EW

Our numerical results show that the results are independent of the angle of measurement for the KPZ anti-advection and the EW cases as well. For the anti-advection case, the two-point correlation function follows the same form as Eq. (5.2) above and the scaling function is a power law with $\nu_2 \simeq 0.44$ (Fig. 5.4, Table 5.1). The probabilty distribution function also scales similarly as Eq. (5.3) above and we have $\delta_2 = \nu_2 \simeq 0.44$ (Fig. 5.4, Table 5.1). Fitting a power law to the scaling function gives $\gamma_2 \simeq 1.78$ (Fig. 5.4, Table 5.1). The data for $P(0, L)$ gives us the value of $\phi_2 \simeq 1.93$ (Fig. 5.5,

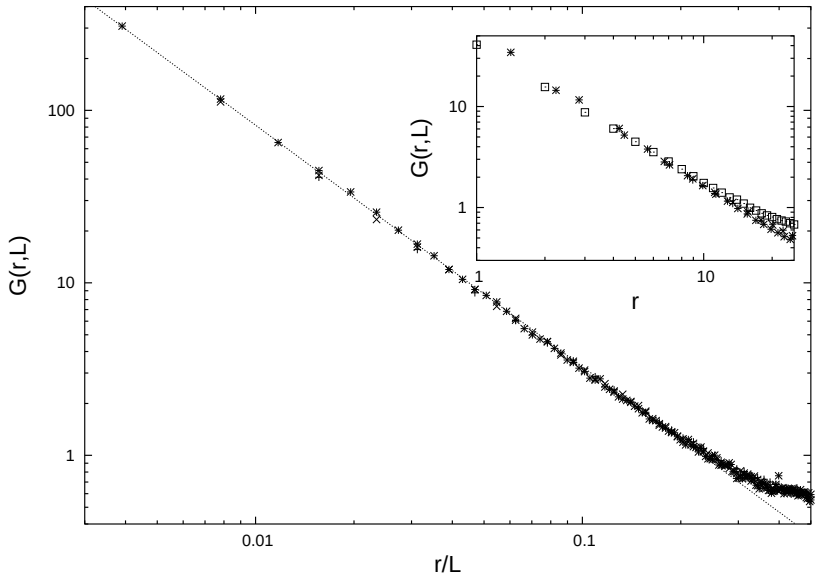

Fig 5.1: KPZ advection: The inset shows $G(r, L)$ versus r for different directions of measurement in two dimensions. The directions are characterised by the angle Θ which is measured with respect to the x-axis. $\Theta = 0, \pi/2$ ($\Box$), $\pi/4$ ($*$), $\pi/6$ ($+$), $\pi/3$ ($\times$). We see that $G(\vec{r}, L)$ is independent of the direction of measurement. The main plot shows the scaling collapse when r is scaled with L. The straight line shows a power law with exponent -1.4. The lattice sizes are $L = 256$ ($*$), 128 ($\times$), 64 ($+$).

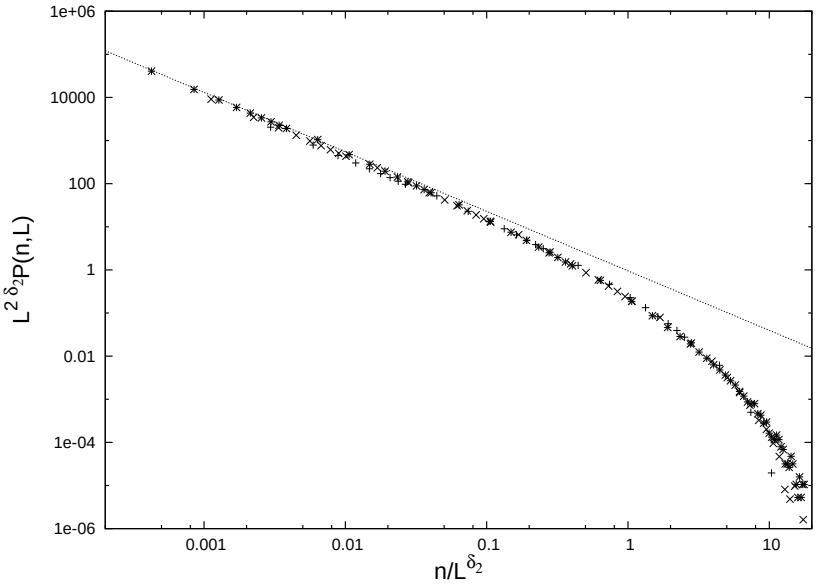

Fig 5.2: KPZ advection: The plot shows $L^{2\delta_2} P(n, L)$ plotted versus n/L^{δ_2} for various values of L in two dimensions. The value of δ_2 is 1.4. The lattice sizes are L= 256 ($*$), 128 ($\times$), 64 ($+$). The straight line shows a power law with exponent -1.38.

Table 5.1) which when used in Eq. (5.12) gives $\gamma_2 = 1.84$. This value is slightly larger than the value from direct numerical fitting.

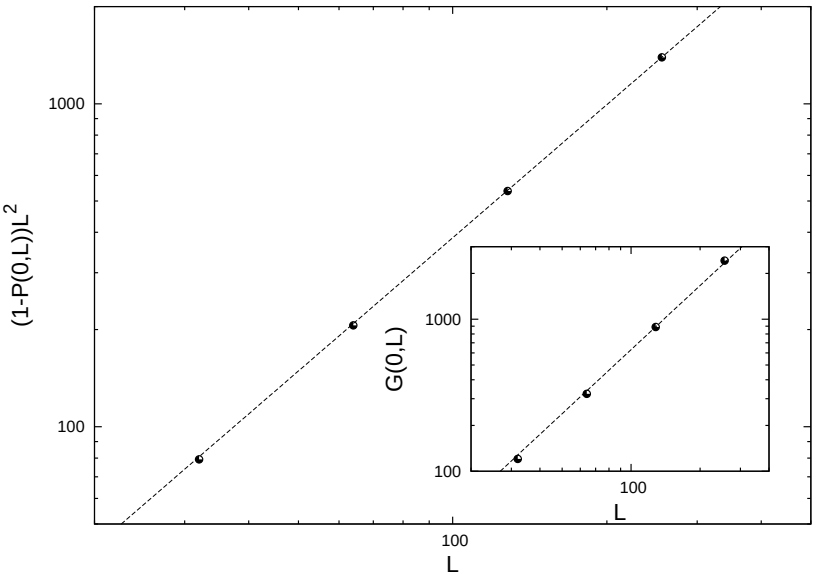

Fig 5.3: KPZ advection: The main plot shows the data for $(1 - P(0, L))L^2$ plotted versus L, the dotted line shows a power law with exponent 1.37 (see Table 5.1). The inset shows $G(0, L)$ plotted versus L and the dotted line shows that $G(0, L) \sim L^{\delta_2}$, the value of δ_2 being 1.4.

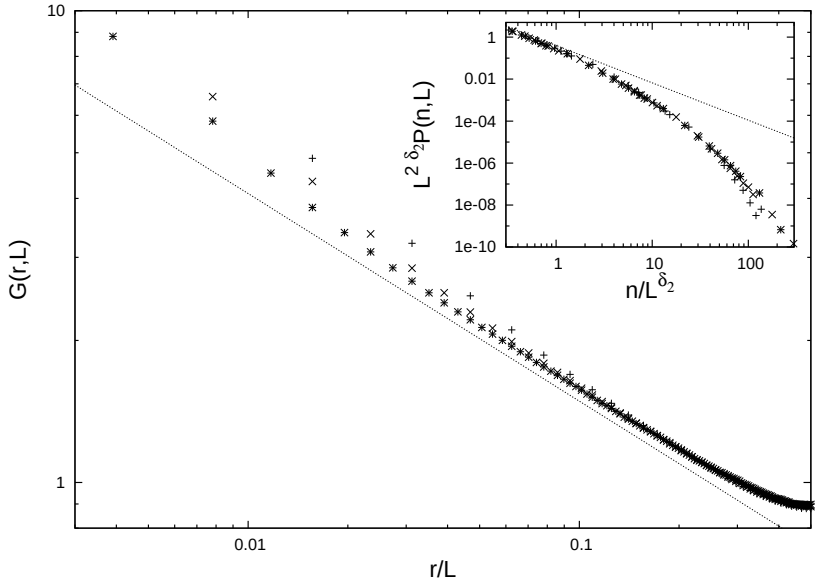

Fig 5.4: KPZ anti-advection: The main plot shows $G(r, L)$ plotted versus r/L for various values of L. The straight line shows a power law with exponent -0.44. The inset shows $L^{2\delta_2}P(n, L)$ plotted versus n/L^{δ_2} for various values of L. The straight line shows a power law with exponent -1.78. The lattice sizes for both plots are $L = 256$ $(*)$, 128 $(\times)$, 64 $(+)$.

The EW dynamics again shows similar behaviour as the KPZ advection and anti-advection cases above and the steady state is an SCS though, as we have mentioned

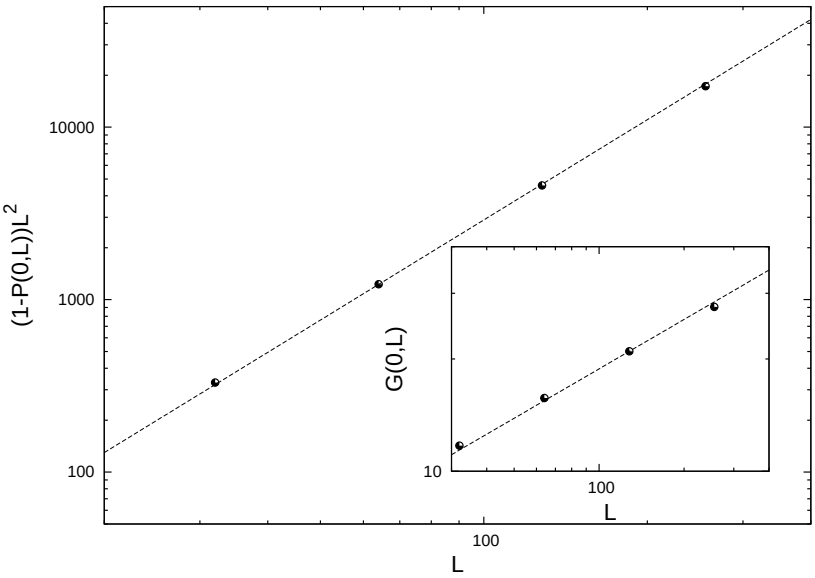

Fig 5.5: KPZ anti-advection: The main plot shows the data for $(1-P(0,L))L^2$ plotted versus L, the dotted line shows a power law with exponent 1.93 (see Table 5.1). The inset shows $G(0,L)$ plotted versus L and the dotted line shows that $G(0,L) \sim L^{\delta_2}$, the value of δ_2 being 0.44.

above, the surface is only logarithmically rough. We see that $\nu_2 = \delta_2 = 0.3$ (Fig. 5.6, Table 5.1). We also find that $\gamma_2 \simeq 1.7$ (Fig. 5.6, Table 5.1) and $\phi_2 \simeq 1.94$ (Fig. 5.7, Table 5.1). Using the values of ϕ_2 and δ_2 in Eq. (5.12) gives $\phi_2 = 1.8$, which is slightly larger than the value from direct numerical evaluation.

	ν_2	δ_2	γ_2	ϕ_2
KPZ Advection	1.40 ± 0.06	1.4 ± 0.2	1.38 ± 0.03	1.37 ± 0.03
KPZ Anti-Adv	0.44 ± 0.02	0.44 ± 0.06	1.78 ± 0.06	1.93 ± 0.03
EW	0.30 ± 0.03	0.3 ± 0.15	1.7 ± 0.2	1.94 ± 0.03

Table 5.1: The values of the exponents in two dimensions for the three kinds of dynamics under consideration — KPZ advection, KPZ anti-advection and EW.

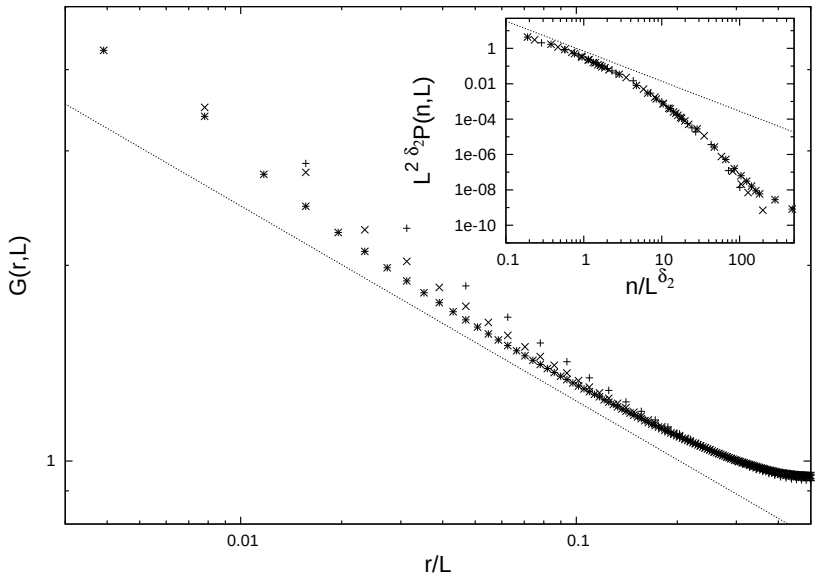

Fig 5.6: EW: The main plot shows $G(r, L)$ plotted versus r/L for various values of L. The straight line shows a power law with exponent -0.3. The inset shows $L^{2\delta_2} P(n, L)$ plotted versus n/L^{δ_2} for various values of L. The straight line shows a power law with exponent -1.7. The lattice sizes for both plots are $L = 256$ $(*)$, 128 $(\times)$, 64 $(+)$.

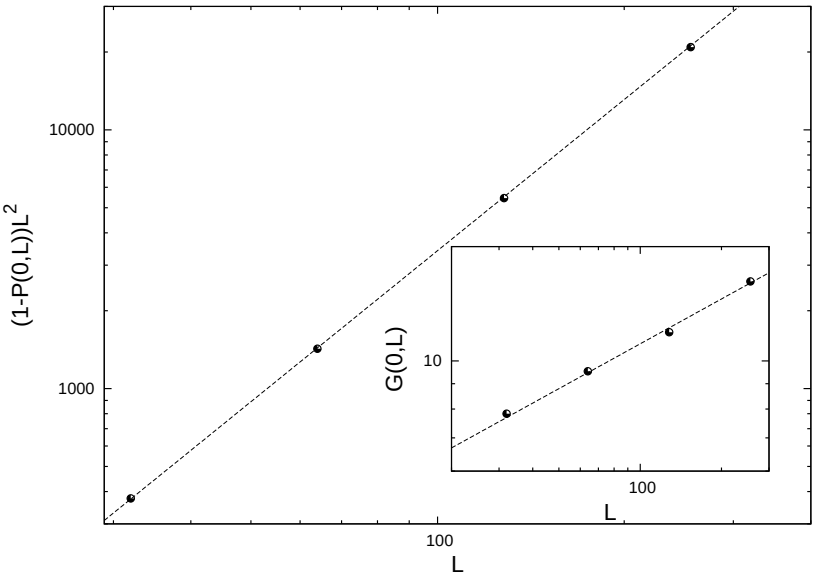

Fig 5.7: EW: The main plot shows the data for $(1 - P(0, L))L^2$ plotted versus L, the dotted line shows a power law with exponent 1.94 (see Table 5.1). The inset shows $G(0, L)$ plotted versus L and the dotted line shows that $G(0, L) \sim L^{\delta_2}$, the value of δ_2 being 0.3.

Conclusions

In this thesis, we have studied the problem of passive, non-interacting particles sliding on fluctuating surfaces which evolve according to the Kardar-Parisi-Zhang (KPZ) and Edwards-Wilkinson (EW) equations. Our results show that the systems under consideration have a new kind of steady state — the Strong Clustering State (SCS), where the passive particles aggregate strongly. This state is characterised by the properties of the two point density-density correlation function $G(r, L)$; we find that $G(r, L)$ is a function of distance r divided by the system size L and shows a divergence at small r/L. The divergence of the scaling function shows a tendency of the particles to form clusters and the scaling with L shows the presence of more than one cluster which are separated from each other at the length scale of the system size.

The KPZ equation breaks the up-down symmetry and in this case, the coupled problem has two sub-cases depending on the relative direction of the surface and particle motion. The sub-case of KPZ advection describes particles and surface moving in the same direction while the KPZ anti-advection sub-case describes particles and surface moving in opposite direction with respect to each other. We have considered both these cases in our work. We have studied the problem in one and two dimensions and also studied the change in the steady state properties under change in relative update speeds and the noise parameter. Our results show that SCS is not limited to a specific dynamics but describes the steady state for a more general set of driving dynamics. We found that the steady state is robust and the exponents are found to be universal within each class of dynamics, e.g. KPZ advection in one dimension.

As described in the introduction, the KPZ equation can be mapped to the Burgers equation in fluid dynamics and our problem is equivalent to that of passive scalars driven by a highly compressible fluid. Thus in the fluid context, our results show that passive scalars driven by a compressible fluid would cluster very strongly in contrast to

the intermittent mixing seen in ink particles in incompressible fluids like water. While this general result agrees with previous work [10, 27, 29], we have been able to obtain a detailed picture of the steady state. While the compressibility of the fluid is an important ingredient for clustering, we should remember that it is the noninteracting nature of the particles that causes the extreme clustering seen in our problem. Our results are to be compared to previous work on a similar problem where the particles interact with each other via hard core repulsion [30, 31]. The steady state in this case is the fluctuation dominated phase ordered (FDPO) state. As the name suggests, there is a phase ordering which is characterised by the cuspy decay of the correlation function. The other important feature of this steady state is the presence of strong fluctuations that persist in the thermodynamic limit. While the cuspy decay is weaker than the power law decay in our case indicating less clustering, the feature of strong fluctuations is a common feature of both the steady states.

In one dimension, we have been able to obtain exact analytic results in the adiabatic limit of a stationary surface with particles moving on it under the effect of temperature. This is an equilibrium problem well known as the Sinai model. We found that even in this equilibrium limit, the state is an SCS and surprisingly, the results match very well with the KPZ advection case.

Our simulations for the problem in two dimensions show that the steady state is again an SCS with the difference that the ordering for the amount of clustering is different from that in one dimension. In one dimension, the KPZ advection case shows the most clustering, followed by the KPZ anti-advection and then the EW case. In two dimensions, the KPZ anti-advection and the EW cases reverse places; the EW surface being only logarithmically rough, shows the least clustering.

6.1 One Dimension

6.1.1 KPZ advection

In the case of KPZ advection in one-dimension, we verified that our result for the two point density-density correlation agrees with the exact result by Derrida [45] on the related problem of second class particles in an ASEP. These second class particles, in the low density regime, behave like our passive sliders and their separation probability goes as $r^{-3/2}$ (r being the separation), the same as for passive sliders in our case. We

varied the values of the parameter ω which characterises the relative update speed of the surface and the particles, and the parameter K which characterises the random noise acting on the particles; we found that SCS continues to be the steady state. Moreover, the values of the exponents characterising the clustering remain the same. For values of ω smaller than one (particles moving faster than the surface), we saw that the probability of a large cluster being present in the system increases; the increased update rate of the particles ensures that they recluster quickly in newly formed valleys. We also found that for the KPZ advection case, the tilting of the surface does not make any difference to the results. This reflects the fact that the extra term which enters due to the tilt, can be simultaneously shifted away from the dynamical equations which govern the dynamics of the surface and the passive particles.

We also compared our results to those by Drossel and Kardar [29], who were the first to study this problem. We found that the form of the correlation function $G(r, L)$ depends strongly on the system size L, a feature not reported in [29]. This scaling with system size affects other results, for example, the form of $G(r, L)$ proposed by us describes the numerical data for the quantity $N(l, L)$ (number of particles in a bin of size l) much better than the $l-$independent form proposed in [29].

Scaling arguments and dimensional analysis are important tools in fluid dynamics which help in deducing various scaling exponents from general considerations and thus provide an understanding of the physics of the problem. A famous example is the Kolmogorov scaling argument [14] which is used to estimate the values of some of the correlation exponents for Navier-Stokes turbulence. Similar arguments have been used for the study of the Burgers turbulence [14, 53], and also for the study of passive scalar turbulence in incompressible fluids [9]. It would be interesting to see if it is possible to formulate similar arguments for passive scalars in compressible fluids, specifically the Burgers fluid, and compare the results with our numerical results.

6.1.2 KPZ anti-advection

For the KPZ anti-advection case, we found that the steady state is again an SCS and clustering is less than the KPZ advection case. The particles tend to cluster in the local valleys and the local valleys in this case are highly dynamic, causing declustering. We found that the variation of ω and K again does not change the exponents characterising clustering.

Drossel and Kardar [29] have suggested that the dynamical exponent, which characterises the motion of the particles, varies continuously as a function of K. Our numerical evidence suggests that there is in fact a single value of z describing the RMS displacement data for various values of K.

6.1.3 EW dynamics

In case of the driving surface being governed by the EW equation, we found that the steady state, as in the above two cases, is an SCS and the amount of clustering is less than the KPZ advection but more than the KPZ anti-advection case. We again found that a change in ω does not affect the clustering properties of the particles.

Gopalakrishnan [37] has suggested that the dynamical exponent might have two different values depending on whether the particles move faster than the surface or vice-versa. We found by a careful analysis of the numerical data that the dynamical exponent does not change under the variation of the ratio of particle and surface update speeds; rather, there is a slow crossover which might come across as an apparent change in exponent.

6.2 Equilibrium Sinai limit

We have seen that the extreme limit of $\omega \to 0$ does not commute with the limit of $L \to \infty$. While the limit $\omega \to 0$ followed by $L \to \infty$ leads to a nonequilibrium SCS with increased clustering of particles, the reverse limit leads to the equilibrium limit of particles moving on a stationary surface under the effect of noise. This equilibrium limit is the well known Sinai model of random walkers moving on a random landscape. Since we are considering a stationary surface, the only important quantity is the static distribution of heights. In one dimension, the KPZ and the EW surface have the same distribution of heights in the steady state and thus the equilibrium limit is the same for both of them. The relevant time scale for this equilibrium problem is $\tau \sim e^{A\sqrt{L}}$ — the time it would take the particles to cross the largest hills in the landscape.

The distribution of the passive particles moving on the surface under the effect of temperature t is governed by the Gibbs-Boltzmann distribution $\rho(r) = e^{-\beta h(r)}/Z$, where Z is the partition function. To calculate the relevant quantities, we took an average over all possible configurations of the stationary surface. In our calculations,

we followed the approach of Comtet and Texier of mapping the problem to a quantum mechanics problem. The various surface configurations for the Sinai model map to various possible paths of a quantum particle in the new problem. Using this mapping, we were able to obtain exact analytic results for the quantities of our interest — the correlation function $G(r, L)$ and the probability distribution $P(n, L)$. We found that not only do these functions follow the same scaling form but the scaling functions also match very well with our results from the KPZ advection problem. The temperature is a free parameter in the equilibrium Sinai problem and can be chosen to fit our numerical results. We found that the two quantities $G(r, L)$ and $P(n, L)$ fit the numerical data for different values of the temperature. A heuristic argument for the agreement of the results is that the temperature has a similar effect on the particles in the case of the Sinai problem as the surface fluctuations in the case of the KPZ surface.

To summarise, we found that the exact results for the equilibrium Sinai limit of a stationary surface show a remarkable similarity to the nonequilibrium KPZ advection case results. This study throws open further questions — While the Sinai limit is common to the KPZ advection, anti-advection and the EW dynamics, why do the results agree for only the KPZ case? Why are different temperature values needed to fit different quantities?

6.3 Two dimensions

We performed Monte-Carlo simulations on a two dimensional lattice version of the problem and our results show that SCS is the steady state of the problem, even in two dimensions. As expected, the amount of clustering in two dimensions is less than that in one dimension. As mentioned above, the EW surface is only logarithmically rough in two dimensions and thus the EW case shows the least clustering.

6.4 Relevance, possibilities

As we have mentioned in the Introduction chapter, Burgers equation is a simplified approach to modeling fluids and may not be of direct use in practical applications. The purpose of our work is to use this comparatively simple model and bring out aspects of passive scalar clustering caused by compressibility. We thus cannot provide a precise scenario where experimental measurements might show an SCS kind of steady state.

Rather, we can speculate about possible scenarios where our study might be relevant in providing a general understanding. At this concluding stage, we would also like to make connections of the important features of our strong clustering state (SCS) to other systems where those features are present.

The Burgers equation provides a simple model for systems as diverse as road traffic to the early universe [11]. In the context of cosmology and the early universe, one is interested in the formation of structures, beginning from a random distribution of particles. Simulations using the low viscosity limit of the Burgers equation show formation of structures that are very similar to those obtained from other, more realistic models, involving gravitation interactions between particles. These models consider the universe to be composed of a single kind of particle for the simplicity of modeling. One can consider a more complicated model where one can have more than one kind of particle. One set of particles interact via gravity and cluster by forming structures, these particles can be thought of as the fluid. There can be another set of particles which are like passive scalar particles and interact with the "fluid" particles via short range interactions. One would expect that the dynamics of these passive particles would reveal features similar to our passive scalars. In the context of particles driven by fluctuating surfaces, we have mentioned that the motivation of Drossel and Kardar [5] to study this problem was to develop a model for growing binary films. It is expected that in some region of the parameter space, the domain walls between two kinds of materials might behave like the passive scalars in our system. Although the number of domain walls is not conserved in the dynamics of binary films, it would be interesting to study their properties and compare them with our results.

While we are interested in a specific problem in the general area of coupled systems, the phenomena of clustering and strong fluctuations are seen in more general scenarios. It would be interesting to contrast and compare our system with others which possess these general features. One of the examples we would like to consider is clustering in granular systems. Consider a system of granular particles which have been provided with some initial kinetic energy and are distributed homogeneously in space. Due to the presence of inelastic interaction, the particles will lose energy as time progresses. It has been observed that while these particles lose energy, the spatial homogeneity of the system gives way to a state in which particles form clusters, and with an increase in energy loss, these clusters "cool down" and become more and more dense [54, 55, 56]. The clustering in this system is different from our system in that it is caused by energy

loss and not by correlations which have developed due to a driving field. Also in the granular case, the system under study is relaxing towards a steady state while our studies have focussed on the steady state properties. It would be interesting to study in our case, the evolution towards a clustered steady state from a homogeneous initial state and compare the results to those from granular systems. One expects that with better imaging techniques, it would be possible to perform measurements in the above granular system experimentally and study the correlations. It would be interesting to compare our results with results from such experiments.

Another important feature of our steady state is the presence of strong fluctuations. As we have discussed in the first chapter, fluctuations that do not damp down in the thermodynamic limit are also seen when the passive particles interact via hard core repulsion [30, 31, 33]. Recent work by Ramaswamy et. al. [57] and Mishra and Ramaswamy [58] has shown that this feature of strong fluctuations is also present in a system of rod like particles in a driven, nematic steady state. The system they consider is that of rod like particles spread on a two dimensional surface which is being shaken to constantly provide energy to the particles and keep them in a driven state. This system can be modeled using an equivalent description of passive particles (the rods themselves) driven by a stochastic field (the alignment of the rods) [58]. The particles show nematic ordering, aligning parallel to each other lengthwise and also show phase separation with clustering of particles. These clusters are highly dynamic in nature and show strong fluctuations similar to those in the FDPO steady state. In [58], the authors have also suggested possible experiments where these fluctuations might be observed. It would be most interesting to see this aspect of driven, phase separated states being realised physically.

To conclude, in this thesis, we have reported our results on a specific problem belonging to the area of coupled driven diffusive systems. We have studied in detail, the steady state, and found that it shows a strong clustering of particles, and fluctuations that do not damp in the thermodynamic limit. We hope that through our studies on the model system of sliding particles on fluctuating surfaces, we have been able to provide an understanding of some general aspects of similar systems. We also hope that future experiments and observations might be able to show specific features of the SCS steady state.

Bibliography

[1] A. L. Barabasi and H. E. Stanley, *Fractal Concepts in Surface Growth* , Cambridge University Press, Cambridge (1995).

[2] D. Chowdhury, Physica Scripta, **T 106**, 13 (2003).

[3] L. D. Landau and E. M. Lifshitz, *Fluid Mechanics*, Pergamon Press, England (1959).

[4] J. M. Burgers, *The Nonlinear Diffusion Equation*, D. Reidel, Dordrecht (1974).

[5] B. Drossel and M. Kardar, Phys. Rev. Lett. **85**, 614 (2000).

[6] P. Biswas, A. Majumdar, A. Mehta and J. K. Bhattacharjee, Phys. Rev. E **58**, 1266 (1998).

[7] A. Kunwar et. al., J. Phys. Soc. Japan **73**, 2979 (2004).

[8] M. K. Verma, Phys. Rep. **401**, 229 (2004).

[9] B. I. Shraiman and E. D. Siggia, Nature **405**, 639 (2000).

[10] G. Falkovich, K. Gawedzki and M. Vergassola, Rev. Mod. Phys. **73**, 913 (2001).

[11] U. Frisch and J. Bec, Burgulence, *Les Houches 2000: New Trends in Turbulence*, M. Lesieur (ed.), Springer EDP-Sciences, Berlin (2001).

[12] R. H. Kraichnan, Phys. Rev. Lett. **72**, 1016 (1994).

[13] K. Nishinari, M. Fukui and A. Schadschneider, J. Phys. A, **37**, 3101 (2004).

[14] F. Hayot and C. Jayaprakash, Int. J. Mod. Phys. B, **14**, 1781 (2000).

[15] U. Frisch, *Turbulence*, Cambridge University Press, Cambridge (1995).

[16] K. R. Sreenivasan, Proc. R. Soc. Lond. A **434**, 165 (1991).

[17] D. Mitra and R. Pandit, Phys. Rev. Lett. **95**, 144501 (2005).

[18] E. Balkovsky, G. Falkovich and A. Fouxon, Phys. Rev. Lett. **86**, 2790 (2001).

[19] J. M. Deutsch, J. Phys. A **18**, 1449 (1985).

[20] M. Wilkinson and B. Mehlig, Phys. Rev. E **68**, 040101 (2003).

[21] M. Wilkinson and B. Mehlig, Europhys. Lett. **71**, 186 (2005).

[22] G. Falkovich, A. Fouxon and M. G. Stepanov, Nature **419**, 151 (2002).

[23] T. Elperin, N. Kleeorin and I. Rogachevskii, Phys. Rev. Lett. **77**, 5373 (1996).

[24] J. R. Fessler, J. D. Kulick and J. K. Eaton, Phys. Fluids **6**, 3742 (1994).

[25] J. R. Cressman, W. I. Goldburg and J. Schumacher, Europhys. Lett. **66**, 219 (2004).

[26] J. C. Sommerer and E. Ott, Science **259**, 335 (1993).

[27] K. Gawedzki and M. Vergassola, Physica D **138**, 63 (2000).

[28] E. Medina, T. Hwa and M. Kardar, Phys. Rev. A. **39**, 3053 (1989).

[29] B. Drossel and M. Kardar, Phys. Rev. B **66**, 195414 (2002).

[30] D. Das and M. Barma, Phys. Rev. Lett. **85**, 1602 (2000).

[31] D. Das, M. Barma and S. N. Majumdar, Phys. Rev. E. **64**, 046126 (2001).

[32] A. J. Bray, Adv. Phys. **51**, 481 (2002).

[33] M. Gopalakrishnan and M. Barma, J. Stat. Phys. **110**, 1305 (2002).

[34] S. Chatterjee and M. Barma, Phys. Rev. E. **73**, 011107 (2006).

[35] T. Bohr and A. Pikovsky, Phys. Rev. Lett. **70**, 2892 (1993).

[36] C. S. Chin, Phys. Rev. E **66**, 021104 (2002).

[37] M. Gopalakrishnan, Phys. Rev. E **69**, 011105 (2003).

[38] A. Comtet and C. Texier, *Supersymmetry and Integrable Models*, H. Aratyn, T. Imbo, W. Y. Keung, U. Sukhatme (eds.), *Proceedings Chicago IL* (1997).

[39] B. Derrida, Phys. Rep. **301**, 65 (1998).

[40] T. M. Liggett, *Interacting Particle Systems*, Springer-Verlag, New York (1985).

[41] P. M. Binder, M. Paczuski and M. Barma, Phys. Rev. E. **49**, 1174 (1994).

[42] D. E. Knuth, *The Art of Computing*, Addison-Wesley, Reading, MA (1997).

[43] W. H. Press, S. A. Teukolsky, W. T. Vetterling and B. P. Flannery, *Numerical Recipes in Fortran*, Cambridge University Press, Cambridge (1986).

[44] M. Matsumoto and T. Nishimura, ACM Transactions on Modeling and Computer Simulation: Special Issue on Uniform Random Number Generation **8**, 3 (1998).

[45] B. Derrida, S. A. Janowsky, J. L. Lebowitz and E. R. Speer, J. Stat. Phys. **73**, 813 (1993).

[46] Y. G. Sinai, Theor. Probab. Appl. **27**, 256 (1982).

[47] I. S. Gradshteyn and I. M. Ryzhik, Identity 6.576.4, **676**, *Table of Integrals, Series, and Products*, Academic Press, Florida, (2000).

[48] I. S. Gradshteyn and I. M. Ryzhik, Identity 6.621.3, **692**, *Table of Integrals, Series, and Products*, Academic Press, Florida, (2000).

[49] T. Nattermann and L. Tang, Phys. Rev. A **45**, 7156 (1992).

[50] T. Halpin-Healy and Y, Zhang, Phys. Rep. **254**, 215 (1995).

[51] J. Krug and H. Spohn, Kinetic Roughening of Growing Surfaces, *Solids Far from Equilibrium*, C. Godreche (ed.), Cambridge University Press, Cambridge (1991).

[52] P. Meakin, *Fractals, Scaling and Growth far from Equilibrium*, Cambridge University Press, Cambridge, (1998).

[53] M. K. Verma, Physica A **277**, 359 (2000).

[54] R. P. Behringer and S. R. Nagel, Rev. Mod. Phys. **68**, 1259 (1996).

[55] I. Goldhirsch and G. Zanetti, Phy. Rev. Lett. **70**, 1619 (1993).

[56] S. Das and S. Puri, Europhys. Lett. **61**, 749 (2003).

[57] S. Ramaswamy, R. A. Simha and J. Toner, Europhys. Lett. **62**, 196 (2003).

[58] S. Mishra and S. Ramaswamy, Phys. Rev. Lett. **97**, 090602 (2006).